Towards Autonomous Excavation of Fragmented Rock: Experiments, Modelling, Identification and Control

by

Joshua Alexander Marshall

A thesis submitted to the Department of Mechanical Engineering
in conformity with the requirements for
the degree of Master of Science (Engineering)

Queen's University
Kingston, Ontario, Canada
August, 2001

Abstract

Towards Autonomous Excavation of Fragmented Rock:
Experiments, Modelling, Identification and Control

Joshua Alexander Marshall
Master of Science (Engineering)
Department of Mechanical Engineering
Queen's University
July, 2001

Increased competition and recent globalization in the minerals industry has resulted in further demands for advanced mining equipment technology. The autonomous excavation problem for fragmented rock entails the design of a control system capable of regulating the complicated bucket-rock interactions that occur during excavation operations. A notable amount of previous work has been performed to address the excavation automation problem, although this work has mainly focused on the excavation of granular material such as soil rather than on rock. Moreover, none has resulted in widespread industry adoption of automated rock loading technologies.

This thesis revisits the autonomous excavation problem for fragmented rock from a fresh perspective, and in particular, focuses on the problem of autonomous excavation using load-haul-dump (LHD) underground mining machines. First, an extensive review of the state-of-the-art in autonomous excavation is provided. Then, results of pioneering full-scale experimental studies are provided. These studies were carried out with the intent of identifying the evolution of machine parameters during free-space motions of the employed LHD mechanism, and during a selection of excavation trials conducted by skilled operators in fragmented rock typical of an underground hard-rock mining scenario. It was discovered that information contained within actuating cylinder pressure signals might offer a means for identification of the bucket-rock interaction status.

Having reviewed the conventional techniques for development of robot dynamical equations of motion, the results are presented of modelling the LHD loader mechanism

motions in free-space and while in contact with a rock pile using the nonlinear system identification technique known as parallel cascade identification (PCI). Although the resulting identified models were not as accurate as might have been hoped, it was concluded, through subsequent observations, that an excavation control system might be realizable by interpretation of measured forces in the LHD machine dump cylinder as an indication of bucket-rock interaction intensity. Based on these findings, a framework is provided for an admittance-type control system, where the bucket is commanded to respond to sensed cylinder forces with prescribed dynamics, providing a basis for the autonomous excavation of fragmented rock.

Acknowledgements

I would like to extend personal thanks to my research supervisor, Dr. Laeeque K. Daneshmend, for his ideas, guidance, and championship, not only in the business of scholarly research, but in matters relating to opportunity and career path. Dr. Daneshmend allowed me a great deal of freedom, yet provided continuous support and personal attention during the course of my stay at Queen's.

I would like to acknowledge Mr. Patrick Murphy for his contribution to commissioning of the field data acquisition system. His sacrificial commitment was instrumental to its success. In addition, I would like to extend thanks to Mr. Dave Sargent and the staff at Tamrock Loaders, Inc. for their exceptionally generous contributions of material and human resources. Furthermore, I would like to recognize Mr. Wayne Lidkea and Inco Limited's Mines Research Department personnel for their donation of fragmented rock, which was put to good use in full-scale excavation studies.

I would also like to tender acknowledgement of Dr. Michael J. Korenberg and Mr. J. Mikael Eklund for offering, on numerous occasions, their advice and expertise with regards to implementation of the parallel cascade identification algorithm. Also, thanks to Mr. David R. Gauldie for his counsel in C language programming.

Many thanks to Dr. Peter M. Wild for his partnership in the project, and for his guidance as professor whom I endeavoured to please as a rookie teaching assistant.

Thanks to members of the administrative and support staff at the Departments of Mining and Mechanical Engineering, for things too numerous to list.

This research was funded in part through a Natural Sciences and Engineering Research Council of Canada (NSERC) PGS A scholarship.

Very special thanks to my parents, David and Sheila, my fiancée Jillian, and the faithful friends who supported me through this research project and graduate degree.

Contents

List of Tables

List of Figures

Nomenclature

A	Integer valued constant used in a PCI model, which is typically selected at random from the set $\{0, 1, \ldots, R\}$
A_H, A_R	Surface areas (m^2) over which the pressures at the head and rod of a given hydraulic cylinder act
C	Real valued constant used in a PCI model, which tends to zero as the mean-square of the residue approaches zero, page 34
$\boldsymbol{C}(\boldsymbol{q}, \dot{\boldsymbol{q}})$	Matrix of centripetal and Coriolis terms
$\boldsymbol{D}(\boldsymbol{q})$	Matrix of inertial coefficients
E	Environment interaction function, mapping cylinder extension/retraction rate to actual bucket-rock interaction force
$\hat{E}$	Environment interaction function, mapping cylinder extension/retraction rate to dump cylinder force
$\boldsymbol{G}$	Velocity loop closure constraint matrix
$H(s)$	Force compensator transfer function
I	Total number of cascades in an identified PCI model
$\boldsymbol{I}_i$	Inertia tensor for the link i about its centre of mass
I_{zzi}	Moment of inertia of link i about the z axis
$\boldsymbol{J}_{v_{ci}}$	Jacobian matrix relating joint velocities to the centre of mass of link i
$\boldsymbol{J}_{\omega_i}$	Jacobian matrix relating joint velocities to the rotation of link i
K	Kinetic energy of a mechanical system
L	Lagrangian function, equivalent to $K-V$ for a mechanical system, page 25
L_i	Dynamic linear system of the i-th cascade of a PCI model
M	Polynomial order of a PCI model

N_i	Static nonlinear system of the i-th cascade of a PCI model
P	Number of parallel cascade models in a MIMO system
Q	Configuration space for a mechanical system
R	Dynamic linear system memory of a PCI model, or is the fraction of material less than the diameter d_s in the Rosin-Rammler equation, page 77
$\boldsymbol{R_i}$	Rotation matrix that transforms vectors from the link frame to the base frame of a mechanical system
R_r	Rolling radius (m) of the LHD vehicle tire
T	Number of data points in a given discrete-time input-output data set
V	Potential energy of a mechanical system
X_i, Z_i	Perpendicular axis for the Denavit-Hartenberg coordinate frames attached to the link i
$Y(s)$	Mechanical admittance, page 100
$Z(s)$	Mechanical impedance, page 99
$\boldsymbol{\Omega}$	Rotational component of the inertial coefficient matrix $\boldsymbol{D(q)}$
$\Re$	Set of real numbers
$\Re^n$	An n-dimensional vector space over $\Re$
$\Re^{m \times n}$	Set of all $m \times n$ matrices with real elements
Σ	Reduced mechanical system
$\tilde{\Sigma}$	Closed-chain mechanical system
δ	Denotes the unit impulse function
$\boldsymbol{\omega_i}$	Rotational velocity vector for link i
ω_N	Nyquist frequency
ω_c	Filter cut-off frequency at -3 dB response
ω_s	Sampling rate
$\boldsymbol{\phi_k}$	Gravitational and externally applied force terms
ϕ_{xxxy}	Third-order cross-correlation of the input x with the output y
ϕ_{xxy}	Second-order cross-correlation of the input x with the output y, page 34

ϕ_{xy}	First-order cross-correlation of the input x with the output y, page 34
τ	Vector of applied forces/torques
τ_k	Externally applied forces/torques
ζ	Probability distribution parameter
a_{im}	Polynomial coefficient corresponding to the order m of the static nonlinear element of the i-th cascade of a PCI model
a_L, a_D	Scaling constants used to compute pressures in the lift and dump cylinders of the trial LHD machine, page 42
a_{ci}	Longitudinal coordinate of the centre of mass of link i
b_{ci}	Lateral coordinate of the centre of mass of link i
c	Cycles per shaft turn of the incremental optical encoder, page 44
c_{ijk}	Christoffel symbols for a mechanical system
d	Translational distance travelled (m) by the LHD vehicle in the direction of its front wheels
d_{ij}	Inertial coefficients for a mechanical system
d_c	Denotes the characteristic size in the Rosin-Rammler equation
d_s	Denotes the size fraction diameter in the Rosin-Rammler equation
e	Equivalent to the mean-squared error, page 35
f	Force in Newtons (N)
$\boldsymbol{f}_a$	Vector of externally applied actuator forces/torques
f_d	Desired cylinder force setpoint
f_e	Force error, page 105
$\boldsymbol{f}_r$	Vector of resistive forces to excavation
$\hat{f}_r$	Measured dump cylinder force, while in contact with a rock pile
f_r	Actual bucket-rock interaction force magnitude
$f(s)$	Force, in the Laplace domain
g	Gravitational constant, page 71
$\boldsymbol{h}(\boldsymbol{q}, \dot{\boldsymbol{q}})$	Vector of centripetal, Coriolis, and gravitational terms, page 29

$h_i(j)$	Impulse response at a time lag given by j of the dynamic linear element of the i-th cascade of a PCI model
i	Typically denotes the link number of a mechanical system or the cascade number in a PCI model
k_n	Volterra series kernels, where $n = 1, 2, \ldots$
l_L, l_D	Lift and dump cylinder lengths (m), page 43
m_i	Mass of link i
$\{m, b, k\}$	Admittance model coefficients
n	Denotes the uniformity index in the Rosin-Rammler equation; otherwise, is used as a counter in PCI modelling
p	Pressure in Pascals (Pa)
$p_m(n)$	Polynomial of order m, equal to $u_i^m(n)$ for the i-th cascade of a PCI model
p_H, p_R	Pressures (Pa) at the head and rod of a given hydraulic cylinder
$\boldsymbol{q}$	Vector of generalized coordinates
r	Correlation statistic
$\boldsymbol{r}_{ci}$	Position vector for the centre of mass of link i
$u_i(n)$	Output of the dynamic linear element of the i-th cascade of a PCI model
$\tilde{u}_i(n)$	Dynamic linear system output $u_i(n)$, modified for use in multi-variable systems, page 37
v	Measured voltage in volts (V)
v_L, v_D	Measured lift and dump cylinder string potentiometer voltages (V)
$\boldsymbol{v}_{ci}$	Translational velocity vector for the centre of mass of link i
v_c	Commanded cylinder velocity, page 104
v_d	Desired reference velocity
v_f	Desired velocity change as computed by the force compensator $H(s)$
v_r	Actual dump cylinder extension/retraction velocity
$v(s)$	Velocity, in the Laplace domain
$\boldsymbol{x}$	Machine state vector
$x(n)$	Discrete-time nonlinear system input

$x(s)$	Position, in the Laplace domain
$x(t)$	Continuous-time nonlinear system input
x_f	Desired cylinder position change
$y(n)$	Discrete-time nonlinear system output
$y(t)$	Continuous-time nonlinear system output
$y_i(n)$	Residue remaining after adding the i-th cascade ($i \geq 1$) to a PCI model
$z_i(n)$	Output of the i-th cascade of a PCI model
API	Application program interface
CCD	Charge-coupled device
DEM	Discrete element method
DLL	Dynamically linked library
FEE	Fundamental equation of earthmoving
FSM	Finite-state machine
LHD	Load-haul-dump
MIMO	Multiple-input/multiple-output
MISO	Multiple-input/single-output
MSE	Mean-squared error
PAM	Pulse-amplitude modulation
PCI	Parallel cascade identification
PCMCIA	Personal Computer Memory Card International Association
PC	Personal computer
PFI	Programmable function input
PID	Proportional-integral-derivative
RAM	Random access memory
SISO	Single-input/single-output

Chapter 1

Introduction

There exist very few robot tasks that require as complicated an interaction with the environment as the excavation problem for fragmented rock. Automation of such work requires a system that is responsive to the machine-environment interaction forces experienced during excavation. In addition to providing an extensive review of literature on the subject, the research presented in this dissertation attempts to discover a technique for modelling of the excavation process based on unique full-scale experimental studies. A model which captures the fundamental nature of the events in question is desired, to the extent that new control ideas may be synthesized. Through pioneering full-scale experiments, observations regarding the status of certain operating parameters during excavation are subsequently transformed into a systems approach to excavation control. This introductory chapter provides some background and insight into the unsolved problem of autonomous rock excavation, in addition to a framework for the thesis material that follows.

1.1 Motivation

Due to increased competition and globalization in the mineral industry, mining companies have been attempting to develop and implement new and innovative technolo-

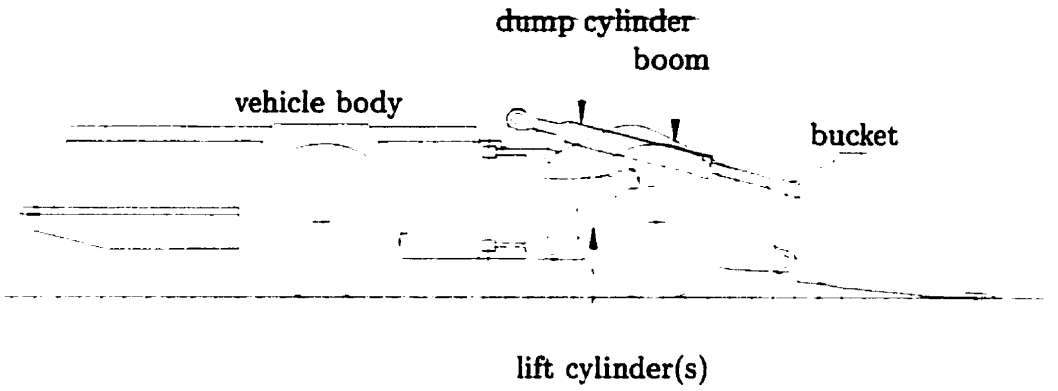

Figure 1.1: Schematic drawing of the load-haul-dump (LHD) machine

gies [6]. Among such efforts has been a move towards automated mobile equipment, including robotic excavation. Although the concept of autonomous excavation has gained some attention in the last decade, few investigations into the development of such technologies have been reported for large and non-homogenous excavation media, such as fragmented rock[1].

In particular, this thesis focuses on the problem of autonomous excavation using a load-haul-dump (LHD) underground mining machine. Such LHD machines are used extensively in underground mining applications to gather and transport ore from drawpoints to haulage vehicles or underground orepasses. These machines are easily recognizable by their characteristic geometry. They are a front-end-loader style, hydraulically actuated, and articulated vehicle. They are typically driven by a diesel engine or electric motors, while steering is accomplished through application of a torque at the vertical steering joint that forms the point of articulation. Figure 1.1 presents a schematic drawing that shows the LHD machine geometry used for the research communicated by this dissertation.

The load-haul-dump cycle is one that is repetitive and hence well suited for au-

[1]Herein, the term *excavation* refers typically to the excavation task carried out in fragmented rock, as opposed to in other excavation media (e.g. soil or gravel).

tomation. Several parties have attempted to automate the tramming (haul) portion of the load-haul-dump cycle, or have at least proposed solutions to the problem [17, 35, 57, 74, 99]. To date, most underground navigation systems rely on installed infrastructure for guidance, although laser and/or camera guided systems are not far from becoming feasible and economical. Obviously, the problem of autonomously dumping the bucket load is one that is relatively simple in comparison to autonomous navigation and bucket loading. Subsequently, the problem of autonomous navigation is thought to be less complex than that of autonomous loading, for reasons that will become evident in the following chapters.

The environments in which LHD machines are required to operate tend to be particularly hazardous in that the loading of ore occurs at underground drawpoints. These drawpoints often pose the dangers of falling or shifting broken rock during loading. In order to increase safety during such operations, remote control and teleoperation technologies have already been developed for LHD operators [48]. The obvious next step is development of a reliable system for autonomous loading of fragmented rock.

In addition to increased safety, automation of the loading task has the potential to provide enhanced productivity, through improved machine utilization and superior machine performance. Unlike a human operator, an automated machine could remain steadily productive, irrespective of environmental conditions or prolonged work hours. In addition, an automated loader might generate more accurate loading, making up for shortcomings in operator skill. Finally, operator abuse and machine wear would most likely be diminished through automation, possibly resulting in better machine reliability and reduced maintenance costs.

As will be seen in chapter 2, despite the fact that a significant amount of previous work, both theoretical and experimental, has been conducted to address the autonomous excavation problem, widespread adoption of automated loading has yet

to occur in the mining industry. Furthermore, literature on the subject indicates that there is a surprising lack of knowledge with regards to the fragmented rock excavation process, and more specifically, with regards to the interpretation of dynamic forces that impact the loader's bucket as it passes through the rock pile. It is perhaps for this reason that effective, systematic techniques for trajectory generation and control have yet to be invented for this task.

1.2 Problem Formulation

A system developed for autonomous excavation of fragmented rock is one that might have numerous potential applications, not only in the underground mining industry, but in other situations, such as for open-pit mining, construction, or even extra-terrestrial exploration. The commonality in these prospective applications lies in the nature of the excavation task. All such tasks utilize an excavation machine that employs some form of bucket as an excavation tool. The bucket is in turn engaged with the environment to remove or extract a particular resource, often under variable and unpredictable working conditions.

Although there exist a variety of potential applications and a number of possible machine types for implementation, as was stated in the previous section, this thesis focuses on the use of LHD underground mining machines for autonomous excavation of fragmented rock as it occurs in an underground mining situation.

What makes the autonomous excavation problem so challenging is the nature of bucket-rock interactions that occur during the excavation process. The performance of an excavator is strongly dictated by the conditions of interaction between the machine and the given pile of fragmented rock. For example, the resistance faced by an excavator bucket as it attempts to penetrate the rock pile may vary significantly depending upon, most notably, the properties of the excavation media (e.g. density

and hardness), the rock pile geometry, and the distribution of particle sizes and shapes. Indeed, it would be very difficult to predetermine the exact nature of future bucket-rock interactions prior to the excavation operation.

As will be discussed in chapter 2, others have formulated the autonomous excavation problem in its broadest meaning, incorporating the need for overall planning of the excavation goal. For example, a possible generalized excavation goal might be: "Remove a pile and clean the site in an area of $D \times E$ m^2 centering at (X_m, Y_m) in the coordinate system P" [91, page 3]. However, in this dissertation, consideration is not given to the problem in this general sense. Instead, focus is devoted to the question of how to compute the necessary actuator control inputs during the loading operation, based on sensor feedback and some understanding of the involved processes, so that the excavator bucket might be filled completely and reliably at each loading iteration. In fact, the problem formulation is narrowed further in that only the lift and dump cylinders are considered as controllable actuators. For the purposes of this dissertation, an assumption was made that any tractive effort supplied by the vehicle is generally constant throughout the loading operation, and that control of the tractive effort would not provide any significant contribution towards an autonomous excavation system (i.e. effective filling of the bucket relies primarily on the appropriate selection of lift and dump cylinder motions). This assumption is reviewed again in chapter 7. The scope of this dissertation, in the problem context given above, is outlined in the section that follows immediately.

1.3 Scope of Work

As will be seen in chapter 2, some previous researchers have considered the problem of capturing the essential aspects of the excavation process for the purposes of simulation and controller development to be extremely difficult, if not impossible. Furthermore,

it was discovered that there have been no reports in the open literature, to the candidate's knowledge, of full-scale data acquisition experiments involving the excavation of fragmented rock. These findings combined to help shape the scope of work for this thesis.

Given the problem formulation and focus described in the previous section, it was learned that there indeed exist significant challenges in the tasks of deriving the machine dynamics and, most notably, modelling the complex dynamics of the loading process (i.e. bucket-rock interaction). Consequently, the scope of this dissertation encompasses the following principal research objectives:

1. A comprehensive review of the state-of-the-art in excavation process modelling, and in research towards autonomous excavation of fragmented rock, with an emphasis on works relating specifically to LHD machine automation;

2. Implement and document the apparatus, methodology, procedure, and results of full-scale experimental excavation studies, conducted using an actual LHD machine operating in fragmented rock typical of a hard-rock mining scenario;

3. Investigate conventional techniques, such as those used in robot design and analysis, for the formulation of machine dynamics towards simulation and control;

4. Endeavour to construct a model that sufficiently captures the necessary aspects of the fragmented rock excavation process, utilizing a nonlinear system identification technique known as parallel cascade identification (PCI), such that the set of identified models might be used for simulation and as a tool for controller design, and;

5. Formulate a systematic strategy for controller development towards autonomous excavation of fragmented rock, based on observations drawn from the experimental and modelling studies.

Although the stated scope of work aims to concentrate on a select few tasks relating to the autonomous excavation problem, it is the candidate's hope that the formulation and findings of this thesis might act as a starting point for future research along similar lines.

1.4 Format of Thesis

In the next chapter, a review of the current literature on the issue of autonomous excavation is provided. Although attention is given to a variety of content, particular consideration is paid to those works that relate specifically the excavation of fragmented rock. In addition, a brief analysis is given of some recently patented technology in connection with autonomous excavation.

In chapter 3, brief appraisals of the pertinent literature in closed-chain mechanism dynamics and in techniques for nonlinear system modelling are supplied. Once again, focus is given to material that is most applicable to the problem at hand. The nonlinear system identification technique known as parallel cascade identification (PCI) is subsequently introduced, followed by some theory and details specific to the algorithm.

Chapter 4 gives a thorough presentation of pioneering experimental studies in rock excavation, performed as an integral part of the research contributing to this dissertation. Full-scale excavation experiments were carried out using a fully-equipped Tamrock EJC 9t model LHD machine in fragmented rock taken directly from an underground mining blast. Ample discussions surrounding the apparatus and methodology are put forward, in addition to a thorough exposition of the experimental results.

In an attempt to tackle a problem that has yet to be successfully solved in the literature, at least in the sense of completeness, chapter 5 attempts to model the dynamics of the loading process through application of the PCI algorithm. The pur-

pose of this chapter is to discover a means by which the excavation process might be simulated, with the intention that the outcome be used as a tool for controller design. An initial attempt to model only the loader mechanism dynamics is provided, without concern for interaction of the bucket with the rock pile. The machine dynamics modelling problem is approached from both analytical and empirical perspectives, applying techniques typical to the analysis of robot manipulators, and finally, using the PCI algorithm. In addition, the use of artificial neural networks or a distinct element method (DEM) as potential alternatives to the PCI approach are briefly discussed.

Based on the experimental and modelling results of chapters 4 and 5, chapter 6 attempts to formulate an approach for control of the loader mechanism towards autonomous excavation using ideas from the field of compliant motion control.

Finally, chapter 7 provides conclusion and summary remarks regarding the research conducted in support of this thesis. In addition, issues for future work are discussed in an effort to provide some incentive for continuation of work towards autonomous excavation of fragmented rock.

Chapter 2

Literature and Technology Review

As was mentioned in chapter 1, there has been a significant amount of previous research conducted in the field of autonomous excavation. Despite this fact, none has resulted in widespread development of autonomous excavation technologies for the mining industry, nor any other relevant industry.

This chapter presents a rather extensive look at the state-of-the-art in autonomous excavation, including a review of the most pertinent literature and a brief analysis of current patented technology. Although a spectrum of literature is presented, particular focus is given to those works relating most specifically to the excavation of fragmented rock, and above all to the automation of LHD mining machines.

2.1 Studies in Fragmented Rock Excavation

Perhaps the most significant number of contributions in the literature pertaining specifically to the problem of automated loading of rock in underground mining has been by Hemami of the *Canadian Centre for Automation and Robotics in Mining* at École Polytechnique in Montréal QC, Canada. Among the first of Hemami's papers was a pioneering exercise in deriving the kinematics and performing a force analysis for a generalized LHD loader mechanism. In this work, Hemami and Daneshmend

[33] presented an analytical study of the loader mechanism geometry and the required hydraulic cylinder forces through treatment of the mechanism as a robot manipulator.

In [27], Hemami acknowledged that the trajectory control of standard industrial robots (e.g. welding or cutting robots) is different than the control required for loading of an LHD bucket. It was suggested that the trajectory a loader bucket should follow through the rock pile not have priority in the control scheme, since the objective is to effectively fill the bucket, not to follow a strictly specified path. Some conceptual discussion was also provided on the topic of motion control. The forces acting on the bucket were described as potentially stochastic in nature, and the need for trajectory alteration in the event of detected prematurely high loads on the bucket was stated. Hemami divided the possible bucket-rock interaction forces into five components: f_1, the weight of the loaded material and that above the bucket; f_2, the force of compacting the material by the bucket; f_3, the sum of frictional forces acting between the bucket and the excavation media; f_4, the digging resistance of the excavation media, and; f_5, the necessary force to move the material in and above the bucket.

Means for analytically determining, or at least approximating, some of these dynamic forces were subsequently presented in [28, 30, 34]. Along with a relatively extensive list of suggested future work, Hemami put forth the following as reasons for the complexity of the excavation problem: (i) the shape, size, geometry and composition of the cutting device may vary from machine to machine; (ii) adding teeth to the cutting edge changes the scenario, and; (iii) material properties are determined by many factors, including hardness, cohesion, uniformity, water content, temperature, size, and compactness.

A method for determining an appropriate bucket trajectory was presented by Hemami in [29]. The proposed trajectory generation technique employed the idea that resistance to compaction described by the force f_2 may be set to zero, so as to minimize the expenditure of energy. However, a method for tailoring the derived

loading trajectory was not explained in any detail, and its potential effectiveness at completely filling the bucket was not determined.

In [31], Hemami essentially repeated the works described above. Nevertheless, there were some additions that are worth noting. A mathematical model for the variation of f_1 was produced using knowledge about the geometry developed during the loading operation. Hemami also concluded that an analysis of the force f_4 should be done experimentally.

Finally, in [32], Hemami provided a lengthy discussion of the fundamental analyses required for the design of an automated excavation machine. One interesting inclusion in this work was the consideration of a mass-spring-damper model for the excavation machine, as well as the excavation media (such as is common in compliant motion analysis). However, it was suggested that this type of model cannot be used in practice, since there is insufficient understanding of the mass, spring, and damper coefficients. In addition, the problem of choosing an entity to be exploited as error, to be measured and used for feedback in a control scheme, was considered. On this, Hemami stated:

> Having taken a look at how an excavating machine is manually operated reveals that the motion of such a machine is continuously corrected and readjusted by the operator. This adjustment is based on the performance of the machine in accomplishing its task... and not the motion itself. The same procedure must be automatically followed in an automated machine [32, page 178].

It was concluded that trajectory control cannot be entirely based on position or velocity errors, nor on a vision system that monitors the progress of the excavation process. A dual-level control was suggested, where a nominal trajectory is followed and modified through higher-level force measurements.

It should be noted that, of the works reviewed to this point in the thesis, none of the given results or ideas were reported as having been verified by experimental means; not in full-scale, nor in laboratory-scale excavation experiments.

Other authors have approached the problem of autonomous rock excavation from a perspective similar to Hemami's. Generalized machine dynamics were set up by Sarata et al. [86], although not actually computed. As will be seen in chapter 5, computation of these dynamics is in fact not an entirely trivial matter. Under a pioneering Russian project, Mikhirev formulated a set of ideas relating to force, motion, and trajectory control for various loader mechanism styles [61, 62]. Mikhirev's analysis was based on a technique using work functions to find an efficient bucket trajectory that would minimize the work for scooping rock masses, with complete filling of the bucket. Additional constraints were determined by the bucket capacity, the natural slope angle, and the pile height. The resistive force modelling portion of this research is discussed further in subsection 2.2.1. However, as a result of rock pile resistance analysis, Mikhirev advocated that measurement of the resistive forces could be used as a signal for automatic activation of the mechanism for bucket rotation in the vertical plane (which, in the case of an LHD machine, would correspond to motions of the dump cylinder). Since reactive forces were thought to decrease as the bucket moved along a continuous curvilinear path towards the pile surface, it was proposed that a force threshold be used to alter the bucket trajectory, resulting in a stepped path (i.e. zig-zag shape) along some nominal trajectory.

In other literature, machine vision has been put forward as a means for autonomous loading of mining machines. In the research of Ji and Sanford [37], a laboratory-scale excavation system was developed that utilized a video camera for environment sensing. Digitized images were then interpreted to develop control and navigation signals. More recent work, using machine vision, has been performed by Petty et al. [73]. Once again, a scale model was developed. However, in this case, the model was constructed to mimic the motions of an LHD vehicle as closely as possible. A loading strategy was formulated such that the bucket followed one of a range of trajectories developed for various rock pile conditions. In the case of oversize or other

problems, it was suggested that a simple algorithm be used to briefly alter the bucket path. The proposed algorithm included a means of detecting instability in the rock pile as well as choosing the location where scooping should take place at the next iteration.

Similar, though perhaps more rigorous, research techniques were employed by a group at Tohoku University in Japan [104]. A CCD camera vision system was used to obtain images of the rock pile, from which the excavation task was planned based on an estimated contour of the rock pile. Experiments were performed using a scale model excavator, similar in configuration to an LHD machine. The authors suggested that such a camera based system would be advantageous in its capability for recognizing changes in rock pile shape at each iteration towards the excavation goal. Although the results were promising, it was conceded that illumination became an important factor for success, a problem that would likely be compounded in an underground mining situation. This research is of the type described in section 1.2, which falls beyond the scope of this dissertation.

Researchers at the University of Arizona have proposed an autonomous rock excavation system for front-end-loader type machines that uses bucket force/torque feedback, fuzzy logic, and neural networks for control [51, 52, 90]. Lever et al. [51] justified their approach by stating that a mathematical model for the bucket-rock interaction would be too complex and computationally expensive. Instead, a set of basic bucket action sequences, typically used by human operators, was compiled for use by the controller. A method using finite-state machines (FSMs) was described. The FSMs were used to define all feasible action sequences required to accomplish the task, and were derived from "expert excavator operators and detailed analyses of the excavation process" [52, page 137]. Neural networks were used in the FSMs to determine what state to enter following an action or behaviour. A reactive control approach, using fuzzy behaviours, was utilized to compare and act on force/torque

data in order to asses the excavation situation and determine the appropriate control output. Some experimental results using a PUMA 560 robotic arm were also presented. This work is fully disclosed in a recent book by the authors [91].

2.2 Studies in Bucket-Rock Interaction

What makes the excavation of coarse, fragmented rock significantly different than that of ideal, homogeneous materials is that there is not one defined shear plane. In order to force an excavation tool through fragmented rock it is necessary to not only overcome the particle to particle frictional resistance, but also to make the particles move up and over one another [22]. In justifying their behaviour-based control approach to the problem at hand, Lever et al. [51] argued the difficulties of mathematically modelling the excavation tool-media interaction.

> It is impossible to generate a rigorous mathematical model to describe the unstructured environments common in mining operations. The conventional proportional-integral-derivative (PID) or even modern stochastic controllers that read exact sensor values, apply a mathematical model, and generate precise output from the mathematical algorithm are impractical for use here [51, page 18].

However, it is the candidate's view that, although the problem of rock pile interaction modelling may be very difficult to quantify, it should not be considered as a decidedly impossible task, as suggested in the above quotation. Moreover, such difficulties should not preclude the use of an approach to the excavation problem based on ideas from systems and control theory. As will be shown, some headway has been made in this avenue by other researchers in the field.

2.2.1 Empirical Studies

Some interesting empirical work was done by Forsman and Pan [22] regarding the shear properties of fragmented rock. Loose material, such as broken rock, will not

move (i.e. fail) until the applied force reaches a yield level, called the shear strength for granular media. The shear strength of fragmented rock is hence an important property in the context of material loading. Forsman and Pan suggested an improvement over Coulomb's equation, commonly used for modelling fine grained materials, in the form of a mathematical expression, derived empirically, for the shear strength of large grained loose material. It is interesting to note that the material porosity was implied to be related to the size distribution of a fragmented rock pile, as well as the degree of interlocking between particles. In addition, Forsman and Pan related the material porosity to fluctuations of the measured normal force in their experimental results.

Analysis of the resistance of fragmented rock to scooping by a bucket was reported in some Russian literature [21, 61]. With regards to the work by Fabrichnyi and Kolokolov [21], a means for calculation of the scooping resistance to blasted rock was given, based on knowledge of the rock pile's changing shear angle.

> It is known that in general the scooping force is governed by the volume of the rock to be shifted, which in turn depends on the angle between the horizontal and the shear surface of the rock. The experimentally recorded variations in the scooping resistance can only be due to changes in the inclination of the shear surface, leading to increases or decreases in the volumes of rock being shifted [21, page 438].

Unfortunately, key references were made by Fabrichnyi and Kolokolov to obscure experimental work (performed much earlier, circa 1957, and available only in the Russian language) by an investigator named Rodionov [79].

In related work, Mikhirev [61] reported some potentially applicable results. Although techniques for control and bucket trajectory generation were the focus of this research, insight into the forces associated with resistance to movement of the bucket through rock was provided. Mikhirev cited the experimental research of Rodionov, which apparently established that a compact nucleus is created in the pile in front of the working edge of the bucket. The characteristics of this compact nucleus were found to relate most notably to average particle size, bucket shape, and bucket pose.

2.2.2 Analytical Studies

Hemami et al. [34] acknowledged that the forces involved in excavating fragmented rock are functions of a large number of parameters, which makes the study of such forces particularly difficult. In this work, Hemami et al. categorized the various physical factors that contribute to the complexity of the problem. Major categories included the operation to be performed, the form of the excavation tool to be used, the material properties, and other machine or application factors. In further studies of the forces acting on a bucket during a scooping operation, Hemami et al. identified five force components. The cited article gave references to works where analysis of these forces had been attempted (see section 2.1). Some simulation results were also presented. However, it was admitted that random fluctuations of these forces would likely exist in reality.

Perhaps the most relevant and complete research in bucket-rock interaction modelling is some very recent work completed at Tohoku University, in Japan [102, 105]. In this work, Takahashi et al. essentially proposed a means for calculation of each of the resistive forces $\{f_1, \ldots, f_5\}$ described previously by Hemami (again, see section 2.1). For analysis purposes, the loading operation was partitioned into two stages: (i) a penetration phase, where the bucket is inserted into the rock pile, and; (ii) a scooping phase, where the bucket tip is lifted and curled to complete the loading task. Given an assumed bucket trajectory, the resistive forces were computed analytically using geometric and frictional parameters of the bucket and rock pile. Equivalent scale model experimental results confirmed the calculated forces to be approximately valid. Unfortunately, the derived equations failed to capture the inherently stochastic nature of the loading process.

Analytical research has been completed in the area of numerical modelling of granular assemblies. Consider the work by Cundall and Strack [14], where a distinct element method (DEM) was used to numerically model the mechanical behaviour of

assemblies of discs (and spheres in three dimensions). "The method is based on the use of an explicit numerical scheme in which the interaction of the particles is monitored contact by contact and the motion of the particles modelled particle by particle" [14, page 47]. In recent work by Takahashi [101], the ideas of Cundall and Strack were applied to simulation of particle behaviour in a *virtual* rock pile. Excavation of a rock pile having uniformly sized particles was simulated using a DEM approach and the bucket-rock interaction forces were computed for a predetermined trajectory. Once again, equivalent scale model experimental results confirmed the simulated interaction forces to be approximately valid. However, it was also admitted that full-scale experiments would be required to truly validate the given computational results. This technique is discussed further in chapter 5.

2.3 Studies in Soil Excavation

What distinguishes the problem of autonomous excavation of fragmented rock from the research presented in this section is simply the nature of the excavation media. In general, the work discussed in this section concerns itself with the problem of soil excavation. Soil, as opposed to fragmented rock, is generally homogeneous in particle size and typically consists of relatively small particles, such that a bucket may be passed through it without the need for significant trajectory alteration. Soil excavation could be appropriately characterized as a cutting exercise, rather than the task of maneuvering a bucket such that it is properly filled with large and small fragments alike, since forces at the tool would evolve smoothly instead of abruptly. Nonetheless, research in this field shares some common attributes with the problem of rock excavation. Moreover, the lack of commercial technology seems to contrast the fact that there appears to have been a considerable amount of research completed in the field of autonomous soil excavation. In this section, only a selection of the

relevant literature is presented.

The problem of autonomous excavation in soil was approached from a motion and path control perspective by Bernold [9]. Bernold advocated the use of impedance control, utilizing force and position feedback. In the case of robotic excavation, the robot was considered as an impedance, translating motion into force, and the soil as an admittance, reacting with a change in position or motion. A mass-spring-damper model for the tool-soil interaction was presented. An attempt was made to determine an optimal path for excavation. With regards to this effort, Bernold concluded:

> In summary, the selection of an optimal path, resulting in lowest energy consumption per excavated volume, is a nontrivial problem which hinges mostly on the proper characterization of the soil-tool interaction and the soil itself. Although static soil experiments can provide the cohesion factor, the complexity of the remaining coefficients for cutting-moment calculation make a static approach to the problem impossible [9, page 9].

To this end, a method of trajectory selection using pattern recognition was suggested. Experimental work was performed using a scale modelled backhoe style excavator (a modified RM-501 micro-robot). Force and position data were collected to create characteristic patterns for various soil conditions. Results were used only to show that it may be conceivable that soil characteristics could be established while excavating, leading to the possibility for trajectory planning and control for autonomous excavation. A similar approach, using impedance control for backhoe excavation control, was also proposed by Ha et al. [26]. In this recent work, a sliding-mode controller for impedance control was developed. Having developed kinematic and dynamic models for the excavator, the control scheme was subsequently implemented, with apparently promising results, on a retrofitted Komatsu PCI05-7 mini-excavator.

Vähä and Skibniewski [106] presented a method of cognitive force control for an excavator. A dynamic model was developed for the excavator and used in conjunction with a model for the soil (referred to as the *regolith*), which was based on the breakdown of resistive forces into a resistance from cutting, frictional resistance, and the

resistance of the material in the bucket. Further details of the backhoe style excavator dynamic model were derived later in a publication by Koivo et al. [41]. Simulation results compared the preplanned bucket trajectory with its actual trajectory, which was adjusted when hydraulic ram forces exceeded preset limits. In a technique proposed by Bullock and Oppenheim [10], strain gauges were used during a laboratory study to measure the resistive forces encountered by the excavator bucket. A supervisory control scheme, where force feedback data are processed at a higher level to produce low level trajectory changes, was considered as an online tactical planner for excavation.

There exists an apparently ongoing project at the University of Sydney, Australia that aspires to develop a system for autonomous excavation [50]. Although it was stated that the ultimate objective of the project is to demonstrate fully autonomous excavation for a variety of tasks, including excavation not only in soil but also in fragmented rock, the described experimental hardware consisted of a backhoe style mini-excavator. It was implied that future experiments and analyses were to be carried out in soil type media.

Researchers at Carnegie Mellon University [95] proposed a technique for robotic excavators to predict resistive forces during excavation using computer learning methods. Included in the presented work is a development of the mechanics of excavation, resulting in the formation of what is known as the fundamental equation of earthmoving (FEE) for a flat blade moving through soil. The assumptions required to validate the FEE were used by the authors to demonstrate its impracticality in the context of excavation.

More recent work at Carnegie Mellon University [7, 81, 100] has resulted in a patented system for robotic excavation and autonomous truck loading. In summary, the system described utilized two scanning laser range-finders to recognize and localize the truck, measure the soil face, and detect obstacles. Onboard software was used

to make decisions regarding digging and dumping operations. Actual digging was described as executed by a force based closed loop control scheme, after previous research in excavation planning by one of the authors. Dumping and truck detection routines were also included as part of the project.

2.4 Patented Technologies

In this section, a selection of patented technology is presented in order to provide an understanding of the work that has been considered commercially feasible. The majority of existing patents relate to the automation of soil excavation tasks, generally using backhoe style excavators [7, 76, 81, 92, 93, 94]. However, there does exist recent work relevant to autonomous excavation of fragmented rock, using LHD-style machinery, as in an underground mining application. It is these patents that are discussed in the subsections that follow.

2.4.1 Fragmented Rock Excavation Technology

A review of the current patents relevant to the problem of autonomous bucket loading revealed two significant contributions. The most recent, by Dasys et al. [15], as part of a group representing the international mining and metals company Noranda, Inc., revealed a patented system for automated bucket loading of a front shovel loader (i.e. an LHD) that uses "sensor feedback provided by pressure and extension sensors on hydraulic cylinder(s) to control the trajectory of the bucket to be loaded by a computer algorithm" [15]. The described invention does not rely on a model of the rock pile, nor is there any computational attempt to determine an optimal bucket trajectory prior to the scooping operation. Instead, the system reacts, using a decision tree to select actuator commands, only to excessive forces sensed in the actuating cylinders. If excessive forces are encountered, the bucket is tilted so as to attempt to

dislodge the rock or other hinderance causing the disproportionate force.

> The computer... has a [hybrid] controller which controls the hydraulic valve that supplies hydraulic fluid into both ends of the [bucket dump] cylinder... and if too much force is exerted on the bucket by the rock pile, the command for hydraulic fluid intake will be reversed and the fluid will be injected into the opposite side of the piston... so as to reverse the action of the shaft... until the force drops to a predetermined level. Then, the oil intake will be reversed again and the tilting action of the bucket will be resumed until the bucket... is filled and is in the rolled back position... [15].

Furthermore, Dasys et al. claimed a 9% improvement in loading capacity, comparing their invention with human operation in field trials. A paper related to the work by Dasys et al. was put forward at the 5th International Symposium on Mine Mechanization and Automation by representatives from STAS Ltd. [49], partners in the Noranda, Inc. project. Unfortunately, no technical details were given in the paper. However, the user-level features of the product, entitled SIAMload, were presented. It is worth noting that SIAMload required that an operator choose one of three loading modes, depending on the human perceived loading conditions.

2.4.2 Other Excavation Technology

A second relevant patent in autonomous excavation was filed by Rocke, a representative of Caterpillar, Inc. [77]. In Rocke's invention, a control system for automatic loading of a wheel loader (similar in mechanical design to an LHD machine), which is particularly suited to soil excavation, is disclosed. Although references were made to a number of previous patents by the inventor (all of which applied to backhoe style soil excavation), in the current patent, an algorithm that appears very similar to the one that was patented three years later by Dasys et al. (discussed in subsection 2.4.1 above) is given.

> As described,the logic means varies the dump cylinder command signal between a predetermined minimum and maximum value to maintain the

> lift and dump cylinder forces at an effective force range. Accordingly the positions and forces of the lift and dump cylinders are monitored to control the command signals at the desired magnitudes. For example, if the lift or dump cylinder forces fall below the lower predetermined values, the extension of the dump cylinder is halted to prevent the bucket from "breaking-out" of the pile too quickly. Alternatively, if the lift or dump cylinder force exceeds the upper predetermined value, the extension of the dump cylinder is accelerated to prevent the bucket from penetrating too deep in the pile [77].

Furthermore, it should be noted that control of the vehicle tractive effort was not included in the control strategy as stated, and that the machine was preferably directed to the pile of material at full engine throttle. On the matter of adaptability of the system to varying material conditions, the reader was referred to [78], another patent by the inventor, in which a system for selecting one of a plurality of control curves based on a material condition setting, is disclosed.

In essence, the common theme in these two patents [15, 77] is a cylinder motion control scheme based on some interpretation of the changing pressures in the hydraulic cylinders as an indication of the state of the bucket-rock interaction.

Chapter 3

Theory and Background

In this chapter, background reviews of the relevant theory in the formulation of equations of motion for closed-chain kinematic mechanisms and techniques for nonlinear system modelling and identification are provided. The purpose here is to provide a concise theoretical background for the thesis material that follows.

3.1 Closed-chain System Mechanics

In chapter 5, analytical equations of motion for the Tamrock EJC 9t LHD loader mechanism are formulated through treatment of the mechanism as a robot manipulator with closed kinematic chains. Herein, the term *closed-chain system* refers to the class of mechanical systems whose links are not only connected in series, but in parallel, forming one or more closed-link loops. As opposed to an open-chain system (e.g. a serial robot), typically not all joints of a closed-chain mechanism are actuated. Such closed-chain mechanisms have the potential to offer some mechanical advantages over open-chain mechanisms, perhaps most notably, a greater rigidity to weight ratio.

The dynamics of open-chain mechanical systems have been extensively studied in the literature, and there exist well established techniques for the formulation of equations of motion for such mechanisms [53, 98, 107]. In essence, in the absence of

friction and interaction with the environment, equations of motion for an open-chain system may be computed using a standard Newton-Euler or Lagrangian approach.

Although there exists a multitude of literature on the subject, due to the complexity of the kinematic and dynamic analyses, development of a clear-cut technique for the derivation of equations of motion for closed-chain mechanisms remains a topic of research. Ghorbel et al. [25] attempted to categorize the literature on the derivation of dynamic equations of motion for closed-chain mechanisms into three classes: (i) those techniques derived for a particular type of closed-chain structure; (ii) those techniques derived for general closed-chain structures, but most suited for simulation and not model-based controller design, and; (iii) those techniques for which the resulting equations of motion have the same form as those for open-chain structures. Among the reviewed literature [25, 55, 56, 65, 66], the formulation of Murray and Lovell [65], which falls into category (iii) of Ghorbel et al., was selected by the candidate as a framework for use in this dissertation.

The approach proposed by Murray and Lovell [65] involves a relatively straightforward procedure for implementation. The method is founded upon d'Alembert's Principle[1] and is based around a transformation from the dynamics of open-chain mechanisms to closed-chain dynamics through the inclusion of holonomic loop constraints.

3.1.1 Euler-Lagrange Equations

Computation of the dynamics for closed-chain mechanisms, as described above, is based on a transformation from open-chain systems using holonomic constraints. Later in this dissertation, the Euler-Lagrange equations are used in the derivation of equations of motion for an open-chain system (as will be seen in the next sub-

[1] In brief, d'Alembert's Principle, considered perhaps the most all-inclusive principle in the entire field of classical mechanics, states that a system of particles moves in such a way that the total virtual work $\sum_{i=1}^{p}(f - m_i\ddot{x}_i) \cdot \delta x_i = 0$ [97].

section). This section serves to provide an applied introduction to the subject of Lagrangian mechanics as it is relevant to the problem at hand. However, the topic is extensive, and the reader is referred to [53, 98, 107] for further details and formal derivations.

Definition 3.1.1 *A configuration space Q represents the set of possible configurations of a mechanical system.*

Definition 3.1.2 *The set of generalized coordinates $\{q_1, \ldots, q_n\}$ are independent, and sufficient to describe the pose of all particles in a mechanical system with n degrees of freedom.*

Let Q be a configuration space for a mechanical system, so that the vector of generalized coordinates $\boldsymbol{q} \in Q$. The Euler-Lagrange equations are then given by

$$\frac{d}{dt}\left(\frac{\partial L}{\partial \dot{q}_i}\right) - \frac{\partial L}{\partial q_i} = \tau_i \tag{3.1}$$

where $\{q_1, \ldots, q_n\}$ are the coordinates of the system, $\{\tau_1, \ldots, \tau_n\}$ are the applied forces[2] corresponding to independent variations of q_i, and $L = K - V$ is the Lagrangian function describing the given mechanical system, defined as the difference between the total kinetic energy K of the system and the total potential energy V of the system. If the Euler-Lagrange equations of (3.1) are specialized to a case when the kinetic energy is a quadratic function of the vector $\dot{\boldsymbol{q}}$ that has the form

$$K = \frac{1}{2}\sum_{i,j=1}^{n} d_{ij}(\boldsymbol{q})\dot{q}_i\dot{q}_j \tag{3.2}$$

and the potential energy $V = V(\boldsymbol{q})$ is independent of $\dot{\boldsymbol{q}}$, then the Euler-Lagrange equations may be written as

$$\sum_{j=1}^{n}\left(d_{kj}(\boldsymbol{q})\ddot{q}_j + \sum_{i=1}^{n} c_{ijk}(\boldsymbol{q})\dot{q}_i\dot{q}_j\right) + \phi_k(\boldsymbol{q}) = \tau_k \tag{3.3}$$

[2]Herein, the term *force* is used to mean force and/or torque.

for $k = 1, \ldots, n$, and where the terms c_{ijk} are known as *Christoffel symbols* [53, 98]. Equation (3.3) may be written in matrix form, such that

$$\boldsymbol{D}(\boldsymbol{q})\ddot{\boldsymbol{q}} + \boldsymbol{C}(\boldsymbol{q}, \dot{\boldsymbol{q}})\dot{\boldsymbol{q}} + \boldsymbol{g}(\boldsymbol{q}) = \boldsymbol{\tau} \tag{3.4}$$

where the k, j-th element of the matrix $\boldsymbol{C}(\boldsymbol{q}, \dot{\boldsymbol{q}})$ is defined as

$$\begin{aligned} c_{kj} &= \sum_{i=1}^{n} c_{ijk}(\boldsymbol{q})\dot{q}_i \\ &= \sum_{i=1}^{n} \frac{1}{2}\left(\frac{\partial d_{kj}}{\partial q_i} + \frac{\partial d_{ki}}{\partial q_j} - \frac{\partial d_{ij}}{\partial q_k}\right)\dot{q}_i \end{aligned} \tag{3.5}$$

and the vector of gravitational potential terms $\boldsymbol{g}(\boldsymbol{q})$ has the elements

$$\phi_k = \frac{\partial V(\boldsymbol{q})}{\partial q_k}\,. \tag{3.6}$$

3.1.2 Reduced System and Holonomic Constraints

The notion of a *reduced system* is required as the first step in developing the closed-chain mechanism dynamics.

Definition 3.1.3 *A reduced system Σ is an open-chain system obtained by hypothetically removing physical constraints from a closed-chain system $\tilde{\Sigma}$ until no closed kinematic chains exist.*

Therefore, formation of the reduced system involves the construction of an open-chain mechanism, obtained by treating the closed-chain mechanism as if it were cut upon at selected joints such that no closed-loops remain. It is often convenient to strategically choose the constraints to be broken so that the resulting reduced system resembles a serial robot, for which there exist well known techniques for analysis.

Now, if $\tilde{Q} = \Re^m$ is a configuration space for a closed-chain system $\tilde{\Sigma}$ with the actuated joints[3] as generalized coordinates $\tilde{\boldsymbol{q}} \in \tilde{Q}$, then let $Q = \Re^n$ be a configuration

[3]For this research, to match the experimental trials of chapter 4, the actuated and measured joints are collocated, i.e. the coordinates of the closed-chain system are the measured joint variables.

space for the corresponding reduced system Σ, having the generalized coordinates $q \in Q$. To derive the closed-chain mechanism dynamics from the reduced system dynamics, the holonomic[4] loop closure constraints are required, so that

$$q = f(\tilde{q}) . \tag{3.7}$$

The velocity loop closure constraint matrix G, with respect to the actuated joints, is also needed, such that

$$\dot{q} = G\dot{\tilde{q}} \tag{3.8}$$

where the Jacobian matrix $G \in \Re^{m \times n}$. Finally, the acceleration loop closure constraint, stemming from the time derivative of equation (3.8), is required and may be found by the chain rule, giving

$$\ddot{q} = G\ddot{\tilde{q}} + \dot{G}\dot{\tilde{q}} . \tag{3.9}$$

3.1.3 Force Transformation

Consider the set of generalized actuating forces $\{\tau_1, \ldots, \tau_m\}$ for the open-chain system Σ and similarly, $\{\tilde{\tau}_1, \ldots, \tilde{\tau}_n\}$ for the closed-chain system $\tilde{\Sigma}$.

Proposition 3.1.1 *Let G be the Jacobian matrix defining the relation $\delta q = G\delta\tilde{q}$. The vector of generalized forces $\tilde{\tau}$ for $\tilde{\Sigma}$ may be computed from the vector of generalized forces τ for Σ by the transformation*

$$\tilde{\tau} = G^T \tau . \tag{3.10}$$

The proof of proposition 3.1.1 lies in the application of d'Alembert's Principle. A full proof is given by Nakamura and Ghodoussi in [66]. However, since Σ and $\tilde{\Sigma}$ represent the same mechanical system only under different constraints, consider that the virtual

[4] A constraint on the coordinates $\{q_1, \ldots, q_n\}$ is called holonomic if the constraint condition can be expressed as an equation $\phi(q_1, \ldots, q_n, t) = 0$, otherwise it is called non-holonomic [97].

work done by the generalized forces of Σ must equal the virtual work done by the generalized forces of $\tilde{\Sigma}$ if the two systems experience the same applied forces. Hence,

$$\delta\tilde{\boldsymbol{q}}^T\tilde{\boldsymbol{\tau}} = \delta\boldsymbol{q}^T\boldsymbol{\tau} \tag{3.11}$$

where $\delta\tilde{\boldsymbol{q}}$ and $\delta\boldsymbol{q}$ represent the same virtual displacement of the mechanical system. Substituting equation (3.8) into equation (3.11) yields

$$\delta\tilde{\boldsymbol{q}}^T\tilde{\boldsymbol{\tau}} = \delta\tilde{\boldsymbol{q}}^T\boldsymbol{G}^T\boldsymbol{\tau}\,. \tag{3.12}$$

Equation (3.10) follows directly from equation (3.12).

3.1.4 Closed-chain Equations

Given the reduced system dynamics and the holonomic loop closure constraints, the closed-chain mechanism dynamics may be computed. Through application of the generalized actuating force transformation of equation (3.10), which relates the closed-chain mechanism dynamics to the reduced system dynamic model

$$\boldsymbol{G}^T\left[\boldsymbol{D}(\boldsymbol{q})\ddot{\boldsymbol{q}} + \boldsymbol{C}(\boldsymbol{q},\dot{\boldsymbol{q}})\dot{\boldsymbol{q}} + \boldsymbol{g}(\boldsymbol{q})\right] = \tilde{\boldsymbol{\tau}}\,. \tag{3.13}$$

To account for the restriction that the reduced system variables $\{\boldsymbol{q},\dot{\boldsymbol{q}},\ddot{\boldsymbol{q}}\}$ must be realizable by the closed-chain mechanism, the holonomic loop closure constraints are incorporated into equation (3.13) to give

$$\boldsymbol{G}^T\left[\boldsymbol{D}(\boldsymbol{f}(\tilde{\boldsymbol{q}}))\left(\boldsymbol{G}\ddot{\tilde{\boldsymbol{q}}} + \dot{\boldsymbol{G}}\dot{\tilde{\boldsymbol{q}}}\right) + \boldsymbol{C}(\boldsymbol{f}(\tilde{\boldsymbol{q}}),\boldsymbol{G}\dot{\tilde{\boldsymbol{q}}})\boldsymbol{G}\dot{\tilde{\boldsymbol{q}}} + \boldsymbol{g}(\boldsymbol{f}(\tilde{\boldsymbol{q}}))\right] = \tilde{\boldsymbol{\tau}}\,. \tag{3.14}$$

Equation (3.14) may be rewritten as

$$\tilde{\boldsymbol{D}}(\tilde{\boldsymbol{q}})\ddot{\tilde{\boldsymbol{q}}} + \tilde{\boldsymbol{C}}(\tilde{\boldsymbol{q}},\dot{\tilde{\boldsymbol{q}}})\dot{\tilde{\boldsymbol{q}}} + \tilde{\boldsymbol{g}}(\tilde{\boldsymbol{q}}) = \tilde{\boldsymbol{\tau}} \tag{3.15}$$

where the inertial coefficient matrix and vectors representing centripetal, Coriolis, gravitational, and externally applied forces are defined respectively by

$$\tilde{\boldsymbol{D}}(\tilde{\boldsymbol{q}}) = \boldsymbol{G}^T\boldsymbol{D}(\boldsymbol{f}(\tilde{\boldsymbol{q}}))\boldsymbol{G} \tag{3.16}$$

$$\tilde{\boldsymbol{C}}(\tilde{\boldsymbol{q}},\dot{\tilde{\boldsymbol{q}}}) = \boldsymbol{G}^T\boldsymbol{D}(\boldsymbol{f}(\tilde{\boldsymbol{q}}))\dot{\boldsymbol{G}} + \boldsymbol{G}^T\boldsymbol{C}(\boldsymbol{f}(\tilde{\boldsymbol{q}}),\boldsymbol{G}\dot{\tilde{\boldsymbol{q}}})\boldsymbol{G} \tag{3.17}$$

$$\tilde{\boldsymbol{g}}(\tilde{\boldsymbol{q}}) = \boldsymbol{G}^T\boldsymbol{g}(\boldsymbol{f}(\tilde{\boldsymbol{q}}))\,. \tag{3.18}$$

It is sometimes useful to combine the centripetal, Coriolis, and gravitational terms into one vector, hence

$$\tilde{\boldsymbol{h}}(\tilde{\boldsymbol{q}}, \dot{\tilde{\boldsymbol{q}}}) = \tilde{\boldsymbol{C}}(\tilde{\boldsymbol{q}}, \dot{\tilde{\boldsymbol{q}}})\dot{\tilde{\boldsymbol{q}}} + \tilde{\boldsymbol{g}}(\tilde{\boldsymbol{q}}) \,. \tag{3.19}$$

3.1.5 Time Domain Solutions

In order to simulate the closed-chain mechanism forward dynamics, the independent generalized joint accelerations $\ddot{\tilde{\boldsymbol{q}}}$ are obtained by solving the algebraic equations of the closed-chain dynamic model

$$\ddot{\tilde{\boldsymbol{q}}} = \tilde{\boldsymbol{D}}^{-1}(\tilde{\boldsymbol{q}}) \left[\tilde{\boldsymbol{\tau}} - \tilde{\boldsymbol{h}}(\tilde{\boldsymbol{q}}, \dot{\tilde{\boldsymbol{q}}})\right] \,. \tag{3.20}$$

The inertial coefficient matrix $\tilde{\boldsymbol{D}}(\tilde{\boldsymbol{q}})$ is both symmetric and positive-definite for this collocated system, and is therefore invertible. In order to solve the above equations of motion, the equations may be placed in first-order form, where

$$\boldsymbol{x} \triangleq \begin{bmatrix} \tilde{\boldsymbol{q}} \\ \dot{\tilde{\boldsymbol{q}}} \end{bmatrix}_{2n \times 1} \tag{3.21}$$

such that

$$\dot{\boldsymbol{x}} = \begin{bmatrix} \dot{\tilde{\boldsymbol{q}}} \\ \tilde{\boldsymbol{D}}^{-1}(\tilde{\boldsymbol{q}}) \left[\tilde{\boldsymbol{\tau}} - \tilde{\boldsymbol{h}}(\tilde{\boldsymbol{q}}, \dot{\tilde{\boldsymbol{q}}})\right] \end{bmatrix} . \tag{3.22}$$

Numerical integration routines, which employ fixed or possibly variable time steps for greater accuracy, may now be used to simulate the mechanism's model behaviour.

3.2 Identification of Nonlinear Systems

The fundamental problem of system identification lies in choosing the type of model that should be used to capture the desired aspects of a given system or process. There are a number of so-called classical techniques available for linear system identification, in which are included the observation of frequency response, step-input response,

and correlation methods [96]. Where controller design is concerned, identification of a linear model is often desirable over one that is nonlinear in that there exist well known and proven procedures for controller design. However, in the use of a linear model, one must understand the degree of validity of the linearization assumption. For the nonlinear case, most system identification approaches involve error minimization (e.g. least-squares, maximum likelihood, minimum variance, and artificial neural networks) to fit acquired data in an attempt at a general model [60, 80, 96].

In this section, the nonlinear system identification technique known as parallel cascade identification (PCI) is introduced. As a prelude to this introduction, a descriptive review of some nonlinear system theory is provided as it is relevant to understanding the origins of the PCI algorithm.

3.2.1 Volterra and Wiener Theories

In the context of applied mathematics and engineering, the Volterra and Wiener theories for nonlinear systems are explicit models ideally suited to representation of so-called *black box* type nonlinear systems, where the relationship between the input and the output of a system is not easily derivable through the development of a set of equations or other analytical techniques. It can be shown that the Volterra functional series[5] may be used to represent a time invariant nonlinear system. The continuous-time, infinite-order Volterra series has the functional form

$$\begin{aligned} y(t) &= \int_{-\infty}^{\infty} k_1(\tau_1)x(t-\tau_1)d\tau_1 \\ &\quad + \int_{-\infty}^{\infty}\int_{-\infty}^{\infty} k_2(\tau_1,\tau_2)x(t-\tau_1)x(t-\tau_2)d\tau_1 d\tau_2 \\ &\quad + \cdots + \int_{-\infty}^{\infty}\cdots\int_{-\infty}^{\infty} k_n(\tau_1,\tau_2,\ldots,\tau_n)x(t-\tau_1)x(t-\tau_2)\cdots \\ &\quad x(t-\tau_n)d\tau_1 d\tau_2\cdots d\tau_n + \cdots \end{aligned} \tag{3.23}$$

[5]The Volterra functional series was named after the mathematician Vito Volterra, who first studied this functional form during the seventeenth century. However, the first application of the Volterra series to the study of nonlinear systems was by Norbert Wiener in the early 1940s [82, 88].

where $n = 1, 2, \ldots$, $x(t)$ is the nonlinear system input, $y(t)$ is the corresponding output, and $k_n(\tau_1, \ldots, \tau_n) = 0$ for any $\tau_j < 0$, with $j = 1, 2, \ldots, n$. The functions $k_n(\tau_1, \ldots, \tau_n)$ are known as the Volterra kernels of the system. However, there are certain inherent difficulties with the application of the Volterra series to physical problems, some of which include difficulty in the measurement of Volterra kernels, as well as issues concerning convergence of the Volterra series [88]. It was Wiener who circumvented these problems by forming a set of orthogonal functions from the Volterra functionals, which he called G-functionals due to their special orthogonal property when the input is from a Gaussian process. For example, if the set of real functions $w_n(t)$ for $n = 1, 2, \ldots$ is an orthogonal set of functions over the interval $a < t < b$, then the orthogonality condition is given by the equation

$$\int_a^b w_m(t) w_n(t) dt = \begin{cases} \lambda_n & \text{for } m = n \\ 0 & \text{for } m \neq n \end{cases} \tag{3.24}$$

where each λ_n is positive since it is equal to the area under the curve $w_n^2(t)$. In effect, the Volterra and Wiener theories together have provided a basis for significant advances in nonlinear system theory.

Korenberg [47, 44] utilized the Volterra and Wiener theories, along with the results of other related works, to show that any discrete-time, finite-memory, causal, nonlinear system having a finite-order Volterra series representation can be represented by a finite number of parallel cascades consisting of alternating dynamic linear and static nonlinear elements. The stated *causal* requirement necessitates that the system be non-anticipatory, or in other words, that the output at time t_i not depend on values of the input at times t_j, where $j > i$. The discrete-time, finite-order Volterra series that is assumed capable of approximating the nonlinear system has the form

$$y(n) = k_0 + \sum_{m=1}^{M} \left(\sum_{r_1=0}^{R} \cdots \sum_{r_m=0}^{R} k_m(r_1, \ldots, r_m) x(n - r_1) \cdots x(n - r_m) \right) \tag{3.25}$$

for $n = 1, 2, \ldots$, where $x(n)$ and $y(n)$ are the system input and output respectively, M is the order of the series, and $(R + 1)$ is the memory length.

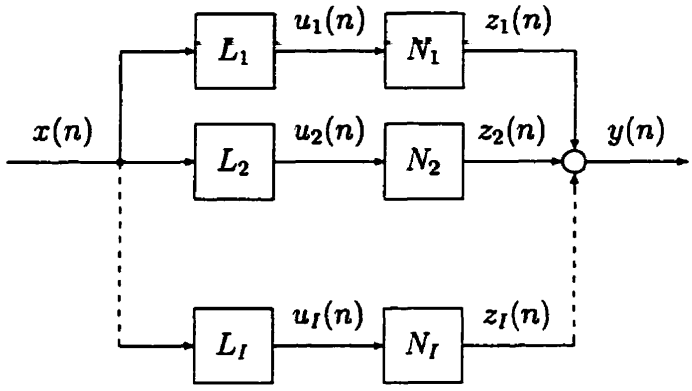

Figure 3.1: Parallel LN cascade schematic model

3.2.2 Parallel Cascade Identification

This subsection summarizes the method of parallel cascade identification (PCI), as it was used in the research described by this dissertation, and as interpreted from the work of Korenberg [44]. Details regarding implementation of the algorithm are provided later, upon use in chapter 5.

Description of the Algorithm

PCI utilizes parallel cascades of alternating dynamic[6] linear L and static nonlinear N elements to represent and identify a nonlinear system. Korenberg [44] showed that the sum of a finite number of parallel LN cascades suffices to represent exactly any discrete-time, finite-memory, finite-order Volterra series, sometimes referred to as a Wiener model. A schematic representation of the proposed parallel cascade model structure is shown in figure 3.1.

For the single-input/single-output (SISO) case, suppose that the nonlinear system to be identified has input $x(n)$ and output $y(n)$, for $n = 0, 1, \ldots, T$. Assume that the system output depends on input delays in the integer set $\{0, 1, \ldots, R\}$, such that $(R+1)$ is the memory length, and that the set of inputs to the system are uniformly

[6] In the current context, the term *dynamic* is used to imply that the system possesses memory.

bounded in that there exists a number $0 < \mathcal{N} < \infty$ such that $|x(n)| < \mathcal{N}$ for all $n \subset [0, T]$. PCI attempts to identify one LN cascade at a time, and computes the succeeding cascade based on the residual of the previous cascades combined. Let $y_i(n)$ be the residue remaining after adding the i-th cascade ($i \geq 1$) to the PCI model, with $y_0(n) = y(n)$. If $z_i(n)$ is computed as the output of the i-th cascade, as shown in figure 3.1, then

$$y_i(n) = y_{i-1}(n) - z_i(n) \tag{3.26}$$

where $i = 1, 2, \ldots, I$ are the number of cascades in the final PCI model, yet to be determined.

Let the output of the dynamic linear element in the i-th cascade be given by

$$L_i: \quad u_i(n) = \sum_{j=0}^{R} h_i(j) x(n-j) \tag{3.27}$$

Now, the delta response $h_i(j)$ of the linear system is chosen using a first- or higher-order cross-correlation of the input with the residue, computed only over the interval $n = R, (R+1), \ldots, T$. For example, by definition

$$\phi_{xy_{i-1}}(j) \triangleq \overline{y_{i-1}(n) x(n-j)} \tag{3.28}$$

$$\phi_{xxy_{i-1}}(j_1, j_2) \triangleq \overline{y_{i-1}(n) x(n-j_1) x(n-j_2)} \tag{3.29}$$

where $\phi_{xy_{i-1}}$ and $\phi_{xxy_{i-1}}$ are first- and second-order cross-correlations of the input with the residue, respectively, and where the over-line denotes the time-average[7] on the interval $n = R, (R+1), \ldots, T$. Assign $h_i(j)$ at random to one of

$$q_1(j) = \phi_{xy_{i-1}}(j) \tag{3.30}$$

$$q_2(j) = \phi_{xxy_{i-1}}(j, A) \pm C\delta(j - A) \tag{3.31}$$

where the integer A is randomly selected from the set $\{0, 1, \ldots, R\}$, the sign of the δ impulse term (added only at diagonal values) is chosen at random, and $C = \{c \mid c \in$

[7] For example, $\overline{x(n)} = \frac{1}{T-R+1} \sum_{n=R}^{T} x(n)$.

$\Re_+, c \neq 0\}$ is adjusted to tend to zero as the mean-square of the residue approaches zero. Korenberg [44] suggested the use of

$$C = \frac{\overline{y_{i-1}^2(n)}}{\overline{y^2(n)}}. \tag{3.32}$$

Once the linear system has been identified and computed using equation (3.27), the static nonlinearity is obtained by least-square fitting a polynomial having input $u_i(n)$ to the residue $y_{i-1}(n)$ over the interval $n = R, (R+1), \ldots, T$, such that

$$N_i: \quad z_i(n) = \sum_{m=0}^{M} a_{im} u_i^m(n) \tag{3.33}$$

where M is the polynomial degree, and the new residue $y_i(n)$ is computed by equation (3.26). Since the resulting polynomial coefficients a_{im} will minimize the mean-square of the new residue over $n = R, (R+1), \ldots, T$, it may be shown that

$$\overline{y_i^2(n)} = \overline{(y_{i-1}(n) - z_i(n))^2} = \overline{y_{i-1}^2(n)} - \overline{z_i^2(n)}. \tag{3.34}$$

Note that the reduction in mean-square error (MSE) by adding the i-th cascade equals the mean-square of the i-th cascade output.

In order to avoid choosing unnecessary cascades that merely fit noise, a standard correlation test may be performed. It can be shown that the correlation statistic of $z_{i+1}(n)$ and $y_i(n)$ over the interval $n = R, (R+1), \ldots, T$ is given by

$$r = \sqrt{\frac{\overline{z_{i+1}^2(n)}}{\overline{y_i^2(n)}}}. \tag{3.35}$$

If the residue were white Gaussian noise (i.e. independent and zero-mean), then for large enough T

$$|r| < \frac{\zeta}{\sqrt{T - R + 1}}. \tag{3.36}$$

For example, if $\zeta = 1.96$, then equation (3.36) holds with a probability of approximately 0.95. Therefore, prior to accepting any given candidate for the $(i+1)$-th cascade, it may be required that the inequality

$$\overline{z_{i+1}^2(n)} > \frac{\zeta^2}{T - R + 1} \overline{y_i^2(n)} \tag{3.37}$$

be satisfied. If equation (3.37) is not satisfied, then a new candidate for the $(i+1)$-th cascade must be constructed, starting with the cascade's linear system through polynomial fitting to the residual of the output. In fact, the desired confidence level may be altered by appropriately changing the value of ζ.

Subsequent parallel cascades should be added to the model until either: (i) a predetermined maximum number of cascades has been reached; (ii) the MSE has been made sufficiently small, or; (iii) there remain no candidate cascades, within a specified number of attempts, that can cause a reduction in MSE exceeding some decidedly small threshold value.

Least-square Fitting of Polynomial Coefficients

Least square fitting of the polynomial in equation (3.33) entails computing the polynomial coefficients a_{im} to minimize

$$e = \overline{\left(y_{i-1}(n) - \sum_{m=0}^{M} a_{im} u_i^m(n)\right)^2} \tag{3.38}$$

where e denotes the MSE for the i-th cascade. Let $p_m(n) = u_i^m(n)$. Differentiating equation (3.38) with respect to the polynomial coefficients a_{im} yields

$$\frac{\partial e}{\partial a_{il}} = 2\overline{\left(y_{i-1}(n) - \sum_{m=0}^{M} a_{im} p_m(n)\right)(-p_l(n))} = 0 \tag{3.39}$$

for $l = 0, 1, \ldots, M$. Rearranging equation (3.39) leaves a system of $(M+1)$ equations and $(M+1)$ unknowns, of the form

$$\begin{bmatrix} \overline{p_0(n)p_0(n)} & \cdots & \overline{p_M(n)p_0(n)} \\ \vdots & \ddots & \vdots \\ \overline{p_M(n)p_0(n)} & \cdots & \overline{p_M(n)p_M(n)} \end{bmatrix} \begin{bmatrix} a_{i0} \\ \vdots \\ a_{iM} \end{bmatrix} = \begin{bmatrix} \overline{y_{i-1}(n)p_0(n)} \\ \vdots \\ \overline{y_{i-1}(n)p_M(n)} \end{bmatrix}. \tag{3.40}$$

Although a classical Gram-Schmidt orthogonalization process might be sufficient to obtain the polynomial coefficients a_{im}, Korenberg [42, 43, 44] suggested the use of a modified Cholesky factorization algorithm (termed the *fast orthogonal search*

algorithm) to compute the needed coefficients. The method relies on an orthogonal approach that does not require the explicit computation of orthogonal functions. The residue after fitting the $(i-1)$-th cascade may be written as

$$\begin{aligned} y_{i-1}(n) &= \sum_{m=0}^{M} a_{im} p_m(n) + e(n) \\ &= \sum_{m=0}^{M} g_m w_m(n) + e(n) \end{aligned} \tag{3.41}$$

where the $w_m(n)$ are orthogonal functions over the interval $n = R, (R+1), \ldots, T$ and the error $e(n)$ is to be minimized. The fast orthogonal search algorithm then works as follows, where $m = 0, 1, \ldots, M$:

1. Let $d_{00} = 1$ and set $d_{m0} = \overline{p_m(n)}$ for $m > 0$;

2. Set $d_{ml} = \overline{p_m(n) p_l(n)} - \sum_{j=0}^{l-1} \alpha_{ml} d_{mj}$ for $l = 1, 2, \ldots, m$;

3. Compute the $\alpha_{ml} = \dfrac{d_{ml}}{d_{ll}}$;

4. Let $c_0 = \overline{y_{i-1}(n)}$ and set $c_m = \overline{y_{i-1}(n) p_m(n)} - \sum_{j=1}^{m-1} \alpha_{ml} c_l$, and;

5. Compute the $g_m = \dfrac{c_m}{d_{mm}}$.

The a_{im} are then computed using the g_m and α_{ml} as follows:

6. Compute the $a_{im} = \sum_{j=m}^{M} g_j v_j$ where $v_m = 1$ and $v_j = -\sum_{l=m}^{j-1} \alpha_{jl} v_l$.

Extension to Multi-variable Systems

The PCI algorithm may be easily extended to model multiple-input/multiple-output (MIMO) systems. Consider that a nonlinear system to be identified has input vector $\boldsymbol{x}(n) = [x_1(n) \cdots x_K(n)]^T$ and output vector $\boldsymbol{y}(n) = [y_1(n) \cdots y_P(n)]^T$. In this case, it is necessary that each output element be modelled individually, resulting in P parallel cascade models. For each output element model, when a new path is to be added

to the parallel array, one element of the input $\boldsymbol{x}(n)$ is selected at random to be the input to the cascade, say $x_k(n)$.

In addition, cross-products of the input may be introduced into the definition of linear elements in the cascade. For example, the i-th cascade of a given output element model may use a cross-correlation of the residue $y_{i-1}(n)$ with the first and second elements in $\boldsymbol{x}(n)$, such that

$$\phi_{x_1 x_2 y_{i-1}}(j_1, j_2) = \overline{y_{i-1}(n) x_1(n - j_1) x_2(n - j_2)} \,. \tag{3.42}$$

The impulse response $h_i(j)$ of the linear system would then equal

$$q_3(j) = \phi_{x_1 x_2 y_{i-1}}(j, A) \tag{3.43}$$

where A is again chosen at random from the set $\{0, 1, \ldots, R\}$. Which one of $\{q_1, q_2, q_3\}$ is used to define the impulse response, or whether a slice of some other possibly higher-order cross-correlation is used, remains to be decided at random. The output $u_i(n)$ of the linear system is calculated using equation (3.27), with $x(n) \triangleq x_k(n)$. Now, using equation (3.27) to compute $u_i(n)$ with $x(n) \triangleq x_1(n)$, let

$$\tilde{u}_i(n) = u_i(n) \pm C x_2(n - A) \tag{3.44}$$

where the sign is chosen randomly, and C, as before, is adjusted to tend to zero as the mean-square of the residue approaches zero. Note that the integer A of equation (3.44) must have the same value as in equation (3.43). Finally, a static nonlinearity with input $\tilde{u}_i(n)$ is least square fitted to the residual of the output.

Chapter 4

Experimental Excavation Studies

Upon detailed inspection of the available literature, it was discovered that there have been no reports of *full-scale* excavation experiments[1] aimed at either further validating existing models for the process of bucket-rock interaction, in an attempt at further understanding the processes involved, or at system identification. There have been a number of reported laboratory-scale experiments, using mini-buckets and small pebbles, often of uniform size distribution, as the excavation media [37, 52, 90, 91, 101, 102, 103, 104, 105]. However, no accessible publications pertaining to full-scale validation of such experiments were found. This is not to say that such information has never been acquired (e.g. development of the patent by Dasys et al. [15] most likely resulted in the generation of similar information), simply that this may be the first occurrence of full-scale operational data for an excavation machine, working in fragmented rock, in the *open* literature. To this end, what follows is an effort at a complete and comprehensive disclosure of the experiments and subsequent results.

Between September 2000 and January 2001, full-scale excavation experiments were conducted with the intent of developing further a practical understanding of the fragmented rock excavation process, and in particular, the interaction that occurs between

[1] It is unclear as to whether the work of Rodionov [79] utilized results from full-scale experimental studies. Even so, this work was available only in the Russian language.

the bucket and rock during the excavation process and its impact on operational parameters such as cylinder pressures and displacement. This chapter presents details regarding the apparatus, methodology, procedure, and results of the aforementioned data collection experiments. Provided first are particulars of the equipment involved, followed by an explanation of the experimental procedure and a qualitative analysis of the ensuing results.

4.1 Apparatus and Methodology

Consider a map of the excavation process, as depicted in figure 4.1. Suppose that the loading process may be decomposed into three physical systems, namely: (i) the mechanism structure (boom, bucket, and vehicle); (ii) the actuators (hydraulic lift and dump cylinders, and possibly the tractive effort of the vehicle) which act on, and are in turn acted upon, by the mechanism structure, and; (iii) the rock pile with which the physical structure interacts during the excavation operation. What is most interesting to note about the system illustrated by figure 4.1 is its suggestion that measured cylinder pressure data contain not only evidence of actuator *input* signals, but also information regarding the machine structure motions and its status of interaction with the rock pile. In fact, experimental observations showed this postulate to hold true.

In an effort to identify the way in which key components of the system change during the loading operation, the trial LHD machine was suitably equipped with instrumentation systems capable of simultaneously measuring the following parameters during excavation operations:

1. External forces acting on the mechanism due to interaction of the bucket with the rock pile, measured as strains on the boom component of the mechanism;

2. Forces applied by hydraulic actuators, and subsequent changes in these forces

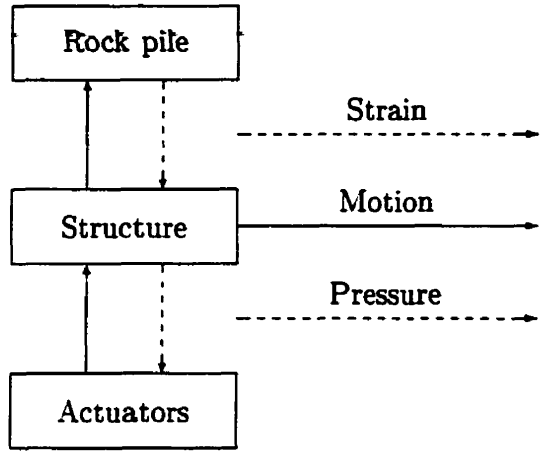

Figure 4.1: A map of the excavation process

as loading proceeded, measured as pressures in the hydraulic cylinders, and;

3. Configuration of the loader mechanism at all times during the loading operation, measured as hydraulic cylinder extensions and vehicle wheel rotations.

It should be noted that no measurement of the vehicle tractive effort was made, which technically also contributes to the "Actuators" block of figure 4.1. This follows directly from the discussion of assumptions given in section 1.2.

Selection and development of the instrumentation and data acquisition systems necessary to perform the types of measurements listed above was an integral part of the work performed towards this dissertation. The following subsections disclose details regarding the loader, instrumentation hardware, and software commissioned specifically for use during the excavation studies.

4.1.1 Loader Specifications

Full-scale excavation experiments using a Tamrock EJC 9t LHD machine, officially known as the EJC 1000 prototype [3] and having geometry as shown previously in figure 1.1 on page 2, were conducted at the facilities of Tamrock Loaders, Inc. of Burlington ON, Canada. A photograph of the actual trial LHD machine is provided

Figure 4.2: Photograph of the Tamrock EJC 9t LHD machine

in figure 4.2. The square frame located at the lower right side of the photograph has outer dimensions 1 yd × 1 yd, included for scale. Table A.1[2] lists some general specifications for the Tamrock EJC 9t LHD machine. The machine was equipped with two lift cylinders (in parallel) and one dump cylinder. The lift and dump cylinder hydraulic system was an open-center system with one gear pump. Table A.2 gives some general specifications for the two types of hydraulic cylinders. The cylinders were operated via a joystick control lever located on the operator console.

The loader was engaged with rock piles of chosen conditions, under the command of skilled operators, as will be described later in this chapter.

4.1.2 Sensors

This subsection describes the sensors employed to measure the parameters stated above. The collection of strain gauge data, measuring the mechanical strain at strategic locations on the mechanism boom, was done in order to possibly identify the forces acting on the mechanism during the loading operation. However, strain gauges were primarily deployed for the purpose of unrelated, although collaborative, research on the subject of component loading analysis [64]. Therefore, details regarding the selec-

[2]Note that specification data for the hardware discussed in this chapter is, for the most part, provided in appendix A, in a tabular format.

tion, configuration, calibration, and commissioning of the strain gauges and related circuitry are not presented here. Instead, the reader is referred to concurrent related work by Murphy [64].

Pressure Transducers

In order to allow for computation of the forces at each cylinder during the loading operation, pressure transducers were placed at both head and rod locations on the dump cylinder and at the same locations on one of the two lift cylinders. Omega Engineering, Inc. of Stamford CT, U.S.A. models PX303-4KG5V (0–4,000 psig) and PX303-7.5KG5V (0–7,500 psig) general purpose, gauge-type transducers were installed on the lift and dump cylinders respectively [1]. Table A.5 gives some specifications for the employed PX303 series transducers.

Measured pressure transducer voltages were converted into corresponding pressures in Pascals by the relationship

$$p = a\,(v - 0.5) \tag{4.1}$$

where p is the pressure in Pascals (Pa), v is the measured output voltage in volts (V), and a is a scaling constant such that $a_L = 6205284$ Pa/V for the lift cylinder transducers (PX303-4KG5V) and $a_D = 10342140$ Pa/V for the dump cylinder transducers (PX303-7.5KG5V). Corresponding cylinder forces were then computed by subtracting the force acting at the cylinder rod from the force at the cylinder head, so that

$$f = p_H A_H - p_R A_R \tag{4.2}$$

where f is the force in Newtons (N), p_H and p_R are the computed pressures at the head and rod respectively, and A_H and A_R are the surface areas (m^2) over which the pressures at the head and rod acted respectively. The areas needed for equation (4.2) were computed using rod and bore specifications for the lift and dump cylinders given in table A.2. Note that, due to the form of equation (4.2), computed cylinder forces

f were positive if acting so as to extend the cylinder. It is also important to note that only one of the two lift cylinders was instrumented. Therefore, having made an assumption that the pressures in both lift cylinders were approximately equal, the measured lift cylinder force was doubled to represent the combined action of both lift cylinders in tandem.

Linear Motion Transducers

Since the configuration of the loader mechanism with respect to the vehicle body may be described completely by two independent coordinates (as will become obvious in chapter 5), the measurement of only two independent position variables was required. Two linear motion transducers, in the form of string potentiometers, were used to record the extension of lift and dump cylinders during the loading operation. Ametek Aerospace, Gulton-Statham Products of Costa Mesa CA, U.S.A. model P-60A string potentiometers were employed for this purpose [5]. Table A.6 lists some specifications for the P-60A linear motion transducer. The transducers were installed in direct line with the orientation of the lift and dump cylinders.

Online calibrations yielded the expressions

$$l_L = 0.4081\, v_L + 1.0609 \tag{4.3}$$

$$l_D = 0.3044\, v_D + 2.3499 \tag{4.4}$$

relating the respective lift and dump cylinder lengths l_L and l_D in meters (m) to measured potentiometer voltages v_L and v_D in volts (V).

Wheel Encoder

In order to sense translational motions of the vehicle, a wheel encoder was installed on the front-right wheel of the trial LHD machine. The encoder was coupled to the tire via a custom manufactured, spring-loaded wheel follower, shown in the photograph

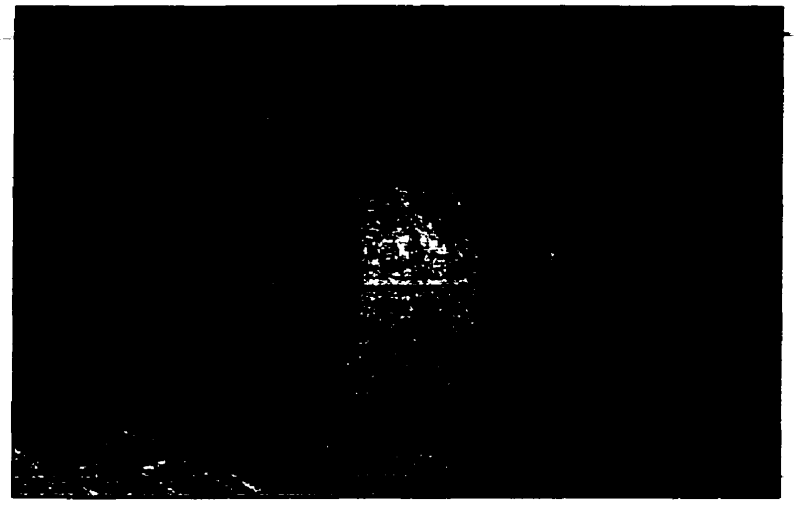

Figure 4.3: Photograph of the H25 incremental optical encoder and wheel coupling mechanism

of figure 4.3. The employed encoder was a BEI Technologies, Inc. of Goleta CA, U.S.A. model H25D-SS-1000-ABZC-4469-LED-EM18 incremental optical encoder [2]. General specifications for the incremental optical encoder are given in table A.7.

Using the wheel coupling mechanism shown in figure 4.3, the encoder itself was found to pass through 10.185 rotations per unit rotation of the LHD vehicle tire, which had a nominal radius of 0.825 m [63]. However, the wheel radius and actual *rolling* radius ($R_r = 0.796$ m) of the LHD vehicle tire differed, since the tire was compressed slightly due to the machine weight. The lateral distance d, in meters, travelled in the direction of the LHD vehicle front wheels, assuming no slippage occurred between the tire and the ground or the tire and the wheel coupling mechanism, was computed as a function of the encoder cycles per shaft turn ($c = 1000$) by

$$d = \frac{2\pi R_r}{10.185\, c} = 4.911 \times 10^{-4}\,\text{m/count}. \tag{4.5}$$

Figure 4.4: Workbench photograph of the two SC-2345 shielded carriers with one opened top, displaying the SCC Series modules within

4.1.3 Signal Conditioning

Conditioning of the voltage signals from the sensors of subsection 4.1.2 was facilitated through the use of two National Instruments Corporation of Austin TX, U.S.A. SC-2345 shielded carriers (with configurable connectors and equipped with SCC-PWR03 power modules) in cooperation with a set of off-the-shelf as well as custom fitted SCC Series modules [67]. In turn, each SC-2345 shielded carrier was connected via a National Instruments Corporation 68-pin E Series cable (model PSHR68-68) to a National Instruments Corporation DAQCard-AI-16E-4 16 channel, 12-bit analog, PCMCIA style personal computer (PC) input device. The two said PCMCIA data input devices were installed in a Toshiba, Inc. model Satellite 330CT notebook computer, having a Pentium processor, 96.0 MB of random-access memory (RAM), 3.81 GB of data storage space, and running the Microsoft, Inc. Windows 98 4.10.1998 operating system.

For the purpose of strain gauge monitoring, two SCC-SG02, two-channel, 350 Ω, quarter bridge completion modules and four SCC-SG04, two-channel, full bridge

modules were utilized. Although discussion of the strain gauge instrumentation is not given here, as per the statement of subsection 4.1.2, it should be noted that the inclusion of 12 channels of strain gauge measurements is what necessitated the second SC-2345 carrier and PCMCIA data input device pair.

Three SCC-FT01, two-channel feedthrough modules were customized to provide buffering, common-mode rejection, and low-pass filtering of sensor signals from the four pressure transducers and two linear displacement transducers described in subsection 4.1.2. A functional circuit diagram for a customized SCC-FT01 module is provided in figure 4.5. Firstly, differential inputs to each of the two SCC-FT01 module channels were passed through an Analog Devices, Inc. of Norwood MA, U.S.A. model AMP04(FP) precision single supply instrumentation amplifier with a chosen gain of one, set by an external 100 kΩ precision resistor [4]. Having rejected common mode signals (at approximately 55 dB for unity gain), the resulting ground referenced signal was then passed through a first-order low-pass filter having a cut-off frequency (defined at -3 dB response) of approximately $\omega_c \approx 1.6$ kHz prior to acquisition by the data input device. Power was provided to the sensors and signal conditioning components via regulated +5 V and $\pm$15 V sources supplied by a SCC-PWR03 power module located on each of the SCC-2345 carriers.

Digital output from the incremental optical encoder was provided in the form of two pulse trains, labelled channels A and B, positioned one-quarter cycle out of phase (i.e. in quadrature) for encoder position and direction measurement. The quadrature encoder data channels A and B were passed respectively to the PFI8 (source) and DIO6 (up/down counter 0) pins of a PCMCIA data input device, via the terminal block provided on the corresponding SCC-2345 carrier unit. A +5 V supply (sourced from the PCMCIA data input device) referenced to the digital ground pin labelled DGND was used to power the encoder circuit.

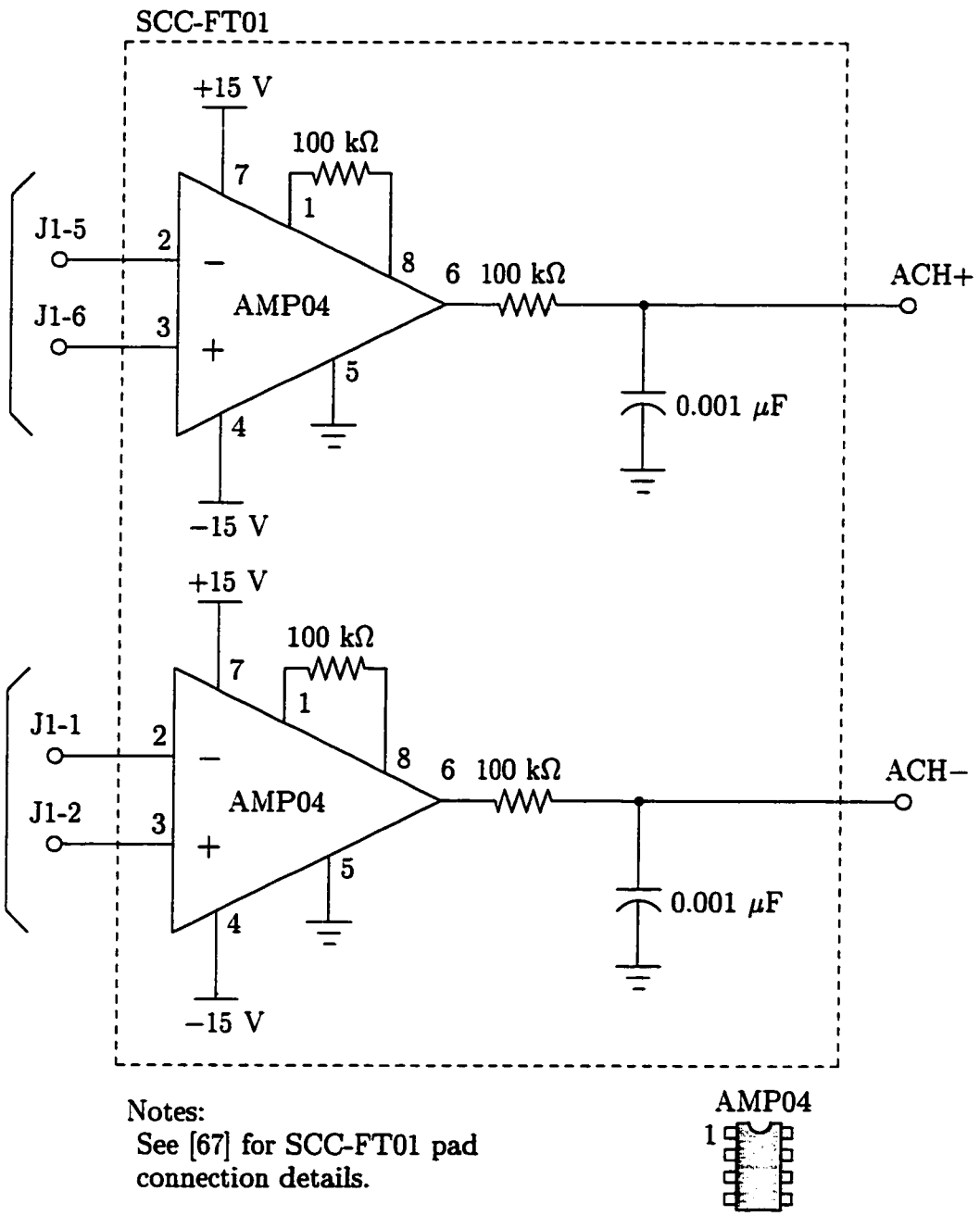

Figure 4.5: Customized SCC-FT01 feedthrough module circuit diagram

4.1.4 Data Acquisition Software Programming

Signals were acquired by the twin PCMCIA data input devices described in subsection 4.1.3, and processed on a PC as described in subsection 4.1.3 running a custom built application in the National Instruments LabVIEW 6i graphical programming environment [68, 69]. The commissioned application, entitled `LHD-DAQ.vi` was written by the candidate so as to facilitate the collection of data during field trials. The application provided a graphical interface for operator input and data visualization pre- and post-acquisition. User definable options included programmable sensor channels, buffer size (samples) and scan rate (Hz) selection, in addition to the choice of using either an ASCII or binary type data storage method.

A sampling of graphical block code for the custom application `LHD-DAQ.vi` is depicted in figure 4.6. The portion of graphical code that handled the actual buffered data acquisition tasks is shown to the left (bottom in figure 4.6), while the remaining code depicts the data storage function of the application. Notice how the first two rows of blocks referred to analog signal acquisition from the two PCMCIA input devices, while the third row dealt with the task of counting rising edges (i.e. digital signal acquisition) from the incoming incremental optical encoder pulse trains.

4.1.5 Acquisition Synchronization

Synchronization of the two PCMCIA input devices was necessary in order to ensure that sampling of data from all analog channels, as well as sampling of the digital counter, was performed simultaneously. To this end, one of the PCMCIA input devices was designated as a *master* device, while the other was designated as a *slave* device. The analog input "AI scan start" (see figure 4.6) signal was physically routed via the PFI7 (programmable function input) pin of the master device to the same pin on the slave device, where it was used as a digital trigger for data acquisition

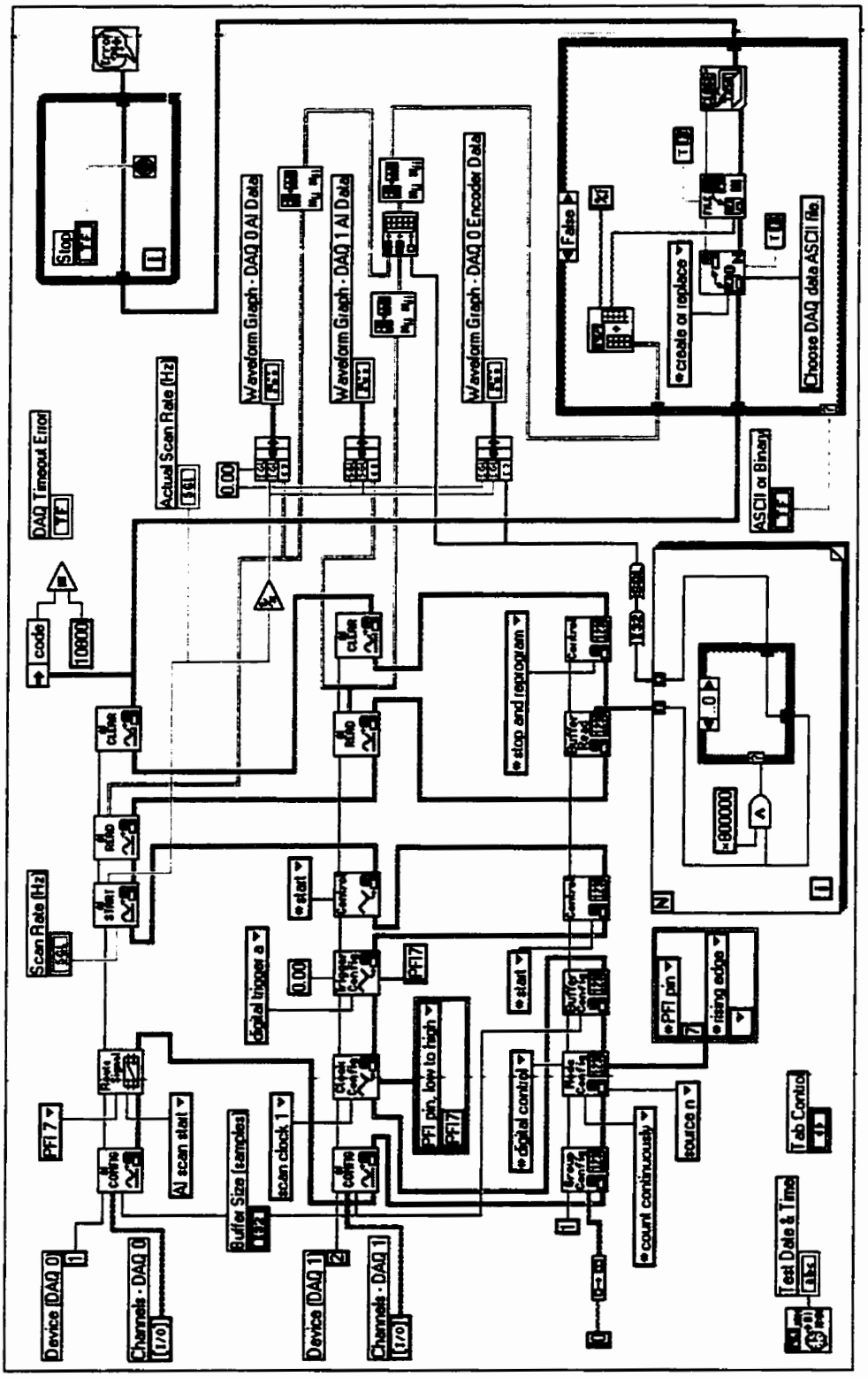

Figure 4.6: Custom application LabVIEW 6i graphical code, illustrating block sequences related to synchronous data acquisition and data storage

synchronization. The same signal was also used as a cue for sampling of the counter value indicating the incremental optical encoder position.

4.1.6 Sampling Rate Selection

A sampling rate of $\omega_s = 3.500$ kHz was selected for all trials, mainly to accommodate the possible high frequency components in strain gauge signals, important to complementary research not discussed in this dissertation [64]. At this rate, according to the Nyquist criterion [8, page 147], signals with frequencies lower than the Nyquist frequency $\omega_N = \omega_s/2 = 1.750$ kHz were sampled accurately. Since all of the signal conditioning modules described in section 4.1.3 included a low-pass filtering stage with a cut-off frequency at $\omega_c \approx 1.6$ kHz, the possibility of aliasing problems due to signals with frequency components above ω_N was essentially eliminated.

4.2 Experimental Procedures and Observations

In order to acquire operational data representative of the excavation process under varying, yet controlled, conditions, the instrumented Tamrock EJC 9t LHD machine was engaged with rock piles (selection was limited) having varying particle size and composition. Excavation studies were conducted under the command of skilled operators having moderately varying operating styles, utilizing documented maneuvers.

The following subsections describe fully the chosen trial excavation scenarios and the degree to which their parameters were known. Finally, a synopsis of the recorded data and observations is offered, accompanied by some qualitative analysis.

4.2.1 Excavation Trial Scenarios

Each of the excavation trials was conducted in one of two rock pile types, labelled: (i) *local roundstone*, and; (ii) *Inco muck*. The local roundstone consisted of generally fine

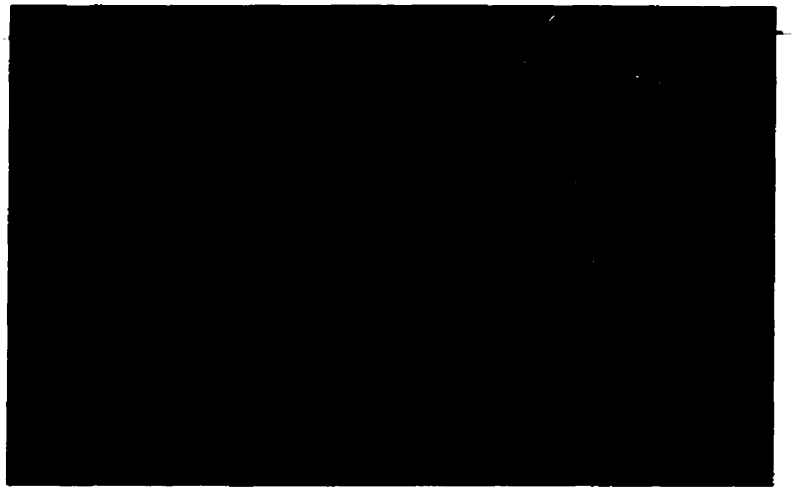

Figure 4.7: Photograph of the trial rock labelled *local roundstone* (with 1 yd × 1 yd frame for scale)

grained sandy material interspersed with larger rounded particles, having a mean size of approximately 10–15 cm, and a relatively low density (2.6 g/cm^3) in comparison with the Inco muck (3.2 g/cm^3). It is this rock, shown in figure 4.7, that testing operators at the Tamrock Loaders, Inc. manufacturing facility have traditionally utilized for loader testing. Admittedly, the low density rounded particles minimize the abrasive damage to new equipment being tested prior to shipment.

To contrast the local roundstone, 33 metric tonnes of Inco muck[3] were shipped from the 7630 drift of Inco Limited's 175 Orebody (an underground hard-rock mine) in Copper Cliff ON, Canada to the trial location at the facilities of Tamrock Loaders, Inc. in Burlington ON, Canada. This rock, shown in figure 4.8, was used in order to lend credibility to the excavation study results in that the Inco muck was extracted from a typical blast at a hard-rock mine located in the Canadian Shield. Note that, in the photograph of figure 4.8, the Inco muck consisted of angular particles having a broad distribution of sizes, including some very large boulders, as is often encountered

[3]In the mining industry, the term *muck* refers typically to freshly blasted (fragmented) rock, in an underground mine, which is ready for transport.

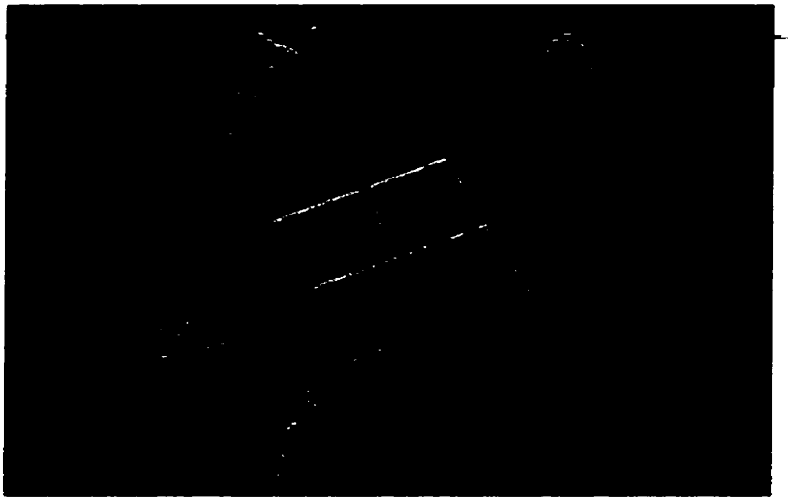

Figure 4.8: Photograph of the trial rock labelled *Inco muck* (with 1 yd × 1 yd frame for scale)

in an underground mining excavation scenario. The muck itself consisted of a fine- to medium-grained, porphyritic amphibole/biotite rich rock known as amphibolite [54].

The executed excavation scenarios were, for the most part, of one of the following two categories: (i) *controlled excavation* trials, or; (ii) *aggressive excavation* trials. Controlled excavation trials were conducted by a single operator, where a predetermined sequence of mechanism actions was prescribed. For example, one prearranged controlled excavation operation kept to the following sequence of steps:

1. Advance loader into the rock pile, with bucket in ready position;
2. *Roll back* with dump cylinder only, while applying constant tractive effort, and;
3. Retreat from the rock pile upon completion.

A variety of controlled excavation trials were conducted in both local roundstone and in Inco muck, so as to observe the effects of both rock pile types on the operational parameters measured by the installed instrumentation.

Aggressive excavation trials were conducted by two skilled operators, different from the single operator used for the controlled excavation trials. For these aggressive excavation trials, the operators were simply instructed to fill the loader bucket

as completely as possible, without concern for following any prescribed sequence of actions. It was hoped that the results of these trials might provide the most significant insight into the evolution of machine parameters (i.e. motion and forces) during excavation, in addition to perhaps an indication of potentially feasible approaches to automation of the loading cycle.

Further to the excavation trial scenarios described above, a number of *free-space motion* trials were conducted, in order to perhaps validate and later identify a model for the loader mechanism behaviour while not in contact with the environment. The loader mechanism was given rich operator inputs, attempting to cover a wide range of possible mechanism configurations. As well, trials were conducted where the operator provided only pulse inputs to the cylinders, and resulting oscillations of the mechanism structure, also observable in the cylinder pressure measurements, were recorded.

4.2.2 Synopsis of Experimental Results and Observations

During the period of study, a very large quantity of data was acquired (on the order of approximately one gigabyte when in ASCII format) for approximately 80 performed excavation trials. In this subsection, a very small sampling of the collected data is presented as it pertains to representative observations, and to the modelling and control investigations that are presented in the chapters that follow. The volume of collected data that is not included here should remain on file at Queen's University for possible distribution and use in further research.

Free-space Motion

Firstly, in order to provide a basis for comparison with the controlled and aggressive excavation trial results, presented in figure 4.9 are representative data from the collection of free-space motion trials. These data illustrate the nature of both the measured pressure (force) signals and hydraulic cylinder length (configuration) sig-

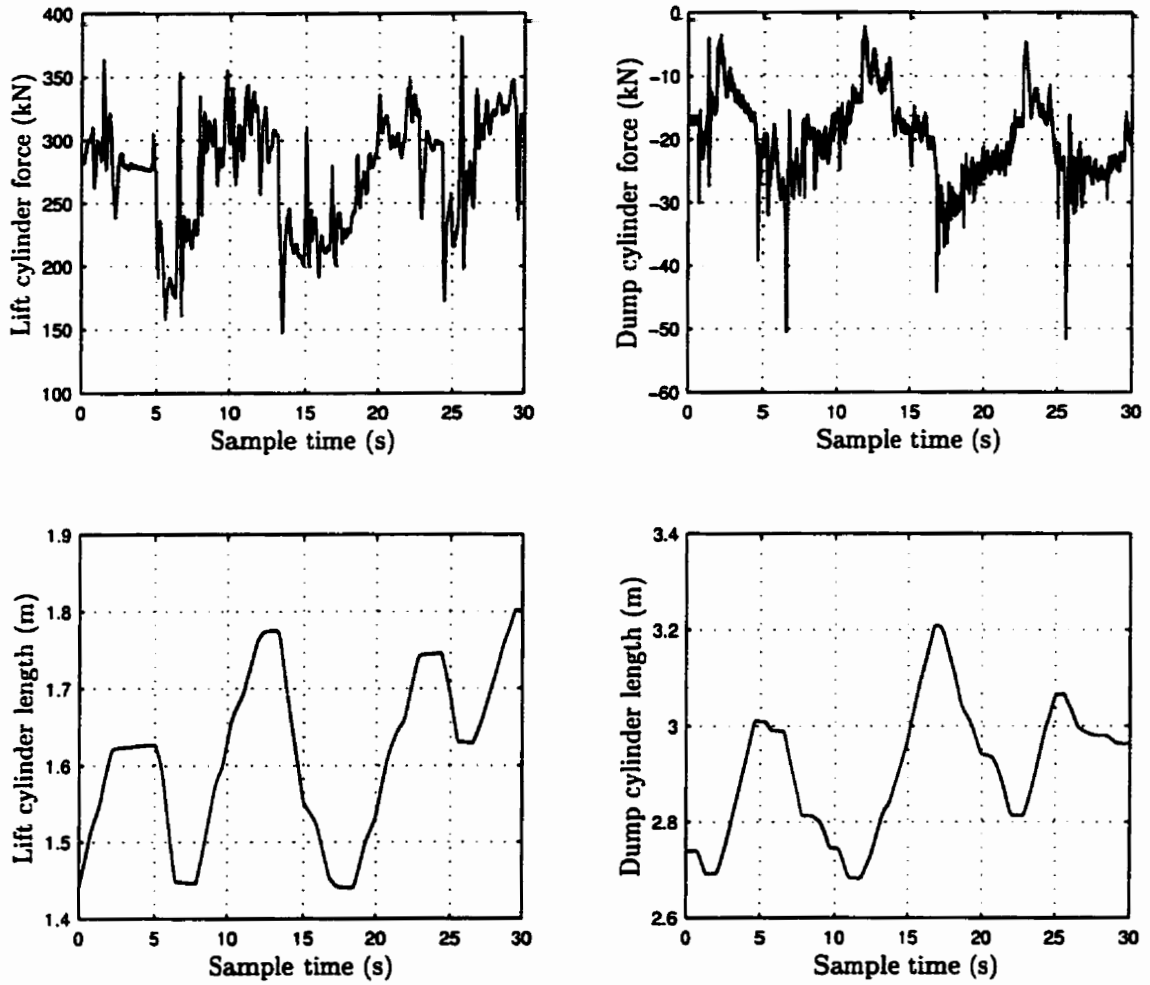

Figure 4.9: Representative free-space motion trial data

nals. The top row of plots in figure 4.9 shows the resulting cylinder forces, computed from cylinder pressures as described in subsection 4.1.2, which corresponded to the cylinder motions shown in the bottom row of plots, on the same independent axis scale. The lift cylinder forces printed in the figure are representative of the actuation provided by both lift cylinders acting in tandem, as though there existed only one lift cylinder supplying twice the actuating force. It should also be reiterated that a negative force corresponded to pressures within the cylinder so as to tend towards a reduction in its length.

Note the comparatively high frequency changes observed in the cylinder forces;

fluctuations not seen in the relatively smooth cylinder displacements. Observed force spikes, and subsequent oscillations, in the cylinders corresponded to sudden changes in motion, for example, an abrupt stop or change in direction. Also, due to the arrangement of the loader mechanism components and actuators, lift and dump cylinder forces were not independent of one another. For reasons that will be reviewed later in this thesis, but which are rather obvious, the lift and dump cylinder forces depended not only on their respective cylinder lengths, but on the overall configuration of the mechanism. For instance, one could not change the lift cylinder length without observing changes in both the lift and dump cylinder forces, although the dump cylinder length may not have measurably changed. Another particular phenomenon that was observed, although not illustrated in figure 4.9, was the extremely high force produced when a cylinder had reached an extension limit. *Hitting the stops*, as it was termed, often resulted in a cylinder force exceeding 4–5 times the nominal.

Controlled Excavation

In the consideration of controlled excavation trials, it was learned that there exist primarily two operator approaches, with regards to lift and dump cylinder actions, to tackling the fragmented rock excavation problem using an LHD machine. The first approach is to attack the rock pile using both the boom and bucket actuators, raising the boom using the lift cylinders whilst rolling back the bucket by retracting the dump cylinder. The second approach, endorsed by the trial LHD machine manufacturer Tamrock Loaders, Inc. [87], aims to utilize only the dump cylinder during the excavation operation, while decisions on how to actuate the dump cylinder are made based on the operator perceived excavation conditions. Obviously, in order to fill the bucket completely and effectively, a significant amount of tractive effort is required, although this parameter was assumed to be approximately constant for the current research (again, see section 1.2).

Therefore, although a number of controlled excavation trials were tried, particular focus was given to trials following the second operator approach, as described above (also given as the example of a controlled excavation operation in the previous subsection, on page 52). A number of controlled excavation trials, as explained, were conducted in the local roundstone. A representative sample from these trials is given in figure 4.10. Only the dump cylinder force and displacement are shown, since for these trials lift cylinder motion was not allowed. The time period up to approximately 7–8 seconds covers the *penetration* phase of the excavation operation. During this phase, the operator was simply pushing the bucket, with its base plate tilted slightly downwards, into the rock pile using the tractive effort of the LHD machine. Note that the dump cylinder remained essentially motionless during this period, but that slight positive forces were measured by the pressure transducers. This is as a result of the rock being pushed into the bucket and causing a moment about the bucket joint so as to try and extend the dump cylinder.

The point labelled (a) in figure 4.10 marks the end of the penetration phase, and the beginning of the *scooping* phase. During this phase, the operator rolled back the dump cylinder causing excavation media to fall deep into the bucket. Note the large negative forces, indicating that the dump cylinder was working hard to tilt the bucket so as to capture the excavation material. As may be seen from the relatively constant slope of the line that represents the change in dump cylinder length, the dump cylinder motion was very smooth and took place at an almost perfectly constant velocity.

The point labelled (b) indicates the time at which breakout[4] occurred. For the case shown in figure 4.10, breakout happened very shortly after the operator commenced the scooping phase, indicating that either the rock pile face had a very shallow slope or that there was insufficient bucket penetration into the rock pile. In this case,

[4]The term *breakout* refers to the event at which the bucket ceases to contact the rock pile, having completed an excavation pass.

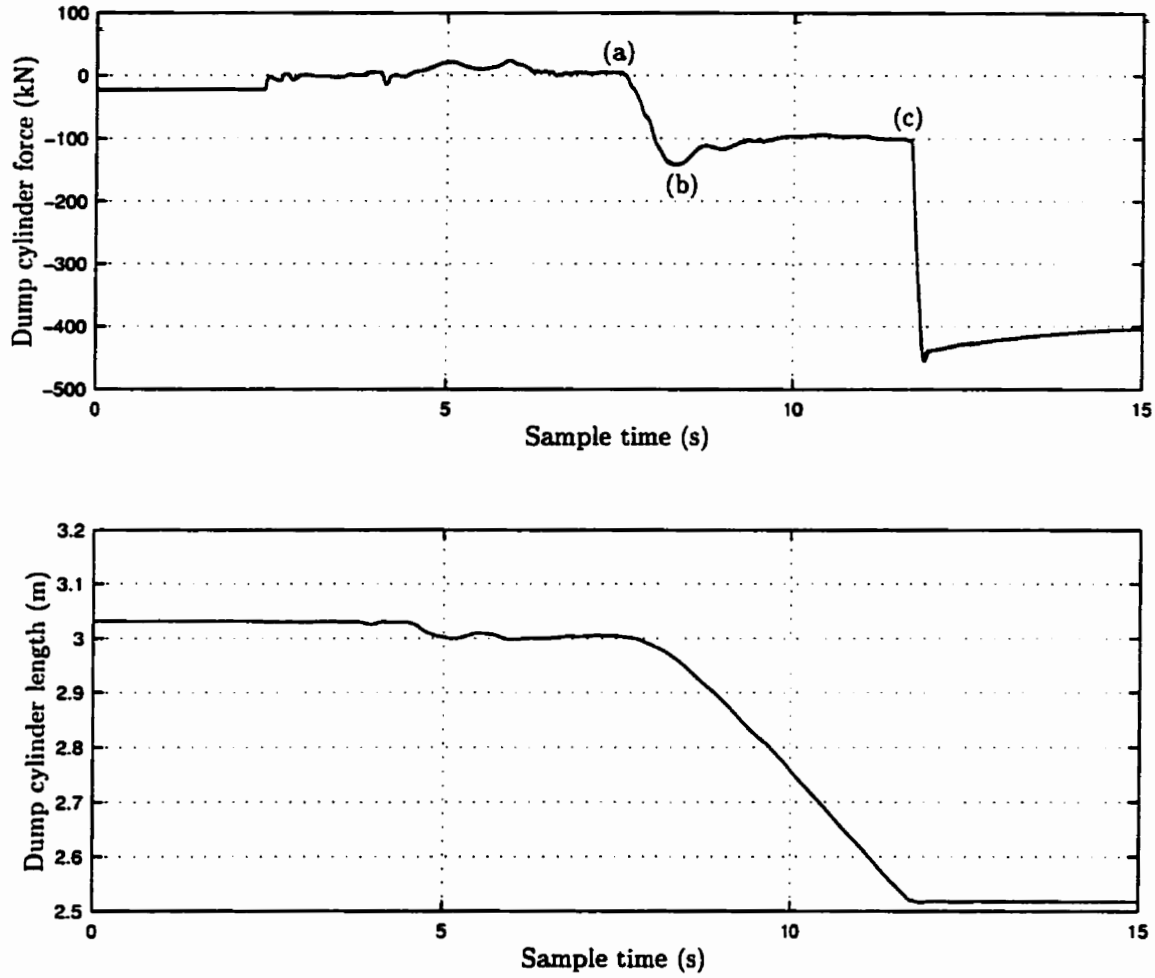

Figure 4.10: Representative controlled excavation trial in local roundstone

it was predominantly the latter that contributed to a somewhat premature breakout. Finally, the point labelled (c) designates the time at which the dump cylinder had reached its retraction limit, resulting in a sudden jump in sensed force, a phenomenon that was introduced previously in the context of free-space motion trial data. Although a full bucket of local roundstone was not achieved in this case, it was observed that data acquired from only the dump cylinder parameters have the potential for exposing a great deal about the excavation operation that took place.

The obvious next step is to compare results from controlled excavation trials carried out in the local roundstone to similar experiments conducted in the Inco muck. A

representative sample of data from trials conducted in Inco muck is provided in figure 4.11. Similar to figure 4.10, only the force and displacement data for the dump cylinder is shown. In figure 4.11, the points labelled (a), (b), and (c) may be interpreted to have the same significance as described for figure 4.10. In the case of excavation trials in Inco muck, as compared with those trials conducted in the local roundstone, very large (positive) forces were encountered during the penetration phase, indicative of the rock characteristics and possibly the applied tractive effort. Similar to the previous case, for the excavation trial shown in figure 4.11, breakout happened a relatively short time after commencement of the scooping phase, indicating a potentially poor result where the objective of completely filling the bucket is concerned. However, one significant difference worth notice is the dump cylinder force at which breakout occurred. In the case of excavation in the local roundstone, the force at breakout in the dump cylinder had a magnitude of approximately 140 kN; whereas, in the case of excavation in the Inco muck, the dump cylinder force at breakout had a magnitude of about 260 kN. This was, for the most part, due to contrasting properties of the excavation media (since the Inco muck was much more dense and had many large particles), although perhaps due in part to slightly better penetration in the case of the operation shown in figure 4.11. Once again, the dump cylinder motion during the scooping phase (and afterwards) was very smooth and took place at an almost constant rate. However, fluctuations in the cylinder force between points (b) and (c) indicate oscillations (of small magnitudes) in the cylinder, possibly due to shifting material within the bucket or cylinder/structural resonance due to contact with the rock pile.

Aggressive Excavation

Aggressive excavation trials were admittedly the most interesting of the conducted experiments. These trials were conducted with the hope of observing patterns in

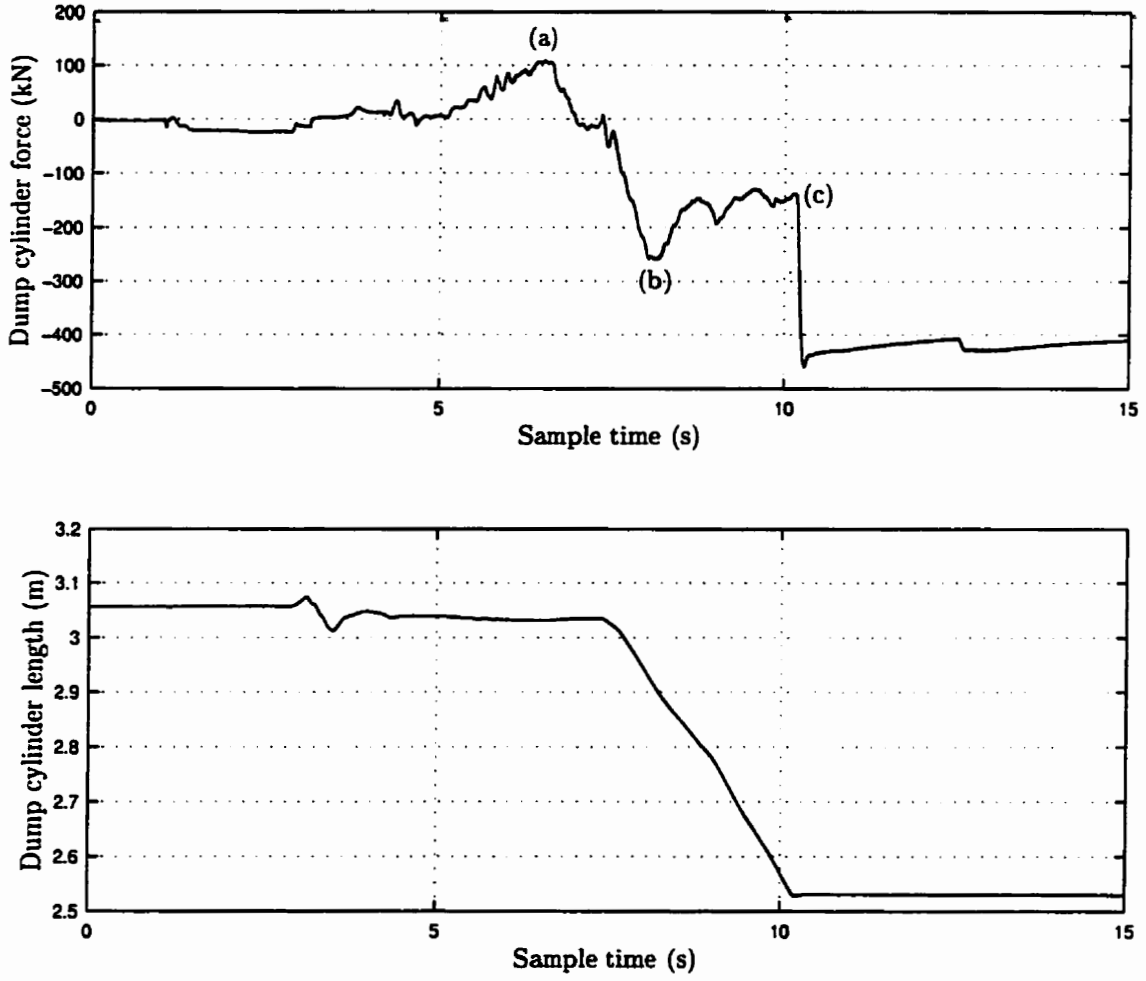

Figure 4.11: Representative controlled excavation trial in Inco muck

the measured machine parameters during excavation, so as to: (i) gain a further understanding of excavation process; (ii) gather data whereby a model capable of identifying and possibly simulating the process might be developed, and; (iii) discover whether machine parameters, such as cylinder pressures, might be used as source of feedback towards the development of a control system for autonomous excavation.

As was mentioned previously, there were two operators available to execute aggressive excavation trials. Both operators were experienced in LHD operation. Furthermore, aggressive excavation trials were carried out solely in Inco muck, since this rock pile duplicated best the conditions under which underground excavation might

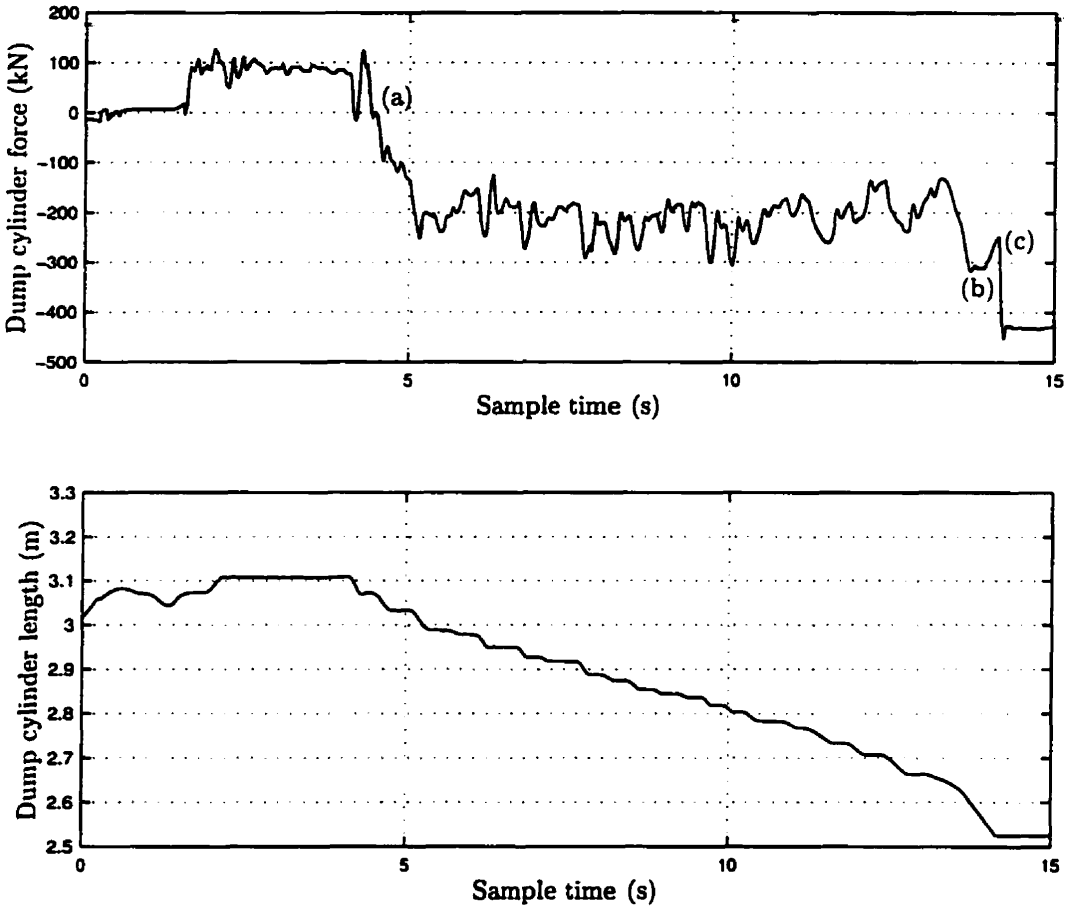

Figure 4.12: Representative aggressive excavation trial for operator (I)

take place. The trial operators were simply instructed to fill the loader bucket as completely as possible at each iteration, which they managed to accomplish exceedingly well. Figures 4.12 and 4.13 present the dump cylinder measurement results of representative excavation trials for two operators numbered (I) and (II) respectively. Once again, the points labelled (a), (b), and (c) may be interpreted to have the same meaning as described for the figures showing controlled excavation trials.

Firstly, it should be reported that both operators chose to control only the dump cylinder during the scooping phase. In both cases, the lift cylinder position remained approximately steady. As opposed to the controlled excavation trials, it was observed that the penetration phase was generally longer and produced higher positive cylinder

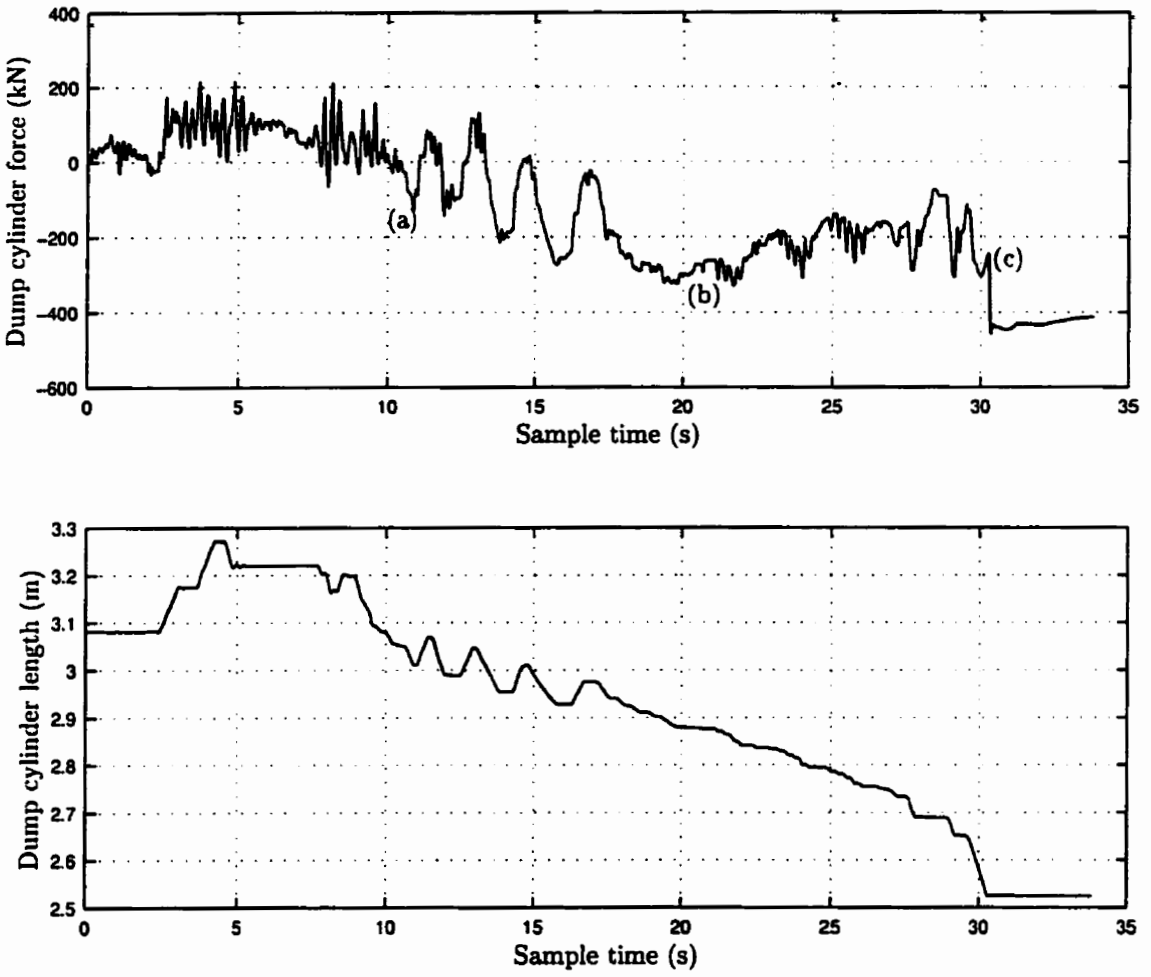

Figure 4.13: Representative aggressive excavation trial for operator (II)

forces in the aggressive excavation trials. As a result, more material was collected in the bucket during the subsequent scooping phase. In the scooping phase, the aggressive excavation trials showed stepped changes in the dump cylinder length, as opposed to the relatively smooth motions observed during controlled excavation trials. These stepped motions, due in part to the response of hydraulic actuators to bucket-rock interaction and in some cases produced by the operators in reaction to their continuous assessment of the situation, resulted in an extended scooping phase as compared with the controlled excavation trials. Consider the difference in dump cylinder retraction rate between the trials shown in figures 4.11 and 4.12.

During controlled excavation trials, a retraction rate of about 140 mm/s was observed, while during aggressive excavation trials, a reduced cylinder retraction rate closer to approximately 35–40 mm/s was noted.

For the cases portrayed in figures 4.12 and 4.13, both operators managed to fill the loader bucket completely. Although both operators utilized only the dump cylinder during excavation, there were some noticeable differences between their individual approaches. During the penetration phase, the angle of attack taken by operator (II) was steeper (longer dump cylinder length) than that used by operator (I), resulting in relatively high forces experienced by the dump cylinder during penetration of the rock pile. Although the cylinder displacement plot for operator (I) indicates that a stepping action was used during retraction of the cylinder in the scooping phase, the cylinder displacement plot for operator (II) indicates the use of significant oscillations, perhaps in an attempt to *fluidize* the rock pile so as to cause rock particles to flow more easily in and around the bucket. This type of action, causing oscillation of the bucket angle, is reminiscent of the algorithm described by the patent of Dasys et al. [15], mentioned in chapter 2. For the case shown in figure 4.12, operator (I) was able to keep the bucket within the rock pile for almost the entire time dump cylinder retraction was taking place. Whereas, operator (II) was able to break out of the pile at an earlier stage of dump cylinder retraction (although it took approximately the same time to pass from point (a) to point (b) in both cases).

At the very least, the aggressive excavation trials have allowed for qualitative and comparative observations to be drawn regarding the excavation of fragmented rock using an LHD machine. Through the collection and analysis of operational data, a clearer understanding of the excavation process and its characteristic stages has been achieved. It is these data that provide the basis for further study in the chapters that follow.

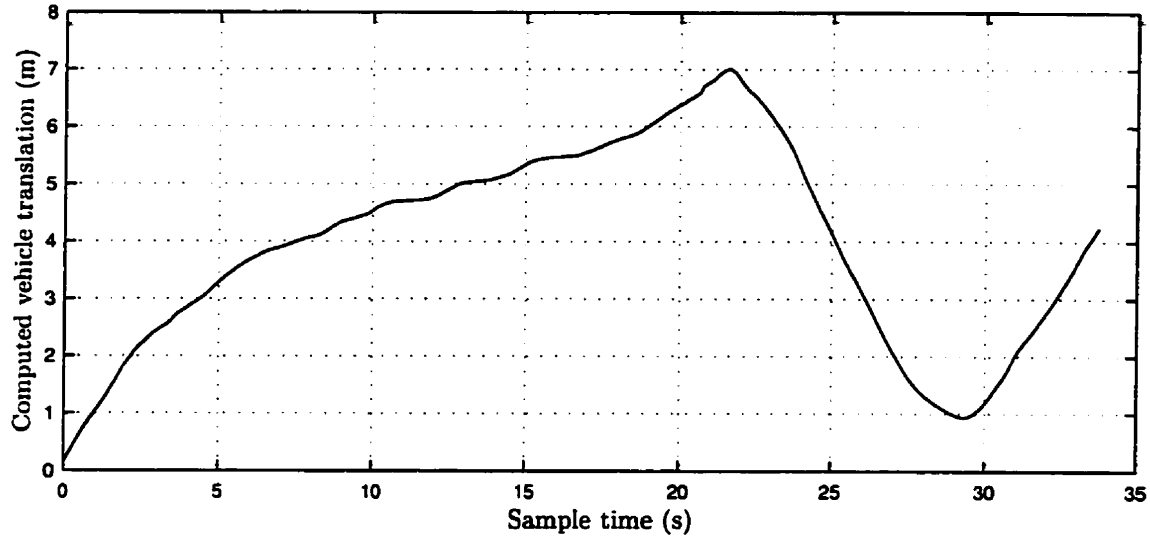

Figure 4.14: Computed vehicle translation, based on incremental encoder measurements, corresponding to the excavation trial of figure 4.13

Wheel Slippage

An issue not discussed to this point is *wheel slippage* during excavation. It was discovered, although too late for any changes to be made, that the use of an incremental wheel encoder for vehicle translation measurement was, in some respects, inappropriate. This unsuitability was due to the significant amount of slippage that occurred between the vehicle tires and the uneven terrain during excavation. Figure 4.14 shows a plot of the vehicle translation, as computed from the incremental encoder data, which corresponds to the aggressive excavation trial of figure 4.13. Notice the small signal fluctuations during the period from 5–15 seconds. Coinciding with this time period were portions of the penetration and scooping phases. In actual fact, the vehicle was barely moving during this time, as opposed to the computed travel of over 3 m.

Nonetheless, the wheel encoder data did have some usefulness in that it provided landmarks for each trial, through which interpretation of the cylinder pressure data was facilitated. Consider the force plot of figure 4.13. It becomes obvious through

inspection of the incremental encoder data of figure 4.14 that breakout had occurred prior to the 22 second mark, since after this time the vehicle was most definitely moving in reverse.

Chapter 5

Dynamics of the Loading Process

It remains clear, in light of the material that has been presented thus far, that further investigations into possible techniques for modelling the underlying dynamics of the excavation process are warranted. In the context of autonomous excavation, the term *dynamics* is used to mean the study of excavator motions under the influence of actuator and rock interaction forces. Although there is no doubt that these dynamics are complex, for feedback control techniques to be considered as a means for development of an autonomous excavation system, the availability of a model that may be used for analysis and possibly simulation is most necessary and useful.

The modelling problem was first approached from an analytical perspective, as an exercise in mechanics and to show potential alternatives to nonlinear system identification. Through the use of techniques from Lagrangian mechanics, based on the material introduced in chapter 3, the loader mechanism dynamics (i.e. motions associated with only the boom, bucket, and actuator links) were modelled as a closed-chain mechanical system. Next, a distinct element method (DEM) and artificial neural networks were considered, although only briefly, as potential alternatives for bucket-rock interaction modelling. Finally, presented in this chapter are the results of efforts to model the machine dynamics, as well as the loader motions during scooping opera-

tions in fragmented rock, using the parallel cascade identification (PCI) technique. Data from aggressive full-scale experimental trials, as described in chapter 4, were used in the identification process for linear and nonlinear elements of PCI models. Attempted modelling scenarios are provided alongside a detailed description of the means by which the PCI algorithm was implemented and applied.

5.1 Euler-Lagrange Formulation

A first attempt at modelling the loader mechanism dynamics (as an exercise in applied mechanics) was done without concern for rock interaction, and through consideration of the mechanism as a robot manipulator, similar to the concepts proposed in [33, 86]. Concurring with the experimental material of chapter 4, only the dynamics resulting from lift and dump cylinder actuation were considered. A Lagrangian approach, as described in chapter 3, was used to derive equations of motion for the given mechanism. This was also recognized by Sarata et al. [86]. However, in [86], only a means through which the equations might be formulated was given, and the technique was never actually implemented.

The loader mechanism of the Tamrock EJC 9t LHD machine used for the current research, by inclusion of the linear actuators, formed a multi-loop, closed kinematic chain of links. It is conceivable that dynamical equations of motion could have been formulated using only the boom and bucket links of the system, through the application of actuator forces as external forces on the resulting serial mechanism. Although this more simplistic perspective might have been acceptable for static force analysis [33], the inertial properties of the actuators and the inclusion of explicit holonomic constraints that define the closed kinematic chains shaped a convincing argument for an attempt at formulation of the system as a closed-chain mechanism.

Schematic drawings of the Tamrock EJC 9t LHD loader mechanism are presented

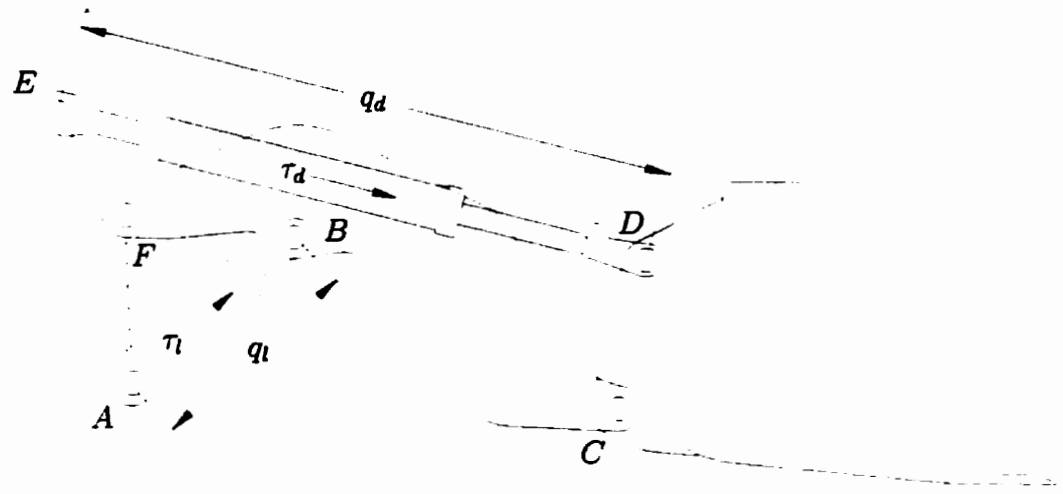

Figure 5.1: Schematic drawing of the loader mechanism

in figures 5.1 and 5.2. The actuated lift and dump cylinder prismatic joints were denoted by $\tilde{q} = [q_l \; q_d]^T \in \Re^2$ and the corresponding actuated cylinder forces denoted by $\tilde{\tau} = [\tau_l \; \tau_d]^T \in \Re^2$. Table A.3 (located in appendix A.1 on page 134) lists the inertial properties[1] for each of the links in the system. Note that, although the boom and bucket links were obviously much larger in mass than the actuators, the cylinder component masses themselves were not entirely insignificant. Table A.4 lists the fixed physical dimensions of the loader mechanism, as illustrated by figure 5.2.

5.1.1 Reduced System Mechanics

As was necessary, the loader mechanism of figure 5.1 was cut open at strategic boom and dump cylinder locations; namely points E and F. The dynamics of the serial reduced system were then modelled through an application of the Euler-Lagrange equations, as described in chapter 3. The Denavit-Hartenberg [16] coordinate frames for the serial reduced system were developed, as shown in figure 5.3, and the joint

[1]Moments of inertia I_{zzi} were taken about the link centre of mass, with reference to the base frame. The constants a_{ci} and b_{ci} were used to locate the centre of mass of link i. Values were computed through computer modelling of the boom and bucket structures; see [64].

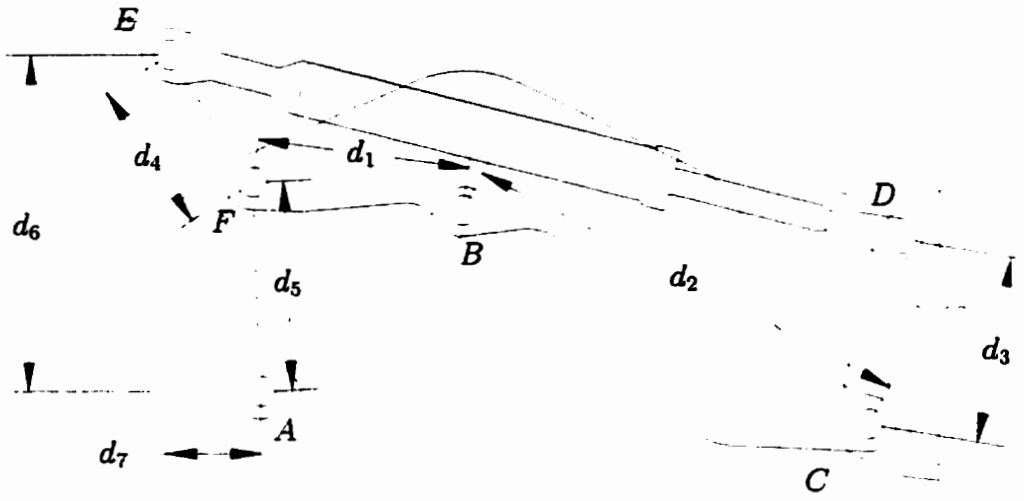

Figure 5.2: Fixed physical dimensions of the loader mechanism

variables were subsequently denoted by $\boldsymbol{q} = [q_1 \dots q_6]^T \in \Re^6$, with q_2 and q_6 being linear displacements corresponding to the lift and dump cylinder extensions. The corresponding generalized actuating forces were denoted by $\boldsymbol{\tau} = [\tau_1 \cdots \tau_6]^T \in \Re^6$.

Kinetic and Potential Energy Expressions

The total kinetic energy of the reduced system was written as

$$K = \frac{1}{2}\sum_{i=1}^{6}\left(m_i \boldsymbol{v}_{ci}^T \boldsymbol{v}_{ci} + \boldsymbol{\omega}_i^T \boldsymbol{I}_i \boldsymbol{\omega}_i\right) = \frac{1}{2}\dot{\boldsymbol{q}}^T \boldsymbol{D}(\boldsymbol{q})\dot{\boldsymbol{q}} \tag{5.1}$$

with

$$\boldsymbol{v}_{ci} = \boldsymbol{J}_{v_{ci}}(\boldsymbol{q})\dot{\boldsymbol{q}} \tag{5.2}$$

$$\boldsymbol{\omega}_i = \boldsymbol{R}_i^T(\boldsymbol{q})\boldsymbol{J}_{\omega_i}(\boldsymbol{q})\dot{\boldsymbol{q}} \tag{5.3}$$

for $i = 1, 2, \dots, 6$ links, where $\boldsymbol{J}_{v_{ci}}(\boldsymbol{q})$ and $\boldsymbol{J}_{\omega_i}(\boldsymbol{q})$ were Jacobian matrices, the matrix $\boldsymbol{R}_i(\boldsymbol{q})$ took care of the fact that the angular velocity $\boldsymbol{\omega}_i$ must be expressed in a frame attached to its respective link, and $\boldsymbol{I}_i$ was the inertia tensor for the link i about its

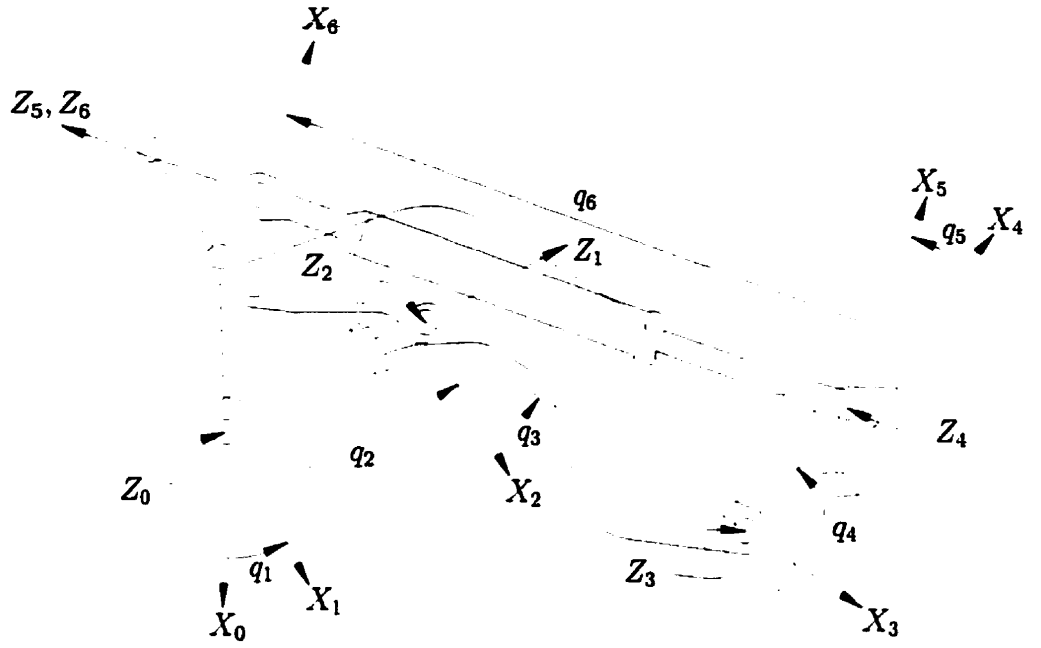

Figure 5.3: Denavit-Hartenberg coordinate frames for the serial reduced system

centre of mass. Given the planar motion of the system, for all links i

$$I_i = \begin{bmatrix} 0 & 0 & 0 \\ 0 & 0 & 0 \\ 0 & 0 & I_{zzi} \end{bmatrix}. \tag{5.4}$$

The centre of mass location vectors r_{ci} were next computed from the coordinate frames of figure 5.3, giving[2]

$$r_{c1} = \begin{bmatrix} -a_{c1}S_1 \\ a_{c1}C_1 \\ 0 \end{bmatrix}$$

$$r_{c2} = \begin{bmatrix} -(q_2 - a_{c2})S_1 \\ (q_2 - a_{c2})C_1 \\ 0 \end{bmatrix}$$

[2]The abbreviations $S_{ij} \triangleq \sin(q_i + q_j)$ and $C_{ij} \triangleq \cos(q_i + q_j)$, commonly used in the robotics literature, were applied as needed to simplify the resulting expressions.

$$
\begin{aligned}
r_{c3} &= \begin{bmatrix} -q_2 S_1 + a_{c3} C_{13} - b_{c3} S_{13} \\ q_2 C_1 + a_{c3} S_{13} + b_{c3} C_{13} \\ 0 \end{bmatrix} \\
r_{c4} &= \begin{bmatrix} -q_2 S_1 + d_2 C_{13} - a_{c4} C_{134} + b_{c4} S_{134} \\ q_2 C_1 + d_2 S_{13} + a_{c4} S_{134} - b_{c4} C_{134} \\ 0 \end{bmatrix} \\
r_{c5} &= \begin{bmatrix} -q_2 S_1 + d_2 C_{13} + d_3 C_{134} + a_{c5} S_{1345} \\ q_2 C_1 + d_2 S_{13} + d_3 S_{134} + a_{c5} C_{1345} \\ 0 \end{bmatrix} \\
r_{c6} &= \begin{bmatrix} -q_2 S_1 + d_2 C_{13} + d_3 C_{134} + (q_6 - a_{c6}) S_{1345} \\ q_2 C_1 + d_2 S_{13} + d_3 S_{134} + (q_6 - a_{c6}) C_{1345} \\ 0 \end{bmatrix} .
\end{aligned} \tag{5.5}
$$

Therefore, the Jacobians $J_{v_{ci}}(q)$ were finally computed such that

$$
J_{v_{ci}}(q) = \begin{bmatrix} \dfrac{\partial r_{ci}}{\partial q_1} & \cdots & \dfrac{\partial r_{ci}}{\partial q_6} \end{bmatrix} \in \Re^{3\times 6} . \tag{5.6}
$$

The resulting Jacobian matrices are not printed here due to their length. Instead, they may be found in appendix B.1 on page 137. Combination of these Jacobian matrices with equation (5.2) produced the translational kinetic energy portion of equation (5.1). It is clear that, for the given serial reduced system,

$$
\begin{aligned}
\omega_1 &= \begin{bmatrix} 0 & 0 & \dot{q}_1 \end{bmatrix}^T \\
\omega_2 &= \begin{bmatrix} 0 & 0 & \dot{q}_1 \end{bmatrix}^T \\
\omega_3 &= \begin{bmatrix} 0 & 0 & \dot{q}_1 + \dot{q}_3 \end{bmatrix}^T \\
\omega_4 &= \begin{bmatrix} 0 & 0 & \dot{q}_1 + \dot{q}_3 + \dot{q}_4 \end{bmatrix}^T \\
\omega_5 &= \begin{bmatrix} 0 & 0 & \dot{q}_1 + \dot{q}_3 + \dot{q}_4 + \dot{q}_5 \end{bmatrix}^T \\
\omega_6 &= \begin{bmatrix} 0 & 0 & \dot{q}_1 + \dot{q}_3 + \dot{q}_4 + \dot{q}_5 \end{bmatrix}^T .
\end{aligned} \tag{5.7}
$$

Fortunately, rotation for all links occurred about parallel axes, so the above expressions remained valid for link-bound frames. Hence, the rotational kinetic energy portion of equation (5.1) was given by

$$\frac{1}{2}\dot{\boldsymbol{q}}^T\boldsymbol{\Omega}\dot{\boldsymbol{q}} = \frac{1}{2}\dot{\boldsymbol{q}}^T \begin{bmatrix} \sum_{i=1}^{6} I_{zzi} & 0 & \sum_{i=3}^{6} I_{zzi} & \sum_{i=4}^{6} I_{zzi} & \sum_{i=5}^{6} I_{zzi} & 0 \\ 0 & 0 & 0 & 0 & 0 & 0 \\ \sum_{i=3}^{6} I_{zzi} & 0 & \sum_{i=3}^{6} I_{zzi} & \sum_{i=4}^{6} I_{zzi} & \sum_{i=5}^{6} I_{zzi} & 0 \\ \sum_{i=4}^{6} I_{zzi} & 0 & \sum_{i=4}^{6} I_{zzi} & \sum_{i=4}^{6} I_{zzi} & \sum_{i=5}^{6} I_{zzi} & 0 \\ \sum_{i=5}^{6} I_{zzi} & 0 & \sum_{i=5}^{6} I_{zzi} & \sum_{i=5}^{6} I_{zzi} & \sum_{i=5}^{6} I_{zzi} & 0 \\ 0 & 0 & 0 & 0 & 0 & 0 \end{bmatrix} \dot{\boldsymbol{q}} \,. \tag{5.8}$$

Next, the potential energy for the reduced system was computed as the sum of the individual link potential energies. For each link, the potential energy was computed as simply its total mass multiplied by the gravitational acceleration $g \approx 9.81$ m/s^2 and the height of its centre of mass above the point A, which gave

$$\begin{aligned} V_1(\boldsymbol{q}) &= -m_1 g a_{c1} S_1 \\ V_2(\boldsymbol{q}) &= -m_2 g (q_2 - a_{c2}) S_1 \\ V_3(\boldsymbol{q}) &= m_3 g (-q_2 S_1 + a_{c3} C_{13} - b_{c3} S_{13}) \\ V_4(\boldsymbol{q}) &= m_4 g (-q_2 S_1 + d_2 C_{13} - a_{c4} C_{134} + b_{c4} S_{134}) \\ V_5(\boldsymbol{q}) &= m_5 g (-q_2 S_1 + d_2 C_{13} + d_3 C_{134} + a_{c5} S_{1345}) \\ V_6(\boldsymbol{q}) &= m_6 g (-q_2 S_1 + d_2 C_{13} + d_3 C_{134} + (q_6 - a_{c6}) S_{1345}) \,. \end{aligned} \tag{5.9}$$

Thus, the total potential energy was

$$V(\boldsymbol{q}) = \sum_{i=1}^{6} V_i(\boldsymbol{q}) \,. \tag{5.10}$$

Inertia Matrix

By equation (5.1), the inertia matrix was formed by adding the matrices computed above, such that

$$\boldsymbol{D}(\boldsymbol{q}) = \sum_{i=1}^{6} m_i \boldsymbol{J}_{v_{ci}}^T(\boldsymbol{q}) \boldsymbol{J}_{v_{ci}}(\boldsymbol{q}) + \boldsymbol{\Omega} \tag{5.11}$$

Carrying out the above multiplications and using standard trigonometric identities led to expressions for the entries of the inertia matrix $\boldsymbol{D}(\boldsymbol{q})$, containing the d_{kj} of equation (3.3) on page 25.

Christoffel Symbols, Potential Terms, and Equations of Motion

The Christoffel symbols $c_{ijk}(\boldsymbol{q})$, embedded in equation (3.5) on page 26, were computed using the definition

$$c_{ijk}(\boldsymbol{q}) \triangleq \frac{1}{2}\left(\frac{\partial d_{kj}}{\partial q_i} + \frac{\partial d_{ki}}{\partial q_j} - \frac{\partial d_{ij}}{\partial q_k}\right). \tag{5.12}$$

Although a number of the computed Christoffel symbols were zero, the results of even non-zero computations are not shown here for brevity. Instead, these computations are printed in appendix B.2 on page 139.

The potential functions ϕ_k defined in equation (3.6) on page 26 were computed, but again, are not shown here for brevity. These potential functions may be found in appendix B.3 on page 146.

Finally, equations of motion for the reduced system were formulated. These differential equations are not printed here since their inclusion would not enhance the content of this dissertation. According to equation (3.3), they are composed of the terms printed above and in appendix B. Additionally, it should be noted that a computer algebra package was used to assist in the derivation of resulting reduced system equations of motion.

5.1.2 Holonomic Constraints

Beginning with the holonomic loop closure constraints, expressions for the reduced system joint angles q_1 and q_3 were computed from geometry, and were given by

$$q_1 = \pi - \varepsilon_1 - \arccos \mathcal{A} \tag{5.13}$$

$$q_3 = \frac{3\pi}{2} - \varepsilon_2 - \arccos \mathcal{B} \tag{5.14}$$

where

$$\mathcal{A} = \frac{d_5^2 + q_l^2 - d_1^2}{2\,d_5 q_l}$$
$$\mathcal{B} = \frac{d_1^2 + q_l^2 - d_5^2}{2\,d_1 q_l}.$$

As a result of the four-bar linkage structure that existed due to the placement of the dump cylinder, between the bucket and vehicle body, computation of holonomic constraints for the joint angles q_4 and q_5 became more complicated. Consider the four-bar linkage structure formed by points $FCDE$ in figure 5.2. The variable ρ was selected to represent the distance $\overline{CE}$, also a function of the lift cylinder length q_l. By the law of cosines

$$\rho = \left(d_4^2 + d_8^2 - 2\,d_4 d_8 \cos(3\pi - 2\,\varepsilon_1 - \varepsilon_2 - \varepsilon_3 - \varepsilon_5 - q_1 - q_3)\right)^{\frac{1}{2}}. \tag{5.15}$$

Next, again utilizing the law of cosines

$$q_4 = \pi + \varepsilon_4 - \arccos\mathcal{D} - \arccos\mathcal{E} \tag{5.16}$$
$$q_5 = \frac{\pi}{2} - \arccos\mathcal{F} \tag{5.17}$$

where

$$\mathcal{D} = \frac{\rho^2 + d_3^2 - q_t^2}{2\,\rho d_3}$$
$$\mathcal{E} = \frac{\rho^2 + d_8^2 - d_4^2}{2\,\rho d_8}$$
$$\mathcal{F} = \frac{d_3^2 + q_t^2 - \rho^2}{2\,d_3 q_t}.$$

The holonomic velocity constraints corresponding to the joints q_l and q_d were found by their equivalency to the time derivatives of equations (5.13), (5.14), (5.16), and (5.17). If the elements of the Jacobian matrix $\boldsymbol{G}$ of equation (3.8) on page 27 are denoted by g_{ij}, then

$$\boldsymbol{G} = \frac{\partial \boldsymbol{f}(\tilde{\boldsymbol{q}})}{\partial \tilde{\boldsymbol{q}}} = \begin{bmatrix} g_{11} & 1 & g_{31} & g_{41} & g_{51} & 0 \\ 0 & 0 & 0 & g_{42} & g_{52} & 1 \end{bmatrix}^T. \tag{5.18}$$

Derivation of the acceleration constraints corresponding to the joints q_l and q_d required the computation of the time derivative of the velocity constraint Jacobian, as per equation (3.9) on page 27. If the individual elements of $\dot{G}$ are denoted by $\dot{g}_{ij} = \frac{d}{dt} g_{ij}$, then

$$\dot{G} = \begin{bmatrix} \dot{g}_{11} & 0 & \dot{g}_{31} & \dot{g}_{41} & \dot{g}_{51} & 0 \\ 0 & 0 & 0 & \dot{g}_{42} & \dot{g}_{52} & 0 \end{bmatrix}^T . \tag{5.19}$$

5.1.3 Closed-chain Mechanism Dynamics

Given the reduced system dynamics and the holonomic loop closure constraints worked out above, the closed-chain mechanism dynamics were subsequently computed through application of the generalized actuating force transformation that relates the closed-chain mechanism dynamics to the reduced system dynamic model, after the technique developed in chapter 3. Furthermore, since the resulting analytical model did not consider the effects of damping or friction in the actuators, it was necessary to include additional terms in an attempt to account for these effects (e.g. $c_l\dot{q}_l$ and $c_d\dot{q}_d$ damping terms). The resulting nonlinear differential equations were complex, having many terms as was expected, necessitating the assistance of a computer algebra package to aid in their development.

Steps were taken to simulate the dynamical equations using a numerical integration routine in the MATLAB® technical computing environment. It was quickly discovered that this process would involve further complications, namely the translation of equations into the appropriate computer code, the occurrence of joint singularities, and the adaptation of experimental data for use as actuator input values. Consequently, it was decided not to tackle these issues in accordance with the bigger picture, since these equations only consider free-space motion of the LHD mechanism.

Although numerical simulations were not attempted, it was felt that communication of the steps taken towards computation of the closed-chain mechanism dynamics

was a worthwhile exercise, as well as complementary to the problem at hand.

5.2 Modelling Alternatives

The analytical approach of section 5.1 considered modelling only the LHD loader mechanism, without consideration for any interaction with its environment, namely a rock pile. In order to have any usefulness towards the problem of autonomous excavation, the given analytical model would have to be extended to include external forces acting on the bucket link. From a mechanical system modelling perspective, this extension would be relatively straight forward in that generalized forces, more specifically their corresponding influence on the chosen coordinates, need simply be appended to the model of section 5.1. This is illustrated in figure 5.4, where $\boldsymbol{f}_a$ represents the vector of externally applied actuator forces, $\boldsymbol{f}_r$ denotes the vector of resistive forces to excavation, and $\boldsymbol{x}$ is the machine state. However, the problem of how to compute, for the purpose of modelling, the forces of resistance during excavation remains unresolved. In section 2.2, it was noted that various empirical and analytical studies have been conducted with the intent of resolving such interaction forces from a mixed set of excavation parameters. For example, consider the work of Takahashi et al. [102, 105], where resistive forces during excavation were computed analytically using assumed geometric and frictional parameters of the bucket and rock pile.

In the subsections that follow, a distinct element method (DEM) and artificial neural networks are considered briefly as two possible approaches to the problem of bucket-rock interaction modelling.

5.2.1 Distinct Element Method

The distinct element method (DEM), after Cundall and Strack [14], entails construction of a numerical model capable of describing the mechanical behaviour of collections

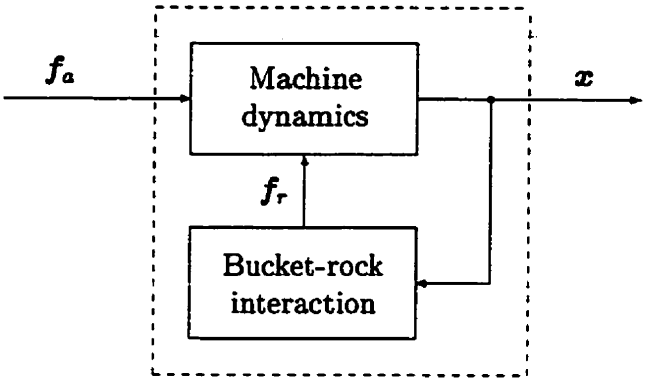

Figure 5.4: A block model for the machine excavation process

of particles, modelled as discs (or spheres in three dimensions). The computational scheme is based on an application of Newton's second law to each individual particle (i.e. disc or sphere), in conjunction with a force-displacement law describing the particle to particle contact forces. Hence, the force-displacement law is used to find particle interaction forces from displacements, while Newton's second law computes the motion of each particle based on the contact forces that act on it.

In reality, the force-displacement law is meant to represent the deformation of individual particles while in forced contact with each other. However, for the purpose of assembly simulation, the particles are simply allowed to overlap one another at contact points. It should be noted, however, that the magnitude of overlap is to be very small in comparison with the individual particle sizes. The resulting contact force is then computed to be in direct proportion with the degree of overlap, as though there existed a spring-type element, connecting the two particles, that acts only in compression. Likewise, a damping element may be added to the model, which again, acts only when the particles are in contact. Models may be constructed to act similarly in both normal and tangential directions of contact, so as to imitate both normal and shear forces acting on each particle, although allowing the variation of parameters to dictate the specific force-displacement relationship in each direction. For arithmetic details of the algorithm, the reader is referred to [14, 101].

As was mentioned in chapter 2, the DEM of Cundall and Strack was conceived for the purpose of modelling granular assemblies having very small particle sizes, at least in relation to the fragmented rock piles described in chapter 4. Nonetheless, the technique was recently applied by Takahashi [101] to simulation of particle behaviour in a *virtual* rock pile. Unfortunately, since the experimental data Takahashi used to validate the DEM model was derived from laboratory scale trials, the constructed DEM model used a particle diameter of only 12 mm. In addition, the model employed a uniform particle size, as well as a predetermined (or prescribed) motion for the excavator bucket. As a result, there remains much room for improvement and extension of the DEM approach to modelling bucket rock interaction forces. For example, consider the use of a DEM model to act as the block titled "Bucket-rock interaction" of figure 5.4. Ideally, the Lagrangian model of section 5.1 could be extended, as previously discussed, and subsequently used as the block titled "Machine dynamics" of figure 5.4. Through combination of the two models in such a way, the simulations performed by Takahashi [101] could be appropriately extended to include the machine dynamics, and the fact that a system for autonomous excavation would necessitate determining the required actuator inputs to overcome bucket-rock interaction forces.

Further to including the machine dynamics, the DEM model could be improved by selecting assemblies of particles having varying sizes, as is typical to the average fragmented rock pile. In fact, there exist already well established techniques for describing particle size distributions for piles of fragmented rock. For example, the Rosin-Rammler equation has been used for blasting analysis [38], which uses techniques from the field of mineral dressing, and has the form

$$R = 1 - e^{-\left(\frac{d_s}{d_c}\right)^n} \tag{5.20}$$

where R is the fraction of material less than the diameter d_s, the constant d_c is called the *characteristic size*, and n is a constant called the *uniformity index*. Therefore, through adjustment of the characteristic size and uniformity index parameters, var-

ious rock pile distributions could be developed, possibly based on actual rock pile measurements, for use in defining a collection of particles to be employed in DEM modelling.

Integration of the above suggested improvements with the available experimental data reported in chapter 4 could provide one alternative to modelling the excavation process. However, some disadvantages of the DEM approach include its numerically intense nature, and the fact that the technique would only be useful in offline simulations, providing little additional knowledge that might be incorporated into a potential controller for autonomous excavation.

5.2.2 Artificial Neural Networks

Another possible approach to modelling the excavation process, whether simply the LHD loader mechanism or the entire excavation process, lies in the application of artificial neural networks. Such neural networks refer to the formulation of systems whose central theme is borrowed from the analogy of biological neural networks [60]. Essentially, artificial neural networks, similar to biological neural networks, consist of an interconnected collection of nodes (analogous to neurons), where each node performs some simple computation over its inputs, or more commonly over the sum of its inputs. Inputs (analogous to synapses) are in turn weighted (analogous to synaptic efficiency) and interconnected based on the desired network function, through a training (analogous to learning) procedure.

Perhaps the most common of the artificial neural network architectures is the multilayer feedforward network where training is accomplished through application of the least mean squared algorithm known as *backpropagation*, popularized by Rumelhart et al. [83]. In the context of applied science and engineering, such artificial neural networks have been utilized for robot control, vehicle control, and even the identification of robot inverse kinematics [60]. In fact, in their work, Shi et al. [90, 91]

employed the backpropagation algorithm to the problem of autonomous excavation, by training their finite-state machines (see section 2.1) for individual tasks based on data collected from observed human operator actions.

Advantages of the artificial neural network approach, in the task of modelling nonlinear systems, lie in its intrinsic simplicity and the ease by which training of the network may be accomplished. There exist, however, several difficulties and disadvantages to the use of neural networks. Firstly, selection of the network structure (i.e. number of layers and nodes per layer) is often arbitrary, often selected by trial and error. Secondly, there exist issues surrounding error convergence to a global minimum and the ability of a given network to generalize. Perhaps most notably, once a network has been developed and identified, there exist no real means by which significance may be attributed to its structure or the values of its connection weights, providing little insight as to the physical nature of the identified process.

5.3 Parallel Cascade Identification

It was decided that an effort to employ the method of parallel cascade identification (PCI) for nonlinear systems might be a worthwhile mission, since the system to be modelled (i.e. the observed excavation process) seemed to fit the criteria communicated by Korenberg in [44]. Furthermore, it had been reported recently that a SISO version of the PCI algorithm had been used successfully by Eklund and Korenberg [19, 20] to simulate aircraft pilot flight controls, having a dynamic model similar in nature to the LHD loader mechanism. Although the analytical model used to represent the flight control system used by Eklund and Korenberg [20, page 74] was markedly less complex than the system described by the proposed Euler-Lagrange equations of section 5.1, it was noted that the PCI algorithm had no troubles identifying even significant hysteresis nonlinearities [19, page 83] in the system.

Moreover, as opposed to the DEM and artificial neural network approaches described in the previous section, a PCI model that could describe the LHD loader mechanism and resulting bucket-rock interactions would have a known internal structure, and hence yield information that might be exploited towards the development of a control system for autonomous excavation. At the very least, an accurate and easily applicable tool would become available for analysis and possibly simulation during controller design.

5.3.1 Algorithm Implementation

A multiple-input/single-output (MISO) version of the PCI algorithm was implemented in the C programming language on a PC having a 450 MHz Pentium II processor and 384 MB of RAM. The C language code was compiled, using a Microsoft 6.0 C/C++ compiler, and called as a dynamically linked library (DLL) for use in the MATLAB® (version 5.3.129215a, release 11.1) technical computing environment, via a proprietary MATLAB application program interface (API). The reason for the use of a C language routine, or so-called C language MEX-file [58], was to circumvent the severe computational bottlenecks (e.g. `while`- and `for`-loops) that do not run fast enough in MATLAB. The resulting C language MEX-file was named suitably `PCI.dll`.

For the most part, the PCI algorithm was coded as it was described previously, in chapter 3, and in the manner published by Korenberg [44]. However, there were some extensions included in the final implementation, not mentioned in chapter 3, which should be noted. Firstly, up to third-order cross correlations were employed (the flight control system model of Eklund and Korenberg [19, 20] was found to require only first-order cross-correlations), resulting in the use of

$$\phi_{xxxy_{i-1}}(j_1, j_2, j_3) \triangleq \overline{y_{i-1}(n)x(n-j_1)x(n-j_2)x(n-j_3)} \tag{5.21}$$

in addition to equations (3.28) and (3.29) on page 33, and subsequently the possible selection of the impulse response for the linear system $h_i(j)$ from

$$q_4(j) = \phi_{xxxy_{i-1}}(j, A_1, A_2) \pm C\delta(j - A_1) \pm C\delta(j - A_2) \tag{5.22}$$

in addition to the functions $q_1(j)$, $q_2(j)$, and $q_3(j)$. In equation (5.22), A_1 was selected from the integer set $\{0, 1, \ldots, R\}$ and A_2 from the integer set $\{A_1, (A_1 + 1), \ldots, R\}$, the sign of each δ-term was chosen at random, and the constant C was computed using equation (3.32) on page 34. Since multiple inputs were allowed, the previously described rules for extension to MIMO systems applied. In particular, cross-correlations of the residue $y_{i-1}(n)$ with the elements of the input vector $\boldsymbol{x}(n)$, as was illustrated in equation (3.42) on page 37, were applied in a similar fashion to third-order cross-correlation calculations.

It was also necessary to limit the number cascade paths allowed in the developed model, so that the number of identified parameters did not exceed the number of data points available for training. Consider that in each cascade, the sum of dynamic linear impulse response parameters and static nonlinear polynomial coefficients totals $(R + M + 2)$ parameters. If there are I cascades in a PCI model, then $I(R + M + 2)$ parameters are identified in total. Although this total number of parameters may not represent the total number of *independent* parameters, it does place an upper bound on the number of possible independent parameters. Therefore, it was ensured that $I(R + M + 2) < (N - R + 1)$, which placed a limit on the number of cascades allowed in the model, such that

$$I < \left\lfloor \frac{N - R + 1}{R + M + 2} \right\rfloor . \tag{5.23}$$

As a means of avoiding numerical overflow from the computation of high-order polynomial terms, it was decided to normalize the input signals to have unity average absolute value over the range of data. Furthermore, the output $u_i(n)$ from each dynamic linear element L_i, which formed the input to a corresponding static nonlinear

element N_i, was also scaled to have unity average absolute value over the interval $n = R, (R+1), \ldots, T$, after the example of Eklund and Korenberg [20]. These scaling procedures were necessary in particular when the inputs to the system to be identified were hydraulic cylinder forces, having a magnitude on the order of 10^5 N.

It is often the case that a model may be improved by including recently past values of the output as an additional input signal. For example, if a system has an input $x(n)$ and an output $y(n)$, a new model may be constructed that has two inputs, namely $x_1(n) = x(n)$ and $x_2(n) = y(n-1)$, and one output $y(n)$ [44]. The option to extend the algorithm to perform this function was incorporated into the `PCI.dll` routine. However, it should be noted that stability of the resulting model was found to be no longer guaranteed with the inclusion of output feedback, as one might have expected. Therefore, to reduce the chance of possible instability, the polynomial order was limited to a maximum of $M = 2$ for cascades that utilized a time delay of the output as input.

Since the intended function of the modelling process was to identify a general model for the system at hand, and not simply memorize a particular set of input/output data, the option was provided in the `PCI.dll` routine to include multiple data sets for training, as is typical in the training of artificial neural networks. This was done by inserting marker points (specifically, data points having a value of 1 000 000) between distinct data sets, which the routine used to recognize the start of a new data set and when to subsequently jump $(R+1)$ steps forward in time.

While the C language code that forms the source for `PCI.dll` is not fully disclosed in this dissertation (as it totalled over 900 lines), the pseudo-code of figure 5.5, written in a C programming style, illustrates the elementary framework of the C language MEX-file source code for the described `PCI.dll` routine. The ellipses "..." mark the omission of large segments of code not necessary to understanding the intended general message of the figure. Note that the `while`-loop was allowed

to continue until either the computed model MSE (denoted e) was less than some desired MSE threshold (denoted MSE), the maximum number of possible cascades had been exceeded, or the number of tried cascade candidates had exceeded 500. It was typical in practice to set the fixed value of MSE to a sufficiently small number, so as to allow the algorithm to try a significant number of possible cascade candidates during system identification.

Once the source code had been compiled as a MEX-file for MATLAB, it was available for use as a function from within the MATLAB technical computing environment. The calling syntax for PCI.dll from within MATLAB was

```
[yApci,yBpci,mseA,mseB,I] = pci(xA,yA,xB,yB,MSE,R,M)
```

where xA and xB were the matrices composed of input vectors for training and testing respectively, yA and yB were the vectors of output data for training and testing respectively, MSE was the target mean-squared error[3], the integers R and M were the specified memory length and polynomial order respectively, yApci and yBpci were the identified PCI model outputs for training and testing respectively, mseA and mseB were the computed mean-squared errors for training and testing, and I was the number of cascades in the identified model. Note that PCI.dll was intended only to implement the PCI algorithm for the purpose of validating the application of PCI to modelling of the LHD loader mechanism and possibly the excavation process. Modifications and/or further coding would be required in order to extract the identified model parameters for subsequent simulations.

Prior to use in modelling of the LHD loader mechanism and the excavation process, the PCI.dll routine was tested on a contrived data set, representative of an invented nonlinear system. The test system was a MISO nonlinear difference equation, derived through modification by the candidate of a SISO nonlinear difference equation that

[3]In all cases, mean-squared error was computed as a percent of the output signal span.

```
#include "mex.h"    // Include the MATLAB MEX-function header.

void pciFunction( ... )
{
    /* The function pciFunction() performs parallel cascade
    identification, building a model based on the algorithm. */

    int i = 0;      // Cascade counter.
    int stop = 0;   // Iteration counter.

    /* Add parallel cascades while conditions are satisfied. */
    while( ( e > MSE ) && ( i < (R + M + 2)/(T - R + 1) )
        && ( stop < 500 ) ) {

        i++;        // Increment the cascade counter.
        stop++;     // Increment the iteration counter.

        /* For each time delay find a delta response. */
        for( r = 0; r < (R + 1); r++ ) {
            ... ;
        }

        /* Compute polynomial coefficients. */
        for( m = 0; m < (M + 1); m++ ) {
            ... ;
        }

        /* Check statistical benefit of cascade. */
        e = ... ;
        if( benefit == false )
            i--;    // Decrement the cascade counter.
    }
}

void mexFunction( int nlhs, mxArray *plhs[],
                  int nrhs, const mxArray *prhs[] )
{
    /* The function mexFunction is the gateway (application
    program interface) routine for MATLAB. */
    ... ;
}
```

Figure 5.5: Pseudo-code illustrating the elementary structure of the C language MEX-file written to implement PCI for use in MATLAB

was borrowed by Korenberg [44, page 443] from McIlroy [59], who employed the said difference equation to model a simulated communications channel. The newly invented system, with input $\boldsymbol{x}(n) = [x_1(n)\ x_2(n)]^T$, was the nonlinear difference equation

$$\begin{aligned} y(n) &= -0.636507 + 1.08717x_2(n-24) + 0.914799x_1^2(n-23) \\ &\quad - 0.698645x_2(n-27) + 0.967739x_2^2(n-25) + 0.787682x_1(n-22) \\ &\quad - 0.630834x_1^3(n-28) + 0.160929x_2(n-30) - 0.209741x_2(n-32) \\ &\quad + 0.397268x_1^5(n-21) - 0.117377x_1(n-29) - 0.49215y(n-2) \\ &\quad + 0.114922y^2(n-5) + 0.129476x_1(n-24)x_1(n-23) \\ &\quad + 0.211136y^2(n-1) - 0.152675x_2(n-24)y(n-6)\,. \end{aligned} \tag{5.24}$$

Using inputs chosen arbitrarily to be of the form

$$x_1(n) = \sin(0.05n)\cos(0.0808n - 0.052) \tag{5.25}$$

$$x_2(n) = \sin(0.033n)\sin(0.025n - 0.08) \tag{5.26}$$

for $n = 1, 2, \ldots$, two sets of input/output data were computed, for training and testing, each 1000 points long. The two sets were then passed as arguments, along with various combinations of memory length and polynomial order, to the `PCI.dll` routine.

Figure 5.6 shows[4] the outcome of one attempt to model the contrived system using equations (5.25) and (5.26) as inputs, plus output feedback. The resulting model had 22 cascades, each with a memory length $R = 35$ and a polynomial order $M = 5$ (except those with output feedback, where the polynomial order was restricted to $M = 2$). The computed MSE for the training data shown in figure 5.6(a) was 0.0457 % over the output span, and the corresponding MSE for the testing data shown in figure 5.6(b) was 0.1382 %. In fact, modelling outcomes were generally successful

[4] In all such figures, the dashed line denotes the PCI model output.

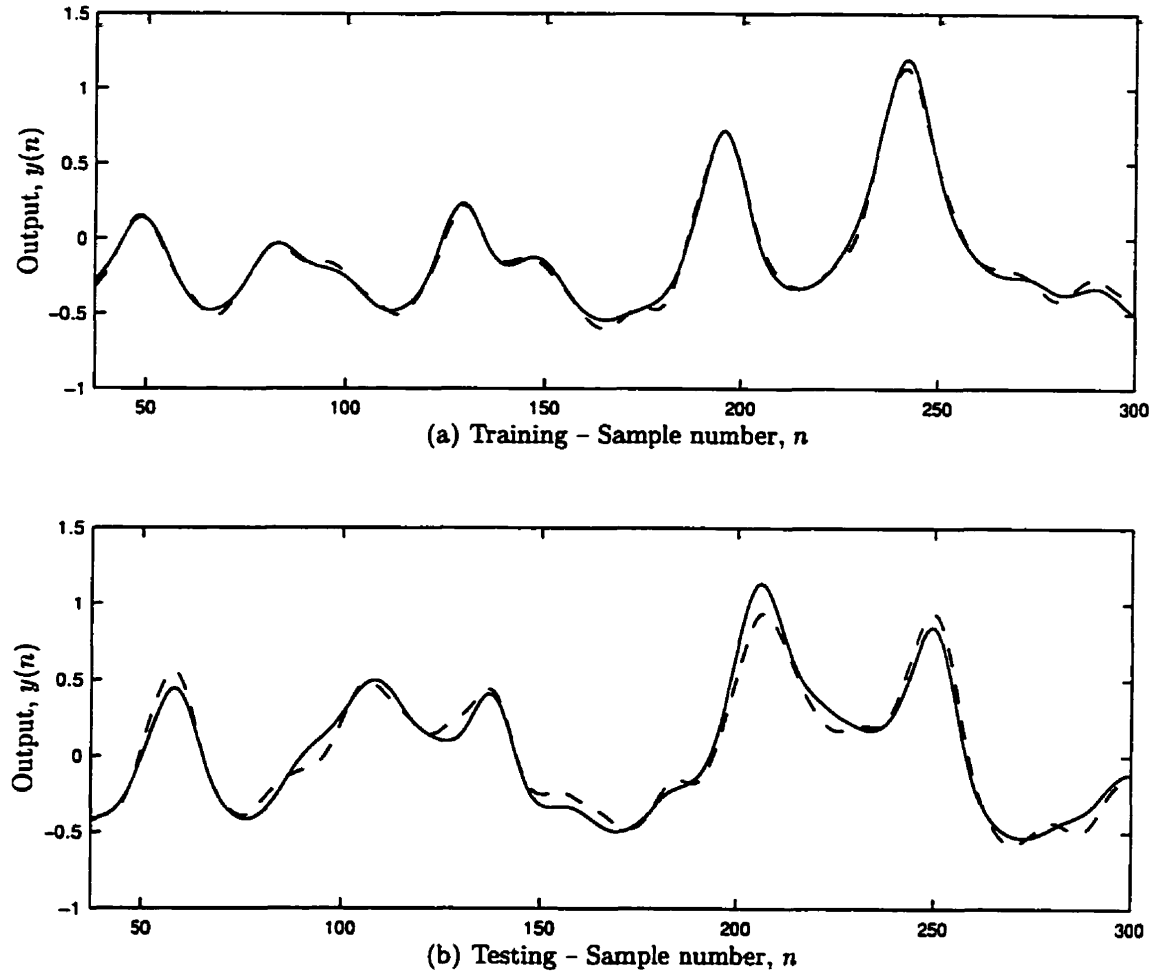

Figure 5.6: Results of PCI (dashed) on contrived data computed from equation (5.24)

even without the inclusion of output feedback. In further testing, random noise was superimposed on input and output data, so as to determine the PCI algorithm's ability to reject uncorrelated noise. Figure 5.7 presents the results of one modelling attempt where random noise having a magnitude in the range of ± 1.00 (relatively significant in relation to the output signal magnitude) was superimposed on the training output data. Note that the algorithm had no problem successfully modelling the testing data, as shown in figure 5.7(b), achieving a MSE of 0.448 % (3 cascades, $R = 35$, $M = 4$, with no output feedback). These results, and others of the sort, confirmed that the encoded `PCI.dll` routine was indeed functioning as intended.

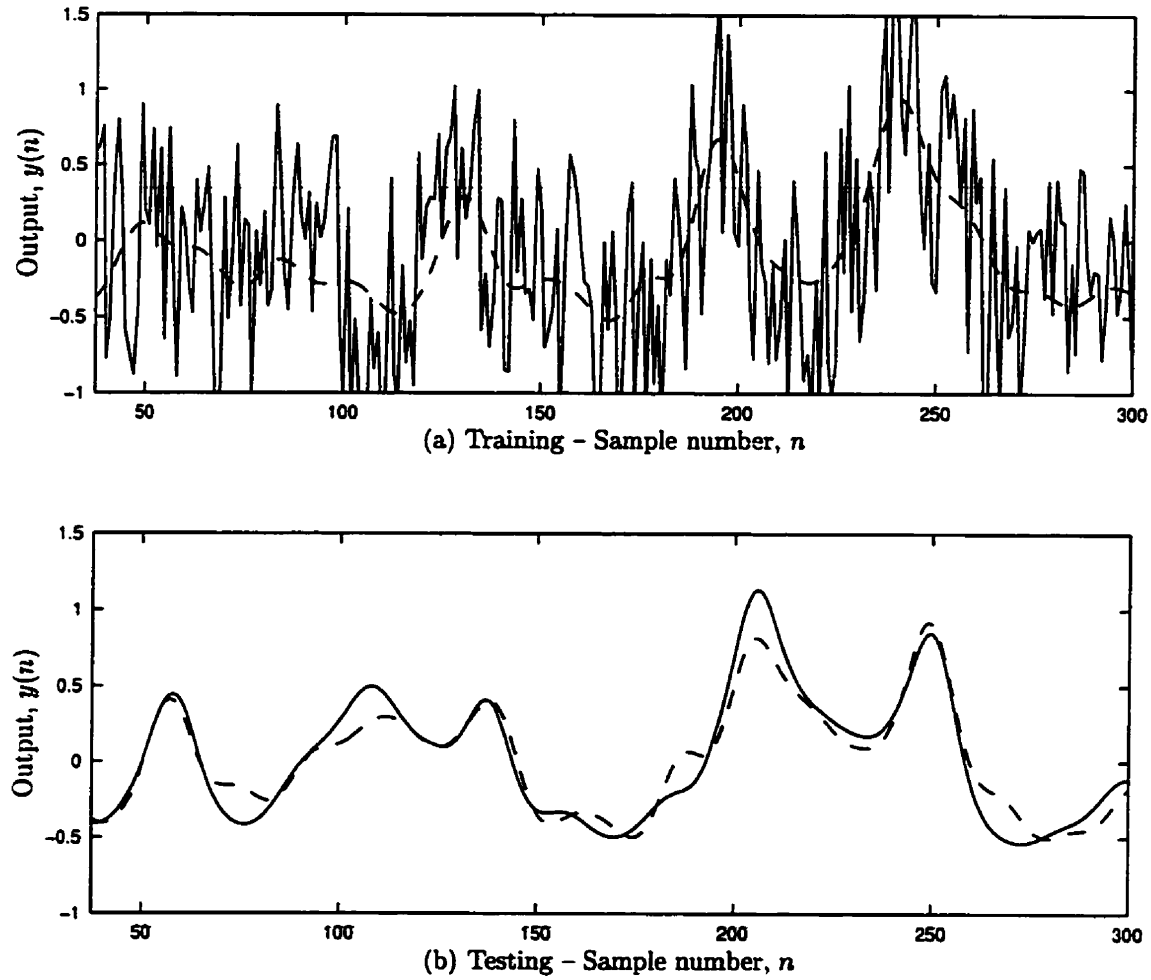

Figure 5.7: Results of PCI (dashed) on contrived data with noise superimposed on the training set output

5.3.2 Model Identification Scenarios

Even though a number of potential PCI modelling scenarios were possible, the following two categories represent the most relevant of those considered. Both presented scenarios endeavoured to model MIMO systems, since in reality the motions of lift and dump cylinders were dependent upon the forces at both cylinders.

Scenario (A): Forward Dynamics in Free Space. Both lift and dump cylinder data were used to model the forward dynamics of the LHD loader mechanism in free space. In this case, cylinder forces were used as inputs, and each cylinder velocity (differentiated length) output was modelled by a separate (i.e. MISO) PCI model. For these modelling attempts, there was no rock pile or other environmental interaction. Moreover, to avoid further nonlinearity complications, only cases where the lift and dump cylinders did not reach their extension limits were considered. The employed input/output data was similar to the representative motions shown in figure 4.9 on page 54.

Scenario (B): Aggressive Excavation. Both lift and dump cylinder data from the aggressive excavation trials, presented in chapter 4, were used in an attempt to identify the excavation process in fragmented rock. Again, cylinder forces were used as inputs, and each cylinder velocity output was modelled by a separate parallel cascade model. Only data from trials conducted by operator (II) were utilized, in order to avoid possible complications due to variations in operator style[5].

Although, as described in chapter 4, the hydraulic cylinder *lengths* were measured at each sampling interval and not the corresponding cylinder extension velocities, both scenarios described above utilized velocity as the output to be modelled. The

[5]The impact of varying operator styles on modelling and identification of the excavation process was a factor not investigated in this research.

reasoning behind this was twofold: (i) in view of Newton's Second Law, one might expect input forces to be more directly related to velocity as opposed to position, and; (ii) integration of resulting motions seemed to provide a more smooth and consistent result for comparison with the measured position data. Therefore, prior to system identification, the derivative of position data was computed using a first-order finite divided difference approximation [11, page 93]. Subsequent integrations were performed by a cumulative trapezoidal numerical integration routine [11, page 478].

The inverse dynamics problem was not considered since for the data collected, if one presumes that it is the application of cylinder forces that results in cylinder motions and not the converse, this situation would represent a system that is not causal in nature. However, for the aggressive excavation trials, it is entirely plausible that external forces on the mechanism result in motions of the boom and bucket links (no matter how small), which in turn cause possibly significant changes in the measured cylinder forces. In fact, it is this postulate that forms a basis for the reactive control schemes proposed in the reviewed patents [15, 77] of chapter 2. By this rationale, the PCI algorithm may not be as applicable as originally thought.

5.3.3 Synopsis of Identification Results and Observations

During this research, various other modelling scenarios were also attempted. Nevertheless, the described scenarios (A) and (B) of the previous subsection provided sufficient results for the purposes of this dissertation.

Scenario (A): Forward Dynamics in Free Space

The free-space motion trial data of section 4.2.2 was employed to fit PCI models using the `PCI.dll` routine under the definition of scenario (A). The results of one such attempt at modelling of the lift cylinder motions is shown in figure 5.8(a), subsampled

to a 35 Hz sampling rate[6]. The resulting PCI model (4 cascades, $M = 7$, $R = 100$) fit the output velocity with a MSE of 1.71 %, having been trained on three sets of free-space motion trial data. Notice the noise due to numerical differentiation in the actual velocity data. As was seen previously in section 5.3.1, the PCI algorithm should have been capable of successful system modelling, even in the presence of such noise. Figure 5.8(b) shows the outcome of integrating the velocity output shown in figure 5.8(a). Note that (here, and in all subsequent examples) as integration proceeded in time the velocity output PCI model errors were also integrated, resulting in a cumulative cylinder position error.

It should also be noted that there were dump cylinder motions taking place at the same time as the lift cylinder motions shown in figure 5.8. Figure 5.9(a) presents the results of one attempt to model the dump cylinder motions, concurrent to the lift cylinder motions above. The ensuing model (4 cascades, $M = 5$, $R = 100$) had a MSE on the testing data of 3.04 %, almost twice the magnitude of the lift cylinder PCI model. Like the model depicted in figure 5.8, training was done using three sets of trial data, subsampled to 35 Hz. Similarly, figure 5.9(b) shows the outcome of integrating the corresponding model velocity output to determine the cylinder length.

Several observations were made with regards to the results achieved in figures 5.8 and 5.9. Firstly, no output feedback was used for the models shown, since the inclusion of output feedback did not significantly improve the results, and simply led to frequent instability of the system. In both cases, since there existed a plurality of random choices to be made during the identification process, it often took several iterations of the PCI algorithm before a model with near acceptable performance was obtained. This was particularly so in dump cylinder system identification. In modelling the contrived data of section 5.3.1, a successful model was achieved at virtually every try. Note that polynomial orders of $M = 7$ and $M = 5$ were used,

[6]Signal aliasing became a possibility, however, this issue was simply ignored.

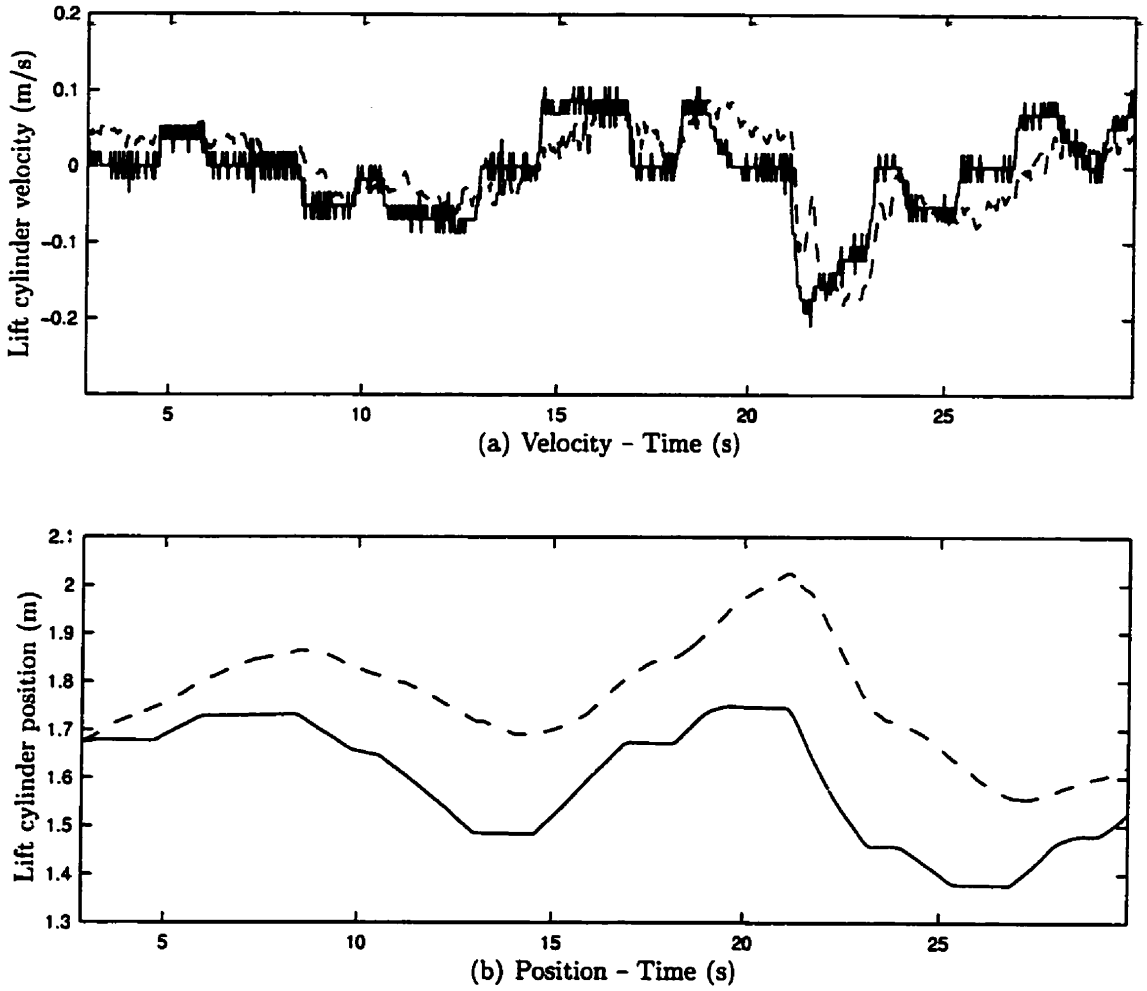

Figure 5.8: Modelling of lift cylinder motions using the PCI (dashed) algorithm

respectively, in the models shown. It was determined that other polynomial orders near to, or less than, these values would typically function as well. However, selection of $M > 9$ tended to cause velocity spikes to show up in the model output, resulting in even larger model errors when integrated. The time-step delay of $R = 100$ used in both examples corresponded to a real time-delay of approximately 2.9 seconds. It was found that variation of the time delay, to even a large extent (even ± 50 %), did not have a significantly observable impact on the system identification outcome.

As was stated previously, for the dump cylinder, a particularly large number of iterations of the PCI algorithm were necessary before a model with near acceptable

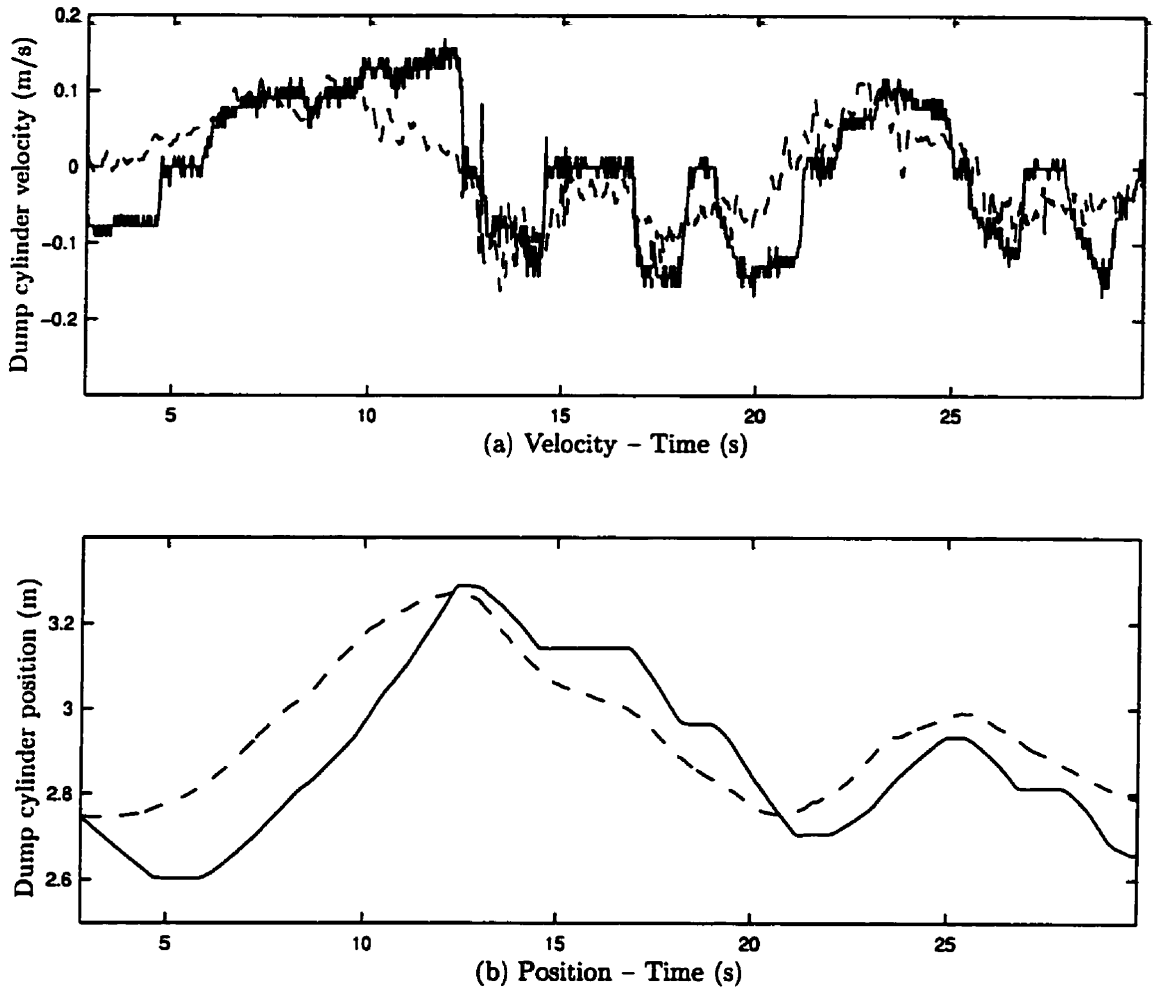

Figure 5.9: Modelling of dump cylinder motions using the PCI (dashed) algorithm

performance was obtained. Even the best of outcomes (e.g. figure 5.9) were not exceptionally good. It was discovered that PCI, in the implementation described, was unable to identify situations where the cylinder was not moving, and abrupt changes in the cylinder motions were not captured by the identification process. These observations were found to be essentially true for both dump and lift cylinder models. Admittedly, the dump cylinder might be considered a more complex nonlinear system in relation to the lift cylinders in that the lift cylinders are directly responsible for, and would impact most predominantly on, motions of only the boom link. Whereas, the dump cylinder itself, as was seen in section 5.1, closes the loop that forms a

four-bar linkage mechanism, causing the dump cylinder to depend more heavily on the configuration of the boom and bucket links combined. This train of thought led to contemplation of the possibility that PCI might be, in some respects, unsuitable to the problem at hand. This is discussed further in section 5.3.4. Nonetheless, it may be possible that PCI, with other variations and combinations in the parameters M,R, sampling rate, total number of samples, and number of training sets, might yield better results [45].

Scenario (B): Aggressive Excavation

Despite the fact that the free-space motion modelling of scenario (A) was only moderately successful, and that an attempt to include bucket-rock interactions into the equation would not likely improve the situation, modelling of the excavation process was attempted as per the definition of scenario (B). As was discussed in section 4.2.2, operators (I) and (II) had similar styles in that they chose to use only the dump cylinder, in combination with tractive effort, during aggressive excavation trials. Hence, figure 5.10 shows the outcome of one attempt to identify the excavation process through dump cylinder motions. The resulting PCI model (7 cascades, $M = 6$, $R = 10$) was again trained using three data sets, and tested on a fourth. The computed MSE on the testing data velocity output was a surprising 1.99 %. One possible reason for the relatively good result is that only the dump cylinder was used by the operator, as opposed to the command of a range of lift and dump cylinder motions, as was the case in scenario (A).

Identification of the aggressive excavation trials differed from the free-space motion trials above in that modelling success was found to be somewhat sensitive to the time-delay. The comparatively short time-delay (approximately 0.3 seconds) indicates that essentially present values of the cylinder forces were identified as being responsible for the motions shown. This makes some sense in that force/motion changes occurred

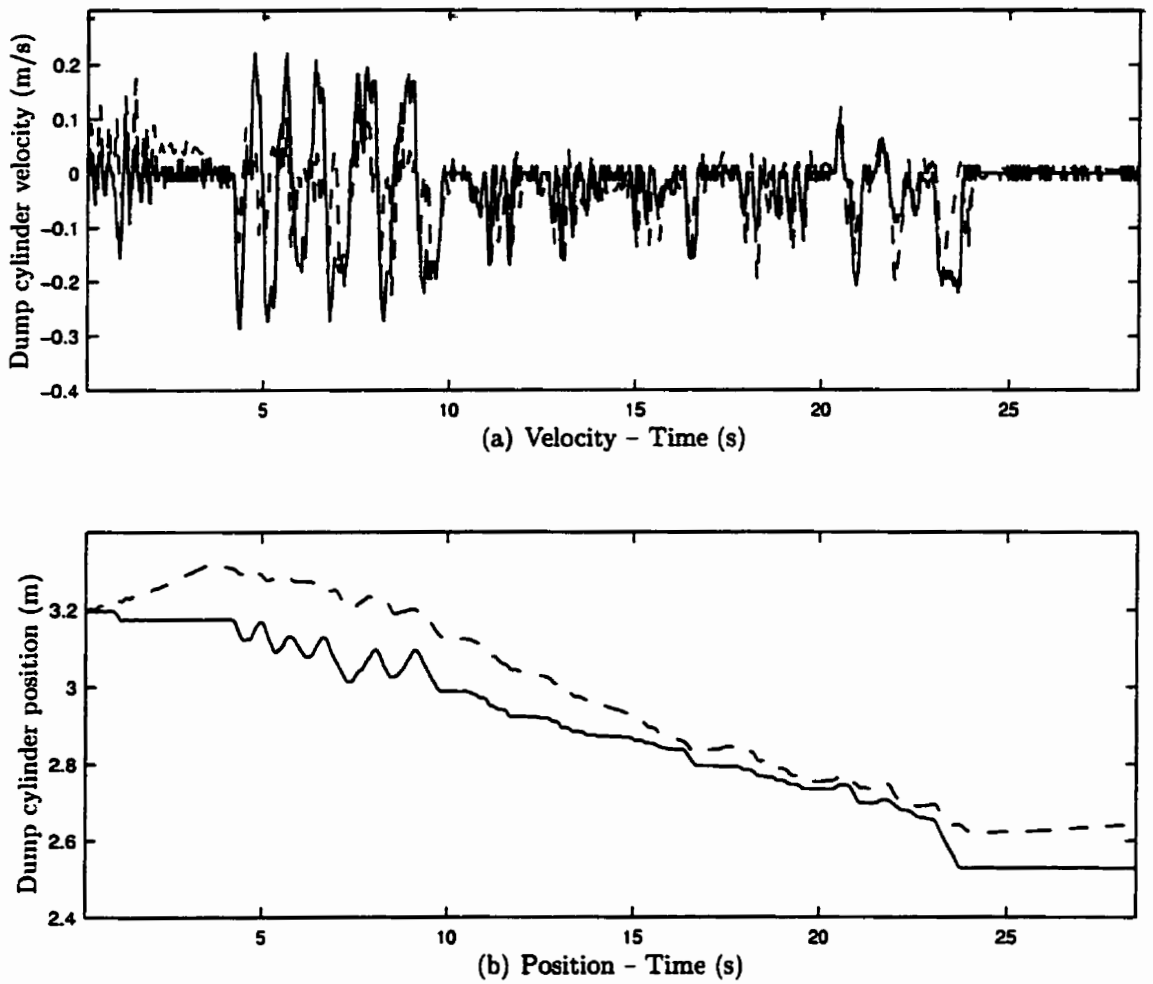

Figure 5.10: Modelling of dump cylinder motions during aggressive excavation operations using the PCI (dashed) algorithm

rapidly as the machine impacted the rock pile, and significant motions seemed to be relatively short in duration. One further point of interest is the fact that the PCI algorithm consistently chose to employ only dump cylinder forces as input (i.e. lift cylinder data was never incorporated into the model). Therefore, PCI reduced the problem to that of modelling only a SISO system. Such a result might indicate that, should only the dump cylinder be utilized for excavation, information concerning the excavation status may be described completely by a system that represents only the motions of that cylinder. Therefore, a control system for autonomous excavation

might only need to consider information feedback from the one actuating cylinder.

5.3.4 Remarks on Modelling Restrictions

Consideration of the fact that the LHD loader mechanism itself forms a somewhat complicated closed link structure, coupled with the only moderately successful results of attempts at system identification, led to deliberation of the possibility that approximation of the given system as a causal nonlinear system representable by a time-invariant, finite-order, finite-memory Volterra series may not be valid. Observation of the PCI implementation's inability to consistently cope with concurrent motions of the two hydraulic cylinders was of particular concern. Of course, some of the discussions that follow below should ideally have taken place prior to attempts at PCI modelling.

Firstly, there was no reason not to believe that sufficient approximation of the system might be achievable via a finite-order representation. Secondly, the potential issue regarding causality of the aggressive excavation trial data has been established previously. Since the aggressive excavation trial identification outcomes were relatively successful, one might assume that motions induced in the LHD loader mechanism due to bucket-rock interaction may have been sufficiently small in magnitude so as to be insignificant as far as the causality restriction is concerned.

However, the time-invariancy assumption is one that merits review. Mathematically speaking, a *time-invariant* system is one for which a translation in time of the inputs results in the same translation in time of the output. Although, envisioning the form of equations of motion for the LHD loader mechanism, the inertial coefficients for the system of links may vary with configuration, in the strictest sense, the system remains time-invariant. Consider that if the initial states are the same and chosen actuator force inputs are the same, then the output motions of the mechanism will always be the same no matter at what instant the forces are applied [12, page

89]. Therefore, the time-invariancy restriction for Volterra series representations is obeyed.

Nevertheless, there does remain one potentially serious issue. If the given mechanism is started in one particular configuration and a unique set of actuator inputs is applied, then a specific motion of the system would result. Then again, if the mechanism is started in a different configuration and the *same* unique set of actuator inputs is applied, then presumably different motions of the system would result. This is mainly due to the dependance of inertial and gravitational characteristics of the mechanism on its configuration. Therefore, in this sense, the outputs of the system will always depend on the initial conditions, a characteristic of systems possessing infinite memory[7]. This revelation might help to understand the results of subsection 5.3.3. From a qualitative viewpoint, the outcome of lift cylinder free-space motion modelling was most definitely better than similar attempts at modelling the dump cylinder motions. This observation might be rationalized by appreciating that lift cylinder motions were less dependent on the initial conditions, since the cylinder itself passed through only small changes in position and orientation in space. This was certainly true in comparison with motions of the dump cylinder, which formed one branch of a four-bar linkage system. As was noted previously, the results of modelling the dump cylinder motions while in contact with the rock pile were unexpectedly good. Though, this may be attributed to the fact that the lift cylinder was not moved at all during these trials, it is perhaps more due to the fact that motions of the dump cylinder were started at essentially the same configuration and passed through almost the same trajectory at each excavation iteration during model training.

In comparison with PCI modelling results corresponding to the contrived data of subsection 5.3.1, as well as its performance as reported by Eklund [19, 20], the

[7]However, this is not to imply that the system has infinite memory in the sense of its inputs.

overall outcome of attempts at excavation machine modelling was inferior. Yet, there exists a fundamental difference between the two stated successful applications and the modelling performed towards this thesis. In both stated successful cases, the data used for training and testing originated from pre-existing algebraic representations. Conversely, the system data identified in this dissertation was derived from *actual* force and position measurements acquired during full-scale experimental studies.

In summary, application of the PCI algorithm to the problem of modelling and identification of the systems that describe the LHD loader mechanism and the excavation process as a whole was attempted. Although the results might not be considered exceptional in that consistent modelling of fine motions and negligible modelling errors were not achieved, in comparison with the analytical approaches discussed earlier in this dissertation, the outcome was in fact a reasonably successful one. Moreover, the availability of developed PCI model structures was found to provide some further insight into the identified excavation processes.

Chapter 6

An Excavation Control Design

As was discussed in chapter 2, the control problem in autonomous excavation evidently requires an approach that is different than any of the well known strategies for trajectory control of industrial robot manipulators. Hemami [27] suggested that the excavator bucket trajectory should not have priority in the chosen control scheme, since the objective is to fill the bucket, and not follow some strictly specified path. The problem is further compounded by the complex nature of bucket-rock interactions, which result in the need for an innovative approach to automating the excavation process. Also, it was discussed in chapter 1 how the autonomous excavation problem may be regarded in its broadest sense to include the challenge of planning a higher-level excavation goal (e.g. excavate a particular area of specified size or volume). However, in this chapter, consideration is not given to the problem in this general sense. Rather, the problem was defined as one of how to select the appropriate actuator inputs so as to control the motion of the LHD loader mechanism to fill its bucket completely and reliably, without any need for operator intervention. Furthermore, only the scooping phase of excavation is considered within the problem scope, as it corresponds with relevant observations made from full-scale excavation and modelling studies.

Though the explicit mathematical formulation and implementation of a control

system for autonomous excavation of fragmented rock lies outside the scope of this dissertation, it was decided that formulation of a controller design concept, based on observations from experimental studies and modelling, would be a worthwhile contribution. Such is the intent of this chapter, which proposes the use of ideas from the field of compliant motion control.

6.1 Compliant Motion Control for Excavation

Controlling the mechanical interaction between a robot manipulator and its environment, such as in manufacturing assembly operations, has been a topic of many discussions in the robotics and control literature. The conceded shortcomings of pure position control in situations where environment interaction must take place have led to the development of techniques for control that lie generally under the label of *compliant motion control*, or sometimes *force control* [36, 39, 75, 98, 108]. Consider the classic example of a window-washing robot, where slight deviations in the manipulator trajectory under pure position control might cause the tool to lose contact with the window surface, or perhaps result in extremely large contact forces and impending disaster. Rather than attempt to follow a strictly specified trajectory, compliant motion control techniques are generally concerned with not only following a prescribed trajectory, but directly regulating the forces of interaction between the manipulator and its environment. One method, termed *impedance control* [36], focuses on the relationship between the manipulator velocity and the forces of interaction with its environment, a relationship that is typically referred to as *mechanical impedance*. In the Laplace domain, mechanical impedance $Z(s)$ may be represented (in one dimension) by the relation

$$Z(s) = \frac{f(s)}{v(s)} \tag{6.1}$$

where $f(s)$ is the environment interaction force and $v(s)$ is the manipulator tool (e.g. LHD bucket) velocity at the point of contact with the environment [98]. It is the task of an impedance controller to produce a response of the mechanism that corresponds to some prescribed impedance $Z(s)$. Therefore, impedance control considers the manipulator as a mechanical impedance, while the environment with which it is coupled is considered as a *mechanical admittance*. As one might expect, mechanical admittance $Y(s)$ may be represented by the relation

$$Y(s) = \frac{v(s)}{f(s)} \tag{6.2}$$

which is in fact the reciprocal of mechanical impedance [70, 89]. Hence, impedances may be seen as systems that accept motion and respond with a force, while admittances as systems that accept force and respond with motion. Hogan [36] argued that, as seen from the manipulator, the environment must be considered as a mechanical admittance, and not an impedance, since kinematically constrained inertial objects (e.g. a window) can always be pushed on, but cannot always be moved. Typical impedance control implementations have focused on either model-based computation of the joint and/or actuator torques necessary for a manipulator to follow a given impedance characteristic [36, 98], or on position-based impedance controlled manipulators [72].

The concept of impedance control has been considered already as one possible approach to controller development for excavation related tasks. Researchers at the University of British Columbia [18, 84, 85] incorporated impedance control into the tele-operation of a miniature backhoe style excavator. As was discussed in chapter 2, Bernold [9] proposed that the use of impedance control (in the excavation of soil type media) would permit the assignment of a target relationship between the actual position of the excavator bucket and its desired position according to some planned nominal path. Also, Ha et al. [26] have recently proposed the implementation of an impedance control scheme for backhoe excavation bucket trajectory following.

However, the above impedance control schemes imply that there exists some predetermined nominal trajectory that the excavation bucket should follow. In the case of tele-operation, this trajectory would presumably come from the command of a remote operator. On the other hand, for autonomous excavation, the path the bucket should follow is not entirely clear, since the ultimate objective is to fill the bucket and not to follow some prearranged trajectory.

6.2 Re-examination of the Control Problem

The reviewed patents [15, 77] circumvented the issue of bucket position trajectory generation in their somewhat common approach to autonomous excavation. Consider the Caterpillar, Inc. patent [77], where lift and dump cylinder forces were monitored and controlled so that they remained within predetermined acceptable upper and lower limits. This was evidently done to keep the intensity of bucket-rock interaction at a level where the eventual achievement of a full bucket was more likely to occur. Should the forces of interaction become too low, it would be expected that an insufficient amount of material would fall into the bucket before breakout occurred. Conversely, should the forces of interaction become too high, the bucket would likely be attempting to penetrate too far into the rock pile, resulting in excessive forces and possibly a prolonged and inefficient excavation cycle. Such reasoning suggests the need for a force-based control scheme that does not give priority to the position trajectory followed by the bucket.

The data from full-scale experimental trials of chapter 4 provide additional evidence that the application of ideas from the field of compliant motion control may be appropriate. Consider the aggressive excavation trial for operator (I) depicted in figure 4.12 on page 60. After having completed the penetration phase, the operator engaged the dump cylinder so as to achieve a cylinder force with a magnitude in the

neighbourhood of 200 kN. The dump cylinder was then continuously commanded by the operator in a fashion that regulated the cylinder force throughout the scooping operation, although the operator was likely not conscious of this underlying fact, until the time at which breakout occurred. The outcome of this operator directed manoeuver was a full bucket of fragmented rock. Moreover, in chapter 5, the system identification results corresponding to attempts at modelling the aggressive excavation trials hinted at the fact that, if the operation is carried out through motions of merely the dump cylinder, force feedback from only the dump cylinder would be sufficient to describe the online excavation status.

To summarize, the proposed theme for autonomous excavation is a control system that is able to interpret measured forces in the dump cylinder of the LHD machine as an indication of the state of bucket-rock interaction.

6.3 Admittance Control for Excavation

Contrary to the conclusion of Hogan [36] that the environment must be an admittance and the manipulator must be an impedance, consider instead that it is wished that the manipulator accept force and respond with motion. Such a situation would be best termed *admittance control*, since a force compensator by design would endeavour to comply with environmental impedance[1] and react to contact forces by changing its motion. Here, the distinction to be made is that by strict definition, impedance control presents a means through which the impedance of a manipulator may be prescribed by the controller that ultimately wishes to follow some predetermined nominal trajectory. Conversely, an admittance control scheme resembles more closely a technique for explicit force control, where the admittance of a manipulator may be defined by a controller that strives to ultimately regulate a chosen force trajectory.

[1] A fragmented rock pile is perhaps best termed a *passive* impedance (after Newman [70]) since it cannot generate or amplify energy.

This noteworthy difference was recognized in Colgate and Hogan [13] and Newman [70], where the term *interaction controller* was coined to extend the generality of force regulation to include desired interaction dynamics other than simply pure force control. Some (e.g. Spong and Vidyasagar [98, page 253]) have suggested that pure position control and pure force control are merely special cases of impedance control, equivalent to infinite impedance and zero impedance, respectively. However, it is argued here that pure force control is more appropriately labelled a special case of admittance control, corresponding to infinite admittance. Thus, what distinguishes the two lies merely in the underlying objective for control.

Hence, given the above verbal description of admittance control and the discussion of section 6.2 regarding the excavation control problem, it might be concluded that an appropriate strategy for control towards autonomous excavation would be the application of an admittance-type control scheme. Such a system would require force feedback to a *force compensator* of sorts, which would in turn compute the necessary actuator control inputs. In the case of position controlled[2] hydraulic actuators, the compensator would be required to compute an appropriately modified trajectory for the position controlled mechanism. Yet, it has already been argued that, for the excavation task, even a nominal position trajectory would have essentially no valuable meaning. On the other hand, the force compensator might more appropriately respond to bucket-rock interaction forces by commanding a change in the actuator *velocity*. For example, should the force compensator, by design, decide that the intensity of bucket-rock interaction is too low, it may choose to direct the proper cylinder to decrease its velocity, so as to not arrive at breakout too early. Alternatively, if the force compensator deems the intensity of bucket-rock interaction to be too high, it may select to instruct the cylinder to increase its velocity to avoid

[2]It is often the case that mechanisms with position controlled actuators are used as a baseline, while modifications of the setpoints are made by an impedance (or admittance) controller to enable the effecting of tasks that call for interaction of the manipulator with its environment [89, 72].

excessive penetration into the rock pile. Again, this approach is similar to a concept alluded to in the Caterpillar, Inc. patent [77]. Except, here the task is formulated as an explicit compliant motion control problem directed at the autonomous excavation of fragmented rock.

In the subsections that follow, one possible method for design of an autonomous excavation control system, based on the methodology of admittance control, is outlined in brief.

6.3.1 Force Compensator Design

The force compensator $H(s)$ design for autonomous excavation should be one that reacts to sensed bucket-rock interaction forces by quickly changing the motion (i.e. velocity) of the bucket. In keeping with previous discussions, only the dump cylinder is regarded as available for use by the controller, and only the measured dump cylinder force is employed as an indicator of the bucket-rock interaction intensity. Consider the velocity-based admittance control scheme block diagram of figure 6.1, adapted from the position-based design of Seraji [89], where f_d is the desired force setpoint to achieve a full bucket of rock, $\hat{f}_r$ is the measured cylinder force, which is assumed to include a component due to ongoing bucket-rock interaction, and v_r and f_r are the actual velocity of the dump cylinder extension/retraction and bucket-rock interaction force respectively. Note that, contrary to previous chapters, forces and velocities corresponding to retraction of the dump cylinder are assumed positive. Using the measured cylinder force $\hat{f}_r$, the force compensator $H(s)$ computes the desired velocity change v_f, which is combined with a desired reference velocity v_d to produce the new velocity command $v_c = v_d + v_f$ to be used by the dump cylinder position controller. For the sake of simplicity, it is assumed that the position-controlled dump cylinder is able to acceptably regulate the cylinder velocity as commanded by the force compensator.

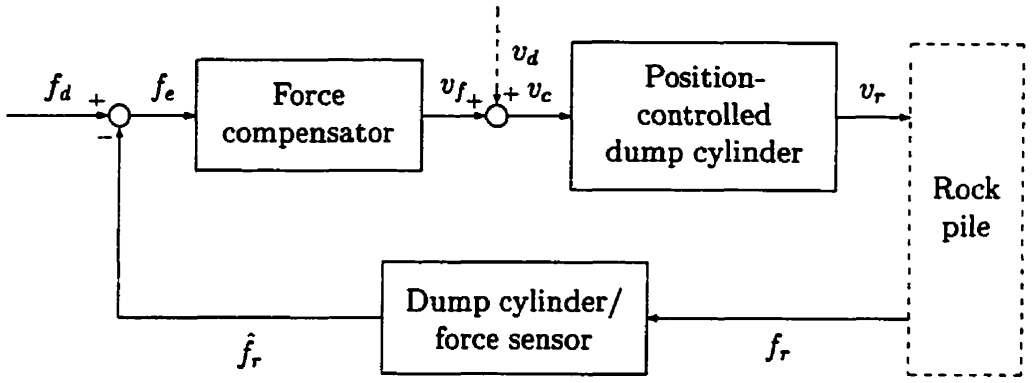

Figure 6.1: Velocity-based admittance control system block diagram

If the force error is given by $f_e = f_d - \hat{f}_r$, then let the force compensator transfer-function be expressed by the mechanical admittance

$$H(s) = \frac{v_f(s)}{f_e(s)} = Y(s) \,. \tag{6.3}$$

For a known equivalent rock pile (environment) stiffness, an admittance $Y(s)$ may be selected to achieve a desirable response of the cylinder to varying bucket-rock interaction forces. In the most simple of possible cases, one might select the force compensator to have constant admittance dynamics

$$H(s) = k \tag{6.4}$$

which, in the time domain, gives the force feedback law

$$v_f = k f_e = k \left(f_d - \hat{f}_r \right) \,. \tag{6.5}$$

In concurrence with the argument for velocity regulation given previously, a gain of $k < 0$ would result in a decrease in magnitude of the cylinder retraction velocity for $\hat{f}_r < f_d$, thus attempting to increase the intensity of bucket-rock interaction, and an increase in magnitude of the cylinder retraction velocity for the case when $\hat{f}_r > f_d$, thus attempting to decrease the intensity of bucket-rock interaction.

Although the simple admittance model of equation (6.4) might provide a means for realization of an approach deemed suitable through full-scale experimental studies and

modelling observations, the compliant motion control methodology affords the ability for greater flexibility in the system dynamics prescribed by the force compensator. For example, consider the extension of equation (6.4) to include higher-order terms, so that

$$H(s) = ms^2 + bs + k \tag{6.6}$$

which leads to the force feedback law

$$v_f = m\frac{d^2}{dt^2}f_e + b\frac{d}{dt}f_e + kf_e\,. \tag{6.7}$$

The parameters $\{m, b, k\}$ would prescribe a desired dynamic response of the system to varying intensities of bucket-rock interaction, as interpreted from dump cylinder force measurements. Presumably, the particular admittance model selected would impact the behaviour of the resulting control system when in contact with rock piles of various composition. For example, the inclusion of the force damping term b might improve the performance of the excavation controller in situations where large rock fragments are present, adjusting the controller to respond appropriately by damping out rapid changes in bucket-rock interaction intensity.

6.3.2 Modelling for Control System Simulation

In the compliant motion control literature, it is often the case that the environment with which a robot manipulator interacts is modelled as a linear spring and damper system; for example as in [40, 71, 89]. In many cases, this is sufficient and convenient to describe the behaviour of simple environments. However, the process of bucket-rock interaction discussed in this thesis is obviously a more complex system, and therefore, its dynamics cannot be modelled by such convenient relationships, as was noted by Hemami [32]. This issue becomes a problem when control system design simulations are desired.

In chapter 5, LHD machine and rock pile dynamics were modelled using PCI, where sensed cylinder forces were considered as inputs to a nonlinear system having cylinder motions as outputs. However, the autonomous excavation problem has just been described as one that responds with motion to bucket-rock interaction forces; hence, the need for an admittance control approach, rather than its reciprocal. Therefore, a model for the block labelled "Rock pile" in figure 6.1 might have the basic form $f_r = E(v_r)$, where the environment interaction function E maps bucket motions in the rock pile to resistive forces acting on the bucket. If the hydraulic dump cylinder itself is utilized as a bucket-rock interaction intensity transducer, then measured cylinder forces may be modelled by some combined function of the form

$$\hat{f}_r = \hat{E}(v_r) \tag{6.8}$$

which is a potential candidate for identification using the PCI algorithm.

Since the assumption, which forms a basis for the admittance control scheme described in this chapter, is that forces of interaction result in pressure changes within the hydraulic cylinders, an attempt was made to identify a model for the mapping $\hat{E}$ using the PCI algorithm on data collected during the experimental studies described in chapter 4. Only the scooping phase of operation was considered, as noted earlier in this chapter. In chapter 5, where a PCI model for the inverse mapping $\hat{E}^{-1}$ was developed, concerns were expressed regarding the potential for violation of the causality restriction. It should be noted that if these concerns existed for the inverse mapping, they must also exist for the mapping $\hat{E}$.

The bottom portion of figure 6.2 presents the outcome of one attempt at identification of the function expressed by equation (6.8), using data from the trials conducted by operator (I). The resulting PCI model (subsampled to 35 Hz, $R = 30$, $M = 4$, no output feedback) was trained on two data sets and had three parallel cascades, where for each cascade the PCI algorithm selected to utilize velocity data from only the dump cylinder. The MSE on the testing data velocity output was computed to

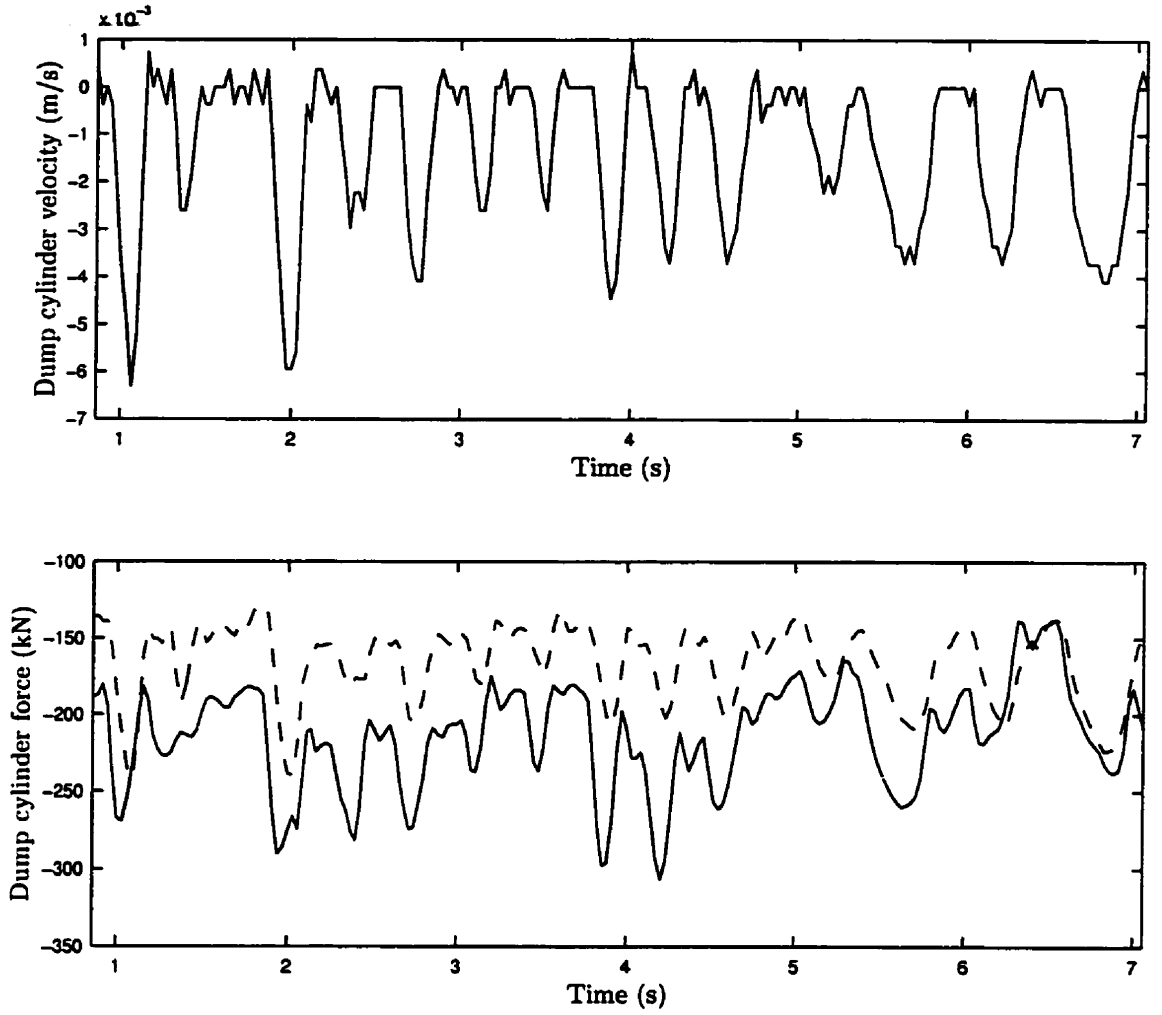

Figure 6.2: Modelling dump cylinder forces using the PCI (dashed) algorithm

be comparatively large, at 10.2 %. However, this was principally due to an offset in the test data output, created by training the model on data representative of trials conduced at lower force magnitudes. The shape of the `PCI.dll` output waveform matched the shape of the test data waveform with acceptable accuracy. These results indicate that simulation, to a certain degree, of the scooping phase of the fragmented rock excavation process may be possible through application of PCI to measured dump cylinder velocity and force data.

6.3.3 Further Remarks on the Excavation Control System

The control scheme proposed in this chapter forms the basis for an admittance controller design towards autonomous excavation of fragmented rock. However, a number of important details, necessary for implementation of the design, were not discussed. Since controller implementation and tuning lies outside the scope of this dissertation, only a qualitative examination of these issues is provided here.

Firstly, there remains the question of how to choose the proper force and velocity setpoints f_d and v_d so as to achieve a full bucket of rock. Obviously, the values assumed by these input arguments would depend heavily on the characteristics of the excavation media. Intuitively, varying rock types and particle size distributions would impact the optimal velocity and interaction intensity at which scooping should take place. For instance, comparing the controlled excavation trials in the local roundstone with those in the Inco muck discussed in chapter 4 (see figures 4.10 and 4.11 on pages 57 and 59), it is evident through observation of the breakout force that a higher force setpoint would be desired for excavation in Inco rock (breakout at 260 kN) in comparison with the local roundstone (breakout at 140 kN). Through inspection of the aggressive excavation trial shown in figure 4.12 on page 60, one might select the constant reference values $f_d \approx 225$ kN and $v_d \approx 35$ mm/s for excavation control. It may be possible that suitable force and velocity setpoints be tuned, online, over a series of excavation iterations, essentially adapting to potentially changing rock pile characteristics.

Moreover, there remains the question of how to select an appropriate admittance model $Y(s)$, and model parameters, to be implemented by the force compensator. This problem is compounded by the requirement that the given control system be stable under varying excavation conditions. Seraji [89] noted that if the environment impedance was known to change, possibly over several orders of magnitude, that a fixed admittance design based on some nominal environment would often lead to

instability. It is reasonable to assume that, as the excavator bucket is passed through any given rock pile, the impedance it sees as a result of bucket-rock interaction would vary as the bucket is filled and particles of diverse sizes and shapes are encountered. This issue was apparently dealt with by Seraji through the development of an *adaptive admittance* technique for use in force control within a compliant motion framework.

It is worth noting that, with respect to a computed change in dump cylinder position $x_f(s) = \frac{1}{s}v_f(s)$, the force compensator design of equation (6.6) is equivalent to a proportional-integral-derivative (PID) regulator [89]. Rewriting the force feedback law of equation (6.7) to compute the desired change in dump cylinder position yields

$$x_f = m\frac{d}{dt}f_e + bf_e + \int_0^t f_e dt \tag{6.9}$$

where the parameters $\{m, b, k\}$ become the derivative, proportional, and integral gains, respectively. Although there exist techniques for tuning PID regulators [23, page 191], it is likely that the necessary regulator gains depend not only on the actuator and mechanism characteristics, but on the conditions and nature of each excavation scenario.

Although control experiments and/or simulations were not performed, the admittance control design proposed in this chapter, based on experimental and modelling observations, and concepts from the field of compliant motion control, offers a first look at one potential technique for control aimed specifically at the development of a system for autonomous excavation of fragmented rock.

Chapter 7

Summary and Conclusions

It is evident that undertaking the design of a system intended to perform autonomous excavation of fragmented rock is a task that involves many unique and varied challenges. Most notably, the conditions necessary for a successful scooping operation are seemingly influenced by the complex nature of bucket-rock interactions that occur during excavation. In chapter 2, a relatively extensive review of the most pertinent literature on this subject was presented, with a focus on those works relating most specifically to the excavation of fragmented rock and to the automation of load-haul-dump (LHD) mining machines. Despite the fact that an apparently broad range of research has already been conducted in the field of autonomous excavation, none has resulted in the prevalence of such technologies in the mining industry, nor in other potentially relevant pursuits.

Previous studies in fragmented rock excavation were found to favour analytical results, not validated through experimental means. For example, consider the analytical force analyses by Hemami [27, 29, 31, 32, 33] and the proposals for trajectory generation by Mikhirev [61, 62]. Some researchers utilized laboratory-scale equipment to validate approaches based on machine-vision [37, 73, 104] and behaviour-control concepts [51, 52, 90]. Furthermore, it was discovered that the legitimacy of reviewed

empirical [21, 22, 61] and analytical [34, 101, 102, 105] studies in bucket-rock interaction had yet to be confirmed by full-scale experimental studies aimed at identifying a control system design suitable for autonomous excavation. Of the relevant patents [15, 77], only one [15] was found to pertain specifically to excavation of fragmented rock. Even so, it was not through a systems and control perspective that autonomous excavation was claimed to have been achieved.

7.1 Experimental Excavation Studies

As a contribution to the task of filling a gap in the existing literature, a wide range of full-scale experiments were conducted using a Tamrock EJC 9t model LHD machine, under excavation conditions comparable to those found in an underground mining situation. The trial LHD machine was instrumented as was deemed appropriate in order to measure certain operational dynamics during scooping. Machine parameters such as hydraulic cylinder forces, loader mechanism configuration, and vehicle translation were recorded, using instrumentation and data acquisition systems built specifically for the described operations, with the intention of subsequent offline analyses and system identification.

The excavation trials were conducted in two very different rock types: (i) a local roundstone, and; (ii) a representative fragmented rock (Inco muck) taken from a blast at an underground hard-rock mine and shipped to the testing site specifically for the planned full-scale excavation trials. In addition to the recording of free-space motion data, controlled and aggressive excavation experiments were conducted using the aforementioned instrumentation and data acquisition systems.

For controlled excavation trials, observations were made regarding the status of machine parameters during the penetration phase, scooping phase, and at breakout. It was remarked that information contained within the dump cylinder force/motion

data was sufficient to expose a great deal about the excavation process. Aggressive excavation trials were primarily intended to provide insight into the evolution of machine parameters during successful scooping operations conducted by experienced operators, and also to hint at potentially feasible approaches to automation of the loading cycle. Hydraulic cylinder retraction rates, force/displacement changes, and patterns in operator tactics were remarked.

7.2 Dynamics of the Loading Process

Having completed the full-scale experimental studies described above, the task of developing a model capable of computing motions of the LHD loader mechanism alone and while in contact with a given rock pile, was addressed. First, an analytical approach for analysis of the LHD loader mechanism as a robot manipulator, using techniques from Lagrangian mechanics, was outlined. Next, the employment of a distinct element method (DEM) and artificial neural networks were examined briefly as modelling alternatives to the subsequently implemented parallel cascade identification (PCI) algorithm.

It was reported recently by Eklund and Korenberg [19, 20] that the PCI algorithm had been used to successfully identify aircraft pilot flight controls having a dynamic model similar in mechanical nature to, although less complex than, the LHD loader mechanism. Therefore, it was decided that an effort to employ the technique of PCI to excavation modelling might be a worthwhile endeavour. Details were provided regarding implementation of the PCI algorithm, for the purpose of validating its applicability to the given system identification problem. The developed C language computer code was tested on contrived data to successfully prove its functionality prior to modelling of systems represented by experimental data from full-scale excavation studies. PCI model identification scenarios pertaining to the LHD loader

mechanism forward dynamics in free-space and aggressive excavation trials were realized. It was discovered that even the best outcomes were not exceptionally good, and that this was particularly true when identifying dump cylinder motions in free-space. However, it was also recognized that the mechanical system to be identified may have depended heavily on its initial conditions, possibly explaining the less favourable results of attempts at modelling the more complicated dump cylinder dynamics. One further point of contention was a possible violation of the causality assumption. The presumption that bucket-rock interaction forces result in measurable cylinder pressure changes formed a basis for the reactive control schemes of the reviewed patents [77, 15] and the admittance control scheme proposed in chapter 6. Yet, the aggressive excavation trial identification outcomes were sufficiently good to indicate that violation of the causality restriction did not play a significant role.

7.3 Future Work in Excavation Control

In chapter 6, a thorough re-examination of the excavation control problem demonstrated the potential applicability of concepts from the field of compliant motion control to the task of autonomous excavation. A case for the formulation of a control system design, founded on an approach labelled admittance control, was argued on the basis of observations from full-scale experiments, modelling efforts, and conclusions drawn in the reviewed literature and patent documents.

Contrary to a common notion that the environment must be an admittance and the manipulator an impedance, a distinction was made that a solution to the problem of autonomous excavation would be best achieved by a control system more closely resembling pure force control. The admittance control approach, which dictates that the manipulator accept force and respond with motion, is one that was found to have not been explicitly explored in the literature pertaining to autonomous exca-

vation. Consequently, a velocity-based force compensation scheme that would allow for transparent definition of the desired manipulator admittance was provided. Although actual implementation was beyond the scope of this dissertation, the described framework provides a sound starting point for future work.

The remaining subsections cover matters deemed worthy of comment under the heading of future work towards autonomous excavation of fragmented rock.

7.3.1 Measurement of Vehicle Translation

Unfortunately, due to significant wheel slippage, the use of a wheel encoder setup was found to be ineffective at measurement of the vehicle's translational motion during excavation (see section 4.2.2 on page 63) . In future, it is suggested that perhaps a means external to the vehicle should be used for absolute position measurement (e.g. a laser distance transducer). This would be of particular interest if combined with measurements of the vehicle tractive effort during excavation operations.

7.3.2 Operator Commanded Signals

Consider the block model structure of figure 5.4 on page 76, used to portray the overall excavation process. In retrospect, it would have been beneficial to have obtained measurements of the *commanded* actuator inputs denoted by $\boldsymbol{f}_a$ in the figure, and not only the hydraulic cylinder forces during excavation operations. This would have allowed for removal of the operator commanded force component from the measured cylinder forces, further isolating the actual force components due only to bucket-rock interaction. Furthermore, such data might possibly have allowed for improved identification of the excavation process based on purely operator (control signal) inputs, avoiding the causality issue, and perhaps permitting simulation or even prediction of the bucket-rock interaction intensity level.

Similarly, regarding implementation of the control scheme described by figure 6.1

on page 105, and for identification, it would have been advantageous to have measured operator commanded signals analogous to v_c of the control system block diagram, since the actual cylinder velocity v_r is always corrupted to a certain degree by the process of bucket-rock interaction. The extent to which bucket-rock interactions truly influence excavator bucket motion could subsequently be determined. Other issues that relate to this matter are discussed further in subsection 7.3.5.

7.3.3 On Tractive Effort

To reiterate previous statements regarding the issue of tractive effort (i.e. translational force imparted to the rock pile by the wheels), an assumption was made that any tractive effort supplied by the vehicle was generally constant throughout the loading operation, and that tractive effort control would not have provided any significant contribution to solving the autonomous excavation problem. This assumption was weakly supported in the literature in that focus was given primarily to the problem of determining appropriate bucket motions so as to achieve a full bucket of material. For example, in the patent by Rocke et al. it was simply stated that, "... the operator directs the machine to the pile of material, preferably at full throttle" [77].

Nonetheless, it is very much a possibility that measurement of the vehicle tractive effort could provide further insight into the excavation process. Still, there exists a significant challenge in physically measuring the level of tractive effort. Engine speed would not be an effective measure, since the machine's diesel engine is required in most cases to power not only the wheels, but also the hydraulic pump that feeds the actuating cylinders. If reaction forces at the boom link joint could be determined, perhaps through strain gauge instrumentation, then it may also be possible to compute an estimate of the tractive effort by considering it as a purely translational force acting on the vehicle body. In any case, for the purposes of this thesis, the matters surrounding tractive effort are afforded the status of future work.

7.3.4 Parallel Cascade Identification

Further to simply varying the model parameters, as was suggested in subsection 5.3.3 on page 89, there exist additional options for potential improvement of the PCI modelling results of chapter 5. Firstly, it may be possible to enhance the results, and perhaps identify more accurately situations where the cylinder was not moving or capture abrupt changes in motion, by fitting a supplementary PCI model to the error of the initial model [19, 20]. This second model could have a different memory length and nonlinear degree than the original.

Also, in other research utilizing the PCI algorithm, it has been found that the inclusion of a second dynamic linear element in each cascade (i.e. an LNL model) has sometimes provided improved results [24, 46].

7.3.5 Simulation and Controller Development

There remains a great deal of research potential in the task of implementation and application of the admittance control design proposed in chapter 6. Although it was shown in subsection 6.3.2 on page 106 that simulation of the scooping phase of the fragmented rock excavation process is perhaps possible through application of the PCI algorithm, subsequent control simulations were not completed within the scope of this thesis. As was stated in subsection 6.3.3 on page 109, implementation of the admittance control design involves the resolution of issues such as: (i) extraction of the PCI model parameters (not just the $h_i(j)$ and coefficients a_{im}, but also the normalizing coefficients discussed in subsection 5.3.1 on page 80); (ii) how to choose the proper force and velocity setpoints f_d and v_d so as to achieve a full bucket of rock, and; (iii) how to select an appropriate admittance model $Y(s)$ to be implemented by the force compensator $H(s)$, which is effective and results in a stable system under varying operational conditions.

Further inspection of the PCI model input-output behaviour shown in figure 6.2 on page 108 reveals that changes in dump cylinder force correspond well to changes in the cylinder velocity. The question therefore remains as to whether the model input velocity changes v_r are due to bucket-rock interaction, or due to signals commanded by the operator. Strictly speaking, the answer is likely that both are responsible (see figure 5.4 on page 5.4). If the operator in fact commanded significant changes in cylinder velocity, then a control system for autonomous excavation should perhaps not only respond to variations in bucket-rock interaction intensity, but also *induce* such changes, so as to fluidize the rock pile during scooping.

Consider that the pulsating action observed in the top portion of figure 6.2 might be realized through the application of the controller commanded cylinder velocity v_c by means of pulse-amplitude modulation (PAM). For example, given a 50 % duty cycle, a desired cylinder velocity of $v_c = 35$ mm/s might be achieved by pulsating the cylinder to a velocity of 70 mm/s. Subsequent changes to v_c, based on force compensator computations, could then be implemented by modulating the amplitude of velocity pulses. Furthermore, the frequency of pulsation could be related to the size distribution of the rock pile, where lower frequencies intuitively correspond to the presence of large rock fragments, and higher frequencies to smaller particles. For example, in very fine grained material, the described scenario would result in approximately smooth motions through the excavation media. In rock piles having large rock fragments, stepped motions of the cylinder could help to dislodge particles and encourage material to flow more easily into the excavator bucket.

Finally, while numerical simulations would provide valuable insight towards the development of a control system for autonomous excavation, complex environment interactions make validation of the proposed control scheme by experimental means a potentially worthwhile endeavour. Given the availability of appropriate equipment for research, the admittance control strategy is perhaps best tried in the field.

7.4 Closing Remarks

Heightened globalization and competition in the mining industry have lead to demands for new and innovative technologies, including a push towards the automation of mobile equipment. Despite the fact that the autonomous excavation problem has been given considerable attention in the literature, only a small number of investigations into technology development have been reported for large and non-homogeneous excavation media, such as fragmented rock. Furthermore, there exist very few experimental studies in support of proposed ideas.

In summary, this thesis has made the following principal contributions:

1. Provided an extensive review of current literature and technology specific to the subject of autonomous excavation of fragmented rock, with an emphasis on works relating specifically to LHD machine automation, discovering a lack of research involving full-scale excavation studies;

2. Designed, implemented, and documented the apparatus, methodology, procedure, and results of full-scale experimental excavation studies, carried out in fragmented rock by an LHD underground mining machine;

3. As an exercise in applied mechanics, formulated a procedure and computed the equations of motion, using techniques from Lagrangian mechanics, for the trial LHD mechanism;

4. Implemented and applied the PCI technique for nonlinear systems in an attempt to utilize the acquired full-scale experimental data for modelling and analysis of the machine mechanism and fragmented rock excavation process, and;

5. Formulated an admittance-type control system design, based on results and observations from the described experimental studies and modelling endeavours,

that utilizes sensed forces in the hydraulic dump cylinder as an indication of the buck-rock interaction intensity, and hence a feedback signal for control.

It is hoped that the experimental data and foundation material supplied by the research of this thesis will help to establish a basis for further investigations and future work towards the development and implementation of a control system designed for autonomous excavation of fragmented rock.

Bibliography

[1] PX300, 302, 303 and 305 series pressure transducers. Omega Engineering, Inc., Stamford CT, U.S.A, 1996.

[2] Model H25 incremental optical encoder. BEI Technologies, Inc., Goleta CA, U.S.A., November 1998.

[3] Presentation of the EJC 1000 prototype. Tamrock Loaders, Inc. Development & Engineering internal document, Burlington ON, Canada, March 1998.

[4] AMP04 precision single supply instrumentation amplifier, Rev. B. Analog Devices, Inc., Norwood MA, U.S.A., November 2000.

[5] Rayelco linear motion transducer. Ametek Aerospace, Gulton-Statham Products, Costa Mesa CA, U.S.A., 2000.

[6] S. Ashley. Underground mining from above. *Mechanical Engineering*, 117(5), May 1995.

[7] J. Bares, P. C. Leger, P. Rowe, S. Singh, A. Stenz, and N. K. Lay. System for autonomous excavation and truck loading. United Kingdom Patent No. GB2342640, Carnegie Mellon University, April 2000.

[8] T. G. Beckwith, R. D. Marangoni, and J. H. Lienhard V. *Mechanical Measurements*. Addison-Wesley Publishing Company, 5-th edition, 1993.

[9] L. E. Bernold. Motion and path control for robotic excavation. *Journal of Aerospace Engineering*, 6(1):1–18, January 1993.

[10] D. M. Bullock and I. J. Oppenheim. Object-oriented programming in robotics research for excavation. *Journal of Computing in Civil Engineering*, 6(3):370–385, July 1992.

[11] S. C. Chapra and R. P. Canale. *Numerical Methods for Engineers*. McGraw-Hill, Inc., 2-nd edition, 1988.

[12] T-C. Chen. *Linear System Theory and Design*. Holt, Rinehard and Winston, Inc., 1984.

[13] J. E. Colgate and N. Hogan. Robust control of dynamically interacting systems. *International Journal of Control*, 48(1):65–88, 1988.

[14] P. A. Cundall and O. D. L. Strack. A discrete numerical model for granular assemblies. *Géotechnique*, 29(1):47–65, 1979.

[15] A. Dasys, L. Geoffroy, and A. Drouin. Sensor feedback control for automated bucket loading. United States Patent No. 5941921, Noranda, Inc., August 1999.

[16] J. Denavit and R. S. Hartenberg. A kinematic notation for lower-pair mechanisms based on matrices. *Journal of Applied Mechanics*, pages 215–221, June 1955.

[17] R. M. DeSantis. Modelling and path-tracking for a load-haul-dump mining vehicle. *ASME Journal of Dynamic Systems, Measurement and Control*, 119:40–47, 1997.

[18] S. P. DiMaio, S. E. Salcudean, C. Reboulet, S. Tafazoli, and K. Hashtrudi-Zaad. A virtual excavator for controller development and evaluation. In *Proceedings*

of the 1998 IEEE International Conference on Robotics and Automation, volume 1, pages 52–58, 1998.

[19] J. M. Eklund. Aircraft flight control simulation using parallel cascade system identification. M.Sc.(Eng.) thesis, Queen's University, Kingston ON, Canada, March 1998.

[20] J. M. Eklund and M. J. Korenberg. Simulation of aircraft pilot flight controls using nonlinear system identification. *Simulation*, 75(2):72–81, 2000.

[21] Y. F. Fabrichnyi and S. B. Kolokolov. Calculating the resistance of blasted rock to scooping by a bucket. *Soviet Mining Science*, 11(4):438–441, 1975.

[22] B. Forsman and C. L. Pan. Shear properties of fragmented rock masses: Model tests and theories. *International Journal of Rock Mechanics and Mining Science & Geomechanical Abstracts*, 26(1):25–36, January 1989.

[23] G. F. Franklin, J. D. Powell, and A. Emami-Naeini. *Feedback Control of Dynamic Systems*. Addison-Wesley Publishing Company, Inc., 3-rd edition, 1994.

[24] A. S. French, M. J. Korenberg, M. Jarvilehto, E. Kouvalainen, M. Juusola, and M. Weckstrom. The dynamic nonlinear behavior of fly photoreceptors evoked by a wide range of light intensities. *Biophysical Journal*, 65:832–839, 1993.

[25] F. H. Ghorbel, O. Chételat, R. Gunawardana, and R. Longchamp. Modeling and set point control of closed-chain mechanism: Theory and experiment. *IEEE Transactions on Control Systems Technology*, 8(5):801–815, September 2000.

[26] Q. P. Ha, Q. H. Nguyen, D. C. Rye, and H. F. Durrant-Whyte. Impedance control of a hydraulically actuated robotic excavator. *Automation in Construction*, 9(5):421–435, 2000.

[27] A. Hemami. A conceptual approach to automation of LHD-loaders. In *Proceedings of the Canadian Symposium on Mining Automation*, pages 178–183, September 1992.

[28] A. Hemami. Force analysis in the scooping/loading operation of an LHD loader. In *Proceedings of the 2nd International Symposium on Mine Mechanization and Automation*, pages 415–424, 1993.

[29] A. Hemami. Study of bucket trajectory in automatic scooping with load-haul-dump loaders. In *Transactions of the Institution of Mining and Metallurgy, Series A: Mining Industry*, volume 102, pages A37–A42, January–April 1993.

[30] A. Hemami. An approximation of the weight of the loaded material during the scooping operation of a mechanical loader. *Transactions of the Canadian Society for Mechanical Engineering*, 18(3):191–205, 1994.

[31] A. Hemami. Modelling, analysis and preliminary studies for automatic scooping. *Advanced Robotics*, 8(5):511–529, 1994.

[32] A. Hemami. Fundamental analysis of automatic excavation. *Journal of Aerospace Engineering*, 8(4):175–179, October 1995.

[33] A. Hemami and L. K. Daneshmend. Force analysis for automation of the loading operation in an LHD-loader. In *Proceedings of the 1992 IEEE International Conference on Robotics and Automation*, pages 645–650, 1992.

[34] A. Hemami, S. Goulet, and M. Aubertin. Resistance of particulate media to excavation: Application to bucket loading. *International Journal of Surface Mining, Reclamation and Environment*, 8:125–129, 1994.

[35] A. Hemami and V. Polotski. Path tracking control problem formulation of an LHD loader. *The International Journal of Robotics Research*, 17(2):193–199, 1998.

[36] N. Hogan. Impedance control: An approach to manipulation, Parts I, II, and III. *ASME Journal of Dynamic Systems, Measurement, and Control*, 107:1–24, 1985.

[37] Q. Ji and R. L. Sanford. Autonomous excavation of fragmented rock using machine vision. In *Emerging Computer Techniques for the Minerals Industry*, chapter 24, pages 221–228. Society for Mining, Metallurgy & Exploration Inc., Littleton CO, U.S.A., 1993.

[38] P. D. Katsabanis. Fragmentation, vibrations, blast design. MINE321 course notes, Queen's University, Kingston ON, Canada, 1998.

[39] H. Kazerooni, T. B. Sheridan, and P. K. Houpt. Robust compliant motion for manipulators, Parts I and II. *IEEE Journal of Robotics and Automation*, RA-2(2):83–105, June 1986.

[40] H. Kazerooni, B. J. Waibel, and S. Kim. On the stability of robot compliant motion control: Thoery and experiments. *ASME Journal of Dynamic Systems, Measurement, and Control*, 112:417–426, 1990.

[41] A. J. Koivo, M. Thoma, E. Kocaoglan, and J. Andrade-Cetto. Modeling and control of excavator dynamics during digging operation. *Journal of Aerospace Engineering*, 9(1):10–18, January 1996.

[42] M. J. Korenberg. Identifying nonlinear difference equation and functional expansion representations: The fast orthogonal algorithm. *Annals of Biomedical Engineering*, 16:123–142, 1988.

[43] M. J. Korenberg. A robust orthogonal algorithm for system identification and time-series analysis. *Biological Cybernetics*, 60:267–276, 1989.

[44] M. J. Korenberg. Parallel cascade identification and kernal estimation for nonlinear systems. *Annals of Biomedical Engineering*, 19:429–455, 1991.

[45] M. J. Korenberg. Personal communications, June 2001.

[46] M. J. Korenberg. Personal communications, July 2001.

[47] M. J. Korenberg, S. B. Bruder, and P. J. McIlroy. Exact orthogonal kernel estimation from finite data records: Extending Wiener's identification of nonlinear systems. *Annals of Biomedical Engineering*, 16:201–214, 1988.

[48] D. Kumar and N. Vagenas. Performance evaluation of an automatic load-haul-dump vehicle. *CIM Bulletin*, 86(974):39–42, 1993.

[49] Y. Laperrière and F. Miller. Automatic loading of LHDs. In *Proceedings of Telemin 1 and the 5th International Symposium on Mine Mechanization and Automation*, June 1999.

[50] A. T. Le, Q. Nguyen, Q. P. Ha, D. Rye, H. Durrant-Whyte, M. Stevens, and V. Boget. Towards autonomous excavation. In *Proceedings of the International Conference on Field and Service Robotics*, pages 121–126. Australian Robot Association, 1997.

[51] P. J. A. Lever and F-Y. Wang. Intelligent excavator control system for lunar mining system. *Journal of Aerospace Engineering*, 8(1):16–24, January 1995.

[52] P. J. A. Lever, F-Y. Wang, and X. Shi. Using bucket force/torque feedback for control of an automated excavator. In *Transactions*, volume 300, pages 135–139. Society for Mining, Metallurgy & Exploration, 1996.

[53] A. D. Lewis. Lagrangian mechanics, dynamics, and control. MATH439 course notes, Queen's University, Kingston ON, Canada, January 2001.

[54] W. Lidkea. Personal communications, June 2001.

[55] S-K. Lin. Dynamics of the manipulator with closed chains. *IEEE Transactions on Robotics and Automation*, 6(4):496–501, August 1990.

[56] J. Y. S. Luh and Y-F. Zheng. Computation of input generalized forces for robots with closed kinematic chain mechanisms. *IEEE Journal of Robotics and Automation*, RA-1(2):95–103, June 1985.

[57] R. Madhavan, M. W. M. G. Dissanayake, and H. F. Durrant-Whyte. Autonomous underground navigation of an LHD using a combined ICP-EKF approach. In *Proceedings of the 1998 IEEE International Conference on Robotics and Automation*, volume 4, pages 3703–3708, 1998.

[58] The MathWorks, Inc., Natick MA, U.S.A. *Application Program Interface Guide, Version 5*, 1998.

[59] P. J. H. McIlroy. Applications of nonlinear systems identification. M.Sc. thesis, Queen's University, Kingston ON, Canada, 1984.

[60] K. Mehrotra, C. K. Mohan, and S. Ranka. *Elements of Artificial Neural Networks*. Series in Complex Adaptive Systems. Massachusetts Institute of Technology Press, 1997.

[61] P. A. Mikhirev. Theory of the working cycle of automated rock-loading machines of periodic action. *Soviet Mining Science*, 19(6):515–522, 1983.

[62] P. A. Mikhirev. Design of automated loading buckets. *Soviet Mining Science*, 22(4):292–298, 1986.

[63] P. Murphy. Personal communications, November 2000.

[64] P. Murphy. Load-haul-dump vehicle load history data acquisition and analysis. M.Sc.(Eng.) thesis, Queen's University, Kingston ON, Canada, September 2001. Pending submission and acceptance.

[65] J. J. Murray and G. H. Lovell. Dynamic modeling of closed-chain robotic manipulators and implications for trajectory control. *IEEE Transactions on Robotics and Automation*, 5(4):522–528, August 1989.

[66] Y. Nakamura and M. Ghodoussi. Dynamics computation of closed-link robot mechanisms with nonredundant and redundant actuators. *IEEE Transactions on Robotics and Automation*, 5(3):294–302, June 1989.

[67] National Instruments Corporation, Austin TX, U.S.A. *DAQ: SCC Series User Manual*, December 1999.

[68] National Instruments Corporation, Austin TX, U.S.A. *National Instruments LabVIEW Measurements Manual*, July 2000.

[69] National Instruments Corporation, Austin TX, U.S.A. *National Instruments LabVIEW Users Manual*, July 2000.

[70] W. S. Newman. Stability and performance limits of interaction controllers. *ASME Journal of Dynamic Systems, Measurement, and Control*, 114:563–570, December 1992.

[71] M. Pelletier and L. K. Daneshmend. Automatic synthesis of robot compliant motions in dynamic environments. *International Journal of Robotics Research*, 16(6):730–748, 1997.

[72] M. Pelletier and M. Doyon. On the implementation and performance of impedance control on position controlled robots. In *Proceedings of the 1994*

IEEE International Conference on Robotics and Automation, volume 2, pages 1228–1233, 1994.

[73] M. K. Petty, J. Billingsley, and T. Tran-Cong. Autonomous LHD loading. In *Proceedings of the Annual IEEE Conference on Mechatronics and Machine Vision in Practice*, pages 219–224, 1997.

[74] M. Piotte, C. Coache, A. Drouin, P. Gauthier, and L. Geoffroy. Automatic control of underground vehicles at high speed. *CIM Bulletin*, 90(1003):78–81, 1997.

[75] M. Raibert and J. J. Craig. Hybrid position/force control of manipulators. *ASME Journal of Dynamic Systems, Measurement, and Control*, June 1981.

[76] D. J. Rocke. Automatic excavation control system and method. United States Patent No. 5446980, Caterpillar Inc., September 1995.

[77] D. J. Rocke. Control system for automatically controlling a work implement of an earthworking machine to capture material. United States Patent No. 5528843, Caterpillar Inc., June 1996.

[78] D. J. Rocke. Self-adapting excavation control system and method. United States Patent No. 5682312, Caterpillar Inc., October 1997.

[79] G. V. Rodionov. Theory of the working cycle of rock loaders of a periodic action. *Transactions of the Mining and Geological Institute*, 19, 1957. Academy of Sciences of the USSR, Ural Branch (in Russian).

[80] G. J. S. Ross. *Nonlinear Estimation*. Springer Series in Statistics. Springer-Verlag New York, Inc., 1990.

[81] P. S. Rowe. Learning system and method for optimizing control of autonomous earthmoving machinery. United States Patent No. 6076030, Carnegie Mellon University, June 2000.

[82] W. J. Rugh. *Nonlinear System Theory: The Volterra/Wiener Approach.* The Johns Hopkins University Press, 1981.

[83] D. E. Rumelhart, G. E. Hinton, and R. J. Williams. Learning internal representations by error propagation. *Parallel Distributed Processing*, 1, 1986.

[84] S. E. Salcudean, K. Hashtrudi-Zaad, S. Tafazoli, S. P. DiMaio, and C. Reboulet. Bilateral matched impedance teleoperation with application to excavator control. In *Proceedings of the 1998 IEEE International Conference on Robotics and Automation*, pages 133–139, May 1998.

[85] S. E. Salcudean, S. Tafazoli, P. D. Lawrence, and I. Chau. Impedance control of a teleoperated mini excavator. In *Proceedings of the 8th IEEE International Conference on Advanced Robotics (ICAR)*, July 1997.

[86] S. Sarata, K. Sata, and S. Tsukuba. Motion control system for autonomous wheel loader operation. In *Proceedings of the 1998 International Conference on Mine Mechanization and Automation*, pages 13.1–13.12, 1998.

[87] D. Sargent. Personal communications, October 2000.

[88] M. Schetzen. *The Volterra and Wiener Theories of Nonlinear Systems.* John Wiley & Sons, Inc., 1980.

[89] H. Seraji. Adaptive admittance control: An approach to explicit force control in compliant motion. In *Proceedings of the 1994 IEEE International Conference on Robotics and Automation*, pages 2705–2712, 1994.

[90] X. Shi, P. J. A. Lever, and F-Y. Wang. Experimental robotic excavation with fuzzy logic and neural networks. In *Proceedings of the 1996 IEEE International Conference on Robotics and Automation*, volume 1, pages 957–962, April 1996.

[91] X. Shi, P. J. A. Lever, and F-Y. Wang. *Autonomous Rock Excavation: Intelligent Control Techniques and Experimentation*, volume 10 of *Series in Intelligent Control and Intelligent Automation*. World Scientific Publishing Co. Pte. Ltd., 1998.

[92] T. Shinji. Automatic excavation system of loading machine. Japanese Patent No. JP62291335, Komatsu Ltd., December 1987.

[93] T. Shinji. Method and apparatus for automatic excavation of loading machine. Japanese Patent No. JP62185928, Komatsu Ltd., August 1987.

[94] T. Shoji and O. Tomoaki. Automatic control device for hydraulic shovel. Japanese Patent Office Publication No. 09256407, Shin Caterpillar Mitsubishi Ltd., September 1997.

[95] S. Singh. Learning to predict resistive forces during robotic excavation. In *Proceedings of the 1995 IEEE International Conference on Robotics and Automation*, volume 2, pages 2102–2107, 1995.

[96] N. K. Sinha and B. Kuszta. *Modeling and Identification of Dynamic Systems*. Van Nostrand Reinhold Electrical/Computer Science and Engineering Series. Van Nostrand Reinhold Company, 1983.

[97] M. R. Spiegel. *Theory and Problems of Theoretical Mechanics*. McGraw-Hill, Inc., 1967.

[98] M. W. Spong and M. Vidyasagar. *Robot Dynamics and Control*. John Wiley & Sons, Inc., 1989.

[99] J. Steele, C. Ganesh, and A. Kleve. Control and scale model simulation of sensor-guided LHD mining machines. *IEEE Transactions on Industry Applications*, 29(6):1232–1238, 1993.

[100] A. Stentz, J. Bares, S. Singh, and P. Rowe. A robotic excavator for autonomous truck loading. *Autonomous Robots*, 7(2):175–186, 1999.

[101] H. Takahashi. Simulation of the resistive forces acting on the bucket of wheel loader in the robotic scooping by use of DEM. In *Proceedings of the International Association of Science and Technology for Development (IASTED) Conference: Robotics and Automation 2000*, pages 230–235, August 2000.

[102] H. Takahashi, M. Hasegawa, and E. Nakano. Analysis on the resistive forces acting on the bucket of a load-haul-dump machine and a wheel loader in the scooping task. *Advanced Robotics*, 13(2):97–114, 1999.

[103] H. Takahashi, H. Kamata, T. Masuyama, and S. Sarata. Concept and model experiments on automatic shoveling of rocks from the rock piles. *Computers & Industrial Engineering*, 27(1–4):43–46, 1994.

[104] H. Takahashi, H. Kamata, T. Masuyama, and S. Sarata. Autonomous shoveling of rocks by using image vision system on LHD. In *Proceedings of the 1998 International Conference on Mine Mechanization and Automation*, pages 1.33–1.44, 1998.

[105] H. Takahashi, Y. Tsukamoto, and E. Nakano. Analysis of resistive forces acting on the bucket of LHD in the scooping task. In *Proceedings of the 16th International Symposium on Automation and Robotics in Construction*, pages 517–522, 1999.

[106] P. K. Vähä and M. J. Skibniewski. Cognitive force control of excavators. *Journal of Aerospace Engineering*, 6(2):159–166, April 1993.

[107] D. A. Wells. *Theory and Problems of Lagrangian Dynamics*. McGraw-Hill, Inc., 1967.

[108] D. E. Whitney. Force feedback control of manipulator fine motions. *ASME Journal of Dynamic Systems, Measurement, and Control*, pages 91–97, June 1977.

Appendix A

Hardware Specifications

This appendix presents specification data that was not included in the text of chapters 4 and 5. The following tables offer only immediately relevant summary information. For full hardware specification details, refer to the cited references for each table.

A.1 Loader Specifications

Table A.1: General specifications for the Tamrock EJC 9t LHD machine [3]

Carrying capacity	22,000 lbs	10 000 kg
Bucket size	6.0 yd^3	4.6 m^3
Engine power	247 hp	182 kW

Table A.2: Hydraulic cylinder general specifications [3]

	Lift cylinder(s)	—	Dump cylinder	—
Bore diameter	7 in	180 mm	8 in	200 mm
Rod diameter	3.5 in	90 mm	4 in	110 mm
Stroke length	43 in	1100 mm	100 in	2510 mm

Table A.3: Link inertial properties of the Tamrock EJC 9t LHD machine

Link No. (i)	Description	m_i	I_{zzi}	a_{ci}	b_{ci}
1	lift cylinder head	180 kg	10.7 kg·m^2	0.407 m	n/a
2	lift cylinder rod	180 kg	12.1 kg·m^2	0.448 m	n/a
3	boom	2311 kg	1513 kg·m^2	0.515 m	0.103 m
4	bucket	2776 kg	1792 kg·m^2	0.323 m	0.753 m
5	dump cylinder rod	219 kg	62.7 kg·m^2	0.925 m	n/a
6	dump cylinder head	219 kg	81.6 kg·m^2	1.057 m	n/a

Table A.4: Fixed physical dimensions of the Tamrock EJC 9t LHD machine

Parameter	Description	Value
d_1	distance $\overline{FB}$	0.826 m
d_2	distance $\overline{BC}$	1.876 m
d_3	distance $\overline{CD}$	0.780 m
d_4	distance $\overline{EF}$	0.629 m
d_5	distance $\overline{AF}$	0.871 m
ε_1	$\angle$ of $\overline{AF}$ to horizontal (acute)	1.5244 rad
ε_2	$\angle FBC$ (obtuse)	5.9249 rad
ε_3	$\angle$ of $\overline{EF}$ to horizontal (acute)	1.0008 rad
d_6	$d_4 \sin\varepsilon_3 + d_5 \sin\varepsilon_1$	1.400 m
d_7	$d_4 \cos\varepsilon_3 + d_5 \cos\varepsilon_1$	0.380 m
d_8	distance $\overline{CF}$	2.700 m
ε_4	$\angle FCB$ (acute)	0.1121 rad
ε_5	$\angle BFC$ (acute)	0.2459 rad

A.2 Sensor Specifications

Table A.5: PX303 series pressure transducer specifications [1]

Excitation	12–32 V (dc)
Output	0.5–5.5 V (dc)
Accuracy	0.25% F.S.
Minimum Load Resistance	2000 Ω
Response Time	1 ms

Table A.6: P-60A linear motion transducer specifications [5]

Excitation	5.00 V (dc)
Linearity	0.08% F.S.
Potentiometer Resistance	500 Ω
Stroke	60.00 in

Table A.7: Specifications for the model H25 incremental optical encoder [2]

Supply voltage	5–15 V (dc), $v_{in} = v_{out}$
Output format	2 channels in quadrature
Frequency response	100 kHz
Cycles per shaft turn	1000
Maximum speed	12 000 rpm
Shaft diameter	3/8 in (nominal)

Appendix B

Euler-Lagrange Computations

This appendix presents the results of arithmetic computations deemed too lengthy to be printed in the text of chapter 5.

B.1 Reduced System Jacobians

The following are Jacobian matrices not printed in the text of section 5.1.1 on page 70, due to their length.

$$J_{v_{c1}} = \begin{bmatrix} -a_{c1}C_1 & 0 & 0 & 0 & 0 & 0 \\ -a_{c1}S_1 & 0 & 0 & 0 & 0 & 0 \\ 0 & 0 & 0 & 0 & 0 & 0 \end{bmatrix}$$

$$J_{v_{c2}} = \begin{bmatrix} -(q_2 - a_{c2})C_1 & -S_1 & 0 & 0 & 0 & 0 \\ -(q_2 - a_{c2})S_1 & C_1 & 0 & 0 & 0 & 0 \\ 0 & 0 & 0 & 0 & 0 & 0 \end{bmatrix}$$

$$J_{v_{c3}} = \begin{bmatrix} -q_2C_1 - a_{c3}S_{13} - b_{c3}C_{13} & -S_1 & -a_{c3}S_{13} - b_{c3}C_{13} & 0 & 0 & 0 \\ -q_2S_1 + a_{c3}C_{13} - b_{c3}S_{13} & C_1 & a_{c3}C_{13} - b_{c3}S_{13} & 0 & 0 & 0 \\ 0 & 0 & 0 & 0 & 0 & 0 \end{bmatrix}$$

$$J_{v_{c4}} = \begin{bmatrix} j_{4,11} & -S_1 & j_{4,13} & -a_{c4}S_{134} + b_{c4}C_{134} & 0 & 0 \\ j_{4,21} & C_1 & j_{4,23} & a_{c4}C_{134} + b_{c4}S_{134} & 0 & 0 \\ 0 & 0 & 0 & 0 & 0 & 0 \end{bmatrix}$$

$$J_{v_{c5}} = \begin{bmatrix} j_{5,11} & -S_1 & j_{5,13} & -d_3S_{134} + a_{c5}C_{1345} & a_{c5}C_{1345} & 0 \\ j_{5,21} & C_1 & j_{5,23} & d_3C_{134} - a_{c5}S_{1345} & -a_{c5}S_{1345} & 0 \\ 0 & 0 & 0 & 0 & 0 & 0 \end{bmatrix}$$

$$J_{v_{c5}} = \begin{bmatrix} j_{6,11} & -S_1 & j_{6,13} & j_{6,14} & (q_6 - a_{c6})\,C_{1345} & S_{1345} \\ j_{6,21} & C_1 & j_{6,23} & j_{6,24} & -(q_6 - a_{c6})\,S_{1345} & C_{1345} \\ 0 & 0 & 0 & 0 & 0 & 0 \end{bmatrix}$$

where

$$j_{4,11} = -q_2C_1 - d_2S_{13} - a_{c4}S_{134} + b_{c4}C_{134}$$

$$j_{4,13} = -d_2S_{13} - a_{c4}S_{134} + b_{c4}C_{134}$$

$$j_{4,21} = -q_2S_1 + d_2C_{13} + a_{c4}C_{134} + b_{c4}S_{134}$$

$$j_{4,23} = d_2C_{13} + a_{c4}C_{134} + b_{c4}S_{134}$$

$$j_{5,11} = -q_2C_1 - d_2S_{13} - d_3S_{134} + a_{c5}C_{1345}$$

$$j_{5,13} = -d_2S_{13} - d_3S_{134} + a_{c5}C_{1345}$$

$$j_{5,21} = -q_2S_1 + d_2C_{13} + d_3C_{134} - a_{c5}S_{1345}$$

$$j_{5,23} = d_2C_{13} + d_3C_{134} - a_{c5}S_{1345}$$

$$j_{6,11} = -q_2C_1 - d_2S_{13} - d_3S_{134} + (q_6 - a_{c6})\,C_{1345}$$

$$j_{6,13} = -d_2S_{13} - d_3S_{134} + (q_6 - a_{c6})\,C_{1345}$$

$$j_{6,14} = -d_3S_{134} + (q_6 - a_{c6})\,C_{1345}$$

$$j_{6,21} = -q_2S_1 + d_2C_{13} + d_3C_{134} - (q_6 - a_{c6})\,S_{1345}$$

$$j_{6,23} = d_2C_{13} + d_3C_{134} - (q_6 - a_{c6})\,S_{1345}$$

$$j_{6,24} = d_3C_{134} - (q_6 - a_{c6})\,S_{1345}$$

B.2 Christoffel Symbols

For brevity's sake, the following non-zero Christoffel symbols c_{ijk} were not printed in section 5.1.1 on page 72. Note that any symbols not printed here were computed to have a value of zero.

$$
\begin{aligned}
c_{111} &= (-2\,m_5 d_3 a_{c5} + 2\,m_6 d_3 a_{c6} - 2\,m_6 d_3 q_6)\cos(2\,q_1 + 2\,q_3 + 2\,q_4 + q_5) \\
&\quad + (2\,m_6 d_2 a_{c6} - 2\,m_6 d_2 q_6 - 2\,m_5 d_2 a_{c5})\cos(2\,q_1 + 2\,q_3 + q_4 + q_5) \\
&\quad + (2\,m_5 q_2 a_{c5} - 2\,m_6 q_2 a_{c6} + 2\,m_6 q_2 q_6)\sin(2\,q_1 + q_3 + q_4 + q_5) \\
c_{112} &= -m_3 b_{c3}\cos q_3 + m_4 b_{c4}\cos(q_3 + q_4) - m_4 q_2 + m_2 a_{c2} - m_6 q_2 \\
&\quad + (-m_5 a_{c5} + m_6 a_{c6} - m_6 q_6)\cos(2\,q_1 + q_3 + q_4 + q_5) \\
&\quad + (-m_6 d_2 - m_3 a_{c3} - m_4 d_2 - m_5 d_2)\sin q_3 - m_3 q_2 \\
&\quad + (-m_5 d_3 - m_6 d_3 - m_4 a_{c4})\sin(q_3 + q_4) - m_5 q_2 - m_2 q_2 \\
c_{113} &= (-m_3 q_2 a_{c3} - m_6 q_2 d_2 - m_5 q_2 d_2 - m_4 q_2 d_2)\cos q_3 \\
&\quad + (-m_6 q_2 d_3 - m_5 q_2 d_3 - m_4 q_2 a_{c4})\cos(q_3 + q_4) \\
&\quad + (-2\,m_5 d_3 a_{c5} + 2\,m_6 d_3 a_{c6} - 2\,m_6 d_3 q_6)\cos(2\,q_1 + 2\,q_3 + 2\,q_4 + q_5) \\
&\quad + (2\,m_6 d_2 a_{c6} - 2\,m_6 d_2 q_6 - 2\,m_5 d_2 a_{c5})\cos(2\,q_1 + 2\,q_3 + q_4 + q_5) \\
&\quad + m_3 q_2 b_{c3}\sin q_3 - m_4 q_2 b_{c4}\sin(q_3 + q_4) + \\
&\quad (m_6 q_2 q_6 + m_5 q_2 a_{c5} - m_6 q_2 a_{c6})\sin(2\,q_1 + q_3 + q_4 + q_5) \\
c_{114} &= (-m_6 q_2 d_3 - m_5 q_2 d_3 - m_4 q_2 a_{c4})\cos(q_3 + q_4) - m_4 d_2 b_{c4}\cos q_4 \\
&\quad + (-2\,m_5 d_3 a_{c5} + 2\,m_6 d_3 a_{c6} - 2\,m_6 d_3 q_6)\cos(2\,q_1 + 2\,q_3 + 2\,q_4 + q_5) \\
&\quad + (-m_6 d_2 q_6 - m_5 d_2 a_{c5} + m_6 d_2 a_{c6})\cos(2\,q_1 + 2\,q_3 + q_4 + q_5) \\
&\quad + (m_5 d_2 d_3 + m_6 d_2 d_3 + m_4 d_2 a_{c4})\sin q_4 - m_4 q_2 b_{c4}\sin(q_3 + q_4) \\
&\quad + (m_6 q_2 q_6 + m_5 q_2 a_{c5} - m_6 q_2 a_{c6})\sin(2\,q_1 + q_3 + q_4 + q_5) \\
c_{115} &= (-m_6 d_3 q_6 + m_6 d_3 a_{c6} - m_5 d_3 a_{c5})\cos(2\,q_1 + 2\,q_3 + 2\,q_4 + q_5) \\
&\quad + (-m_6 d_2 q_6 - m_5 d_2 a_{c5} + m_6 d_2 a_{c6})\cos(2\,q_1 + 2\,q_3 + q_4 + q_5)
\end{aligned}
$$

$$+ (m_6 q_2 q_6 + m_5 q_2 a_{c5} - m_6 q_2 a_{c6}) \sin(2\,q_1 + q_3 + q_4 + q_5)$$

$$c_{116} = -m_6 d_3 \sin(2\,q_1 + 2\,q_3 + 2\,q_4 + q_5) - m_6 d_2 \sin(2\,q_1 + 2\,q_3 + q_4 + q_5)$$
$$-m_6 q_2 \cos(2\,q_1 + q_3 + q_4 + q_5) + m_6 a_{c6} - m_6 q_6$$

$$c_{121} = c_{211} = m_3 b_{c3} \cos q_3 - m_4 b_{c4} \cos(q_3 + q_4) + m_5 q_2 + m_2 q_2$$
$$+ (-m_5 a_{c5} + m_6 a_{c6} - m_6 q_6) \cos(2\,q_1 + q_3 + q_4 + q_5)$$
$$+ (m_3 a_{c3} + m_6 d_2 + m_5 d_2 + m_4 d_2) \sin q_3 + m_3 q_2 + m_4 q_2$$
$$+ (m_6 d_3 + m_5 d_3 + m_4 a_{c4}) \sin(q_3 + q_4) - m_2 a_{c2} + m_6 q_2$$

$$c_{123} = c_{213} = m_3 b_{c3} \cos q_3 - m_4 b_{c4} \cos(q_3 + q_4)$$
$$+ (-m_5 a_{c5} + m_6 a_{c6} - m_6 q_6) \cos(2\,q_1 + q_3 + q_4 + q_5)$$
$$+ (m_3 a_{c3} + m_6 d_2 + m_5 d_2 + m_4 d_2) \sin q_3$$
$$+ (m_6 d_3 + m_5 d_3 + m_4 a_{c4}) \sin(q_3 + q_4)$$

$$c_{124} = c_{214} = (-m_5 a_{c5} + m_6 a_{c6} - m_6 q_6) \cos(2\,q_1 + q_3 + q_4 + q_5)$$
$$+ (m_6 d_3 + m_5 d_3 + m_4 a_{c4}) \sin(q_3 + q_4) - m_4 b_{c4} \cos(q_3 + q_4)$$

$$c_{125} = c_{215} = (-m_5 a_{c5} + m_6 a_{c6} - m_6 q_6) \cos(2\,q_1 + q_3 + q_4 + q_5)$$

$$c_{126} = c_{216} = -m_6 \sin(2\,q_1 + q_3 + q_4 + q_5)$$

$$c_{131} = c_{311} = (m_5 q_2 d_2 + m_6 q_2 d_2 + m_3 q_2 a_{c3} + m_4 q_2 d_2) \cos q_3$$
$$+ (m_4 q_2 a_{c4} + m_5 q_2 d_3 + m_6 q_2 d_3) \cos(q_3 + q_4)$$
$$+ (-2\,m_5 d_3 a_{c5} + 2\,m_6 d_3 a_{c6} - 2\,m_6 d_3 q_6) \cos(2\,q_1 + 2\,q_3 + 2\,q_4 + q_5)$$
$$+ (2\,m_6 d_2 a_{c6} - 2\,m_6 d_2 q_6 - 2\,m_5 d_2 a_{c5}) \cos(2\,q_1 + 2\,q_3 + q_4 + q_5)$$
$$-m_3 q_2 b_{c3} \sin q_3 + m_4 q_2 b_{c4} \sin(q_3 + q_4)$$
$$+ (m_6 q_2 q_6 + m_5 q_2 a_{c5} - m_6 q_2 a_{c6}) \sin(2\,q_1 + q_3 + q_4 + q_5)$$

$$c_{132} = c_{312} = -m_3 b_{c3} \cos q_3 + m_4 b_{c4} \cos(q_3 + q_4)$$
$$+ (-m_5 a_{c5} + m_6 a_{c6} - m_6 q_6) \cos(2\,q_1 + q_3 + q_4 + q_5)$$
$$+ (-m_6 d_2 - m_3 a_{c3} - m_4 d_2 - m_5 d_2) \sin q_3$$

$$+ (-m_5 d_3 - m_6 d_3 - m_4 a_{c4}) \sin(q_3 + q_4)$$

$$c_{133} = c_{313} = (-2\, m_5 d_3 a_{c5} + 2\, m_6 d_3 a_{c6} - 2\, m_6 d_3 q_6) \cos(2\, q_1 + 2\, q_3 + 2\, q_4 + q_5)$$
$$+ (2\, m_6 d_2 a_{c6} - 2\, m_6 d_2 q_6 - 2\, m_5 d_2 a_{c5}) \cos(2\, q_1 + 2\, q_3 + q_4 + q_5)$$

$$c_{134} = c_{314} = (-2\, m_5 d_3 a_{c5} + 2\, m_6 d_3 a_{c6} - 2\, m_6 d_3 q_6) \cos(2\, q_1 + 2\, q_3 + 2\, q_4 + q_5)$$
$$+ (-m_6 d_2 q_6 - m_5 d_2 a_{c5} + m_6 d_2 a_{c6}) \cos(2\, q_1 + 2\, q_3 + q_4 + q_5)$$
$$+ (m_5 d_2 d_3 + m_6 d_2 d_3 + m_4 d_2 a_{c4}) \sin q_4 - m_4 d_2 b_{c4} \cos q_4$$

$$c_{135} = c_{315} = (-m_6 d_3 q_6 + m_6 d_3 a_{c6} - m_5 d_3 a_{c5}) \cos(2\, q_1 + 2\, q_3 + 2\, q_4 + q_5)$$
$$+ (-m_6 d_2 q_6 - m_5 d_2 a_{c5} + m_6 d_2 a_{c6}) \cos(2\, q_1 + 2\, q_3 + q_4 + q_5)$$

$$c_{136} = c_{316} = -m_6 d_2 \sin(2\, q_1 + 2\, q_3 + q_4 + q_5)$$
$$-m_6 d_3 \sin(2\, q_1 + 2\, q_3 + 2\, q_4 + q_5) + m_6 a_{c6} - m_6 q_6$$

$$c_{141} = c_{411} = (m_4 q_2 a_{c4} + m_5 q_2 d_3 + m_6 q_2 d_3) \cos(q_3 + q_4) + m_4 d_2 b_{c4} \cos q_4$$
$$+ (-2\, m_5 d_3 a_{c5} + 2\, m_6 d_3 a_{c6} - 2\, m_6 d_3 q_6) \cos(2\, q_1 + 2\, q_3 + 2\, q_4 + q_5)$$
$$+ (-m_6 d_2 q_6 - m_5 d_2 a_{c5} + m_6 d_2 a_{c6}) \cos(2\, q_1 + 2\, q_3 + q_4 + q_5)$$
$$+ (-m_6 d_2 d_3 - m_5 d_2 d_3 - m_4 d_2 a_{c4}) \sin q_4 + m_4 q_2 b_{c4} \sin(q_3 + q_4)$$
$$+ (m_6 q_2 q_6 + m_5 q_2 a_{c5} - m_6 q_2 a_{c6}) \sin(2\, q_1 + q_3 + q_4 + q_5)$$

$$c_{142} = c_{412} = (-m_5 a_{c5} + m_6 a_{c6} - m_6 q_6) \cos(2\, q_1 + q_3 + q_4 + q_5)$$
$$+ (-m_5 d_3 - m_6 d_3 - m_4 a_{c4}) \sin(q_3 + q_4) + m_4 b_{c4} \cos(q_3 + q_4)$$

$$c_{143} = c_{413} = + (-m_6 d_2 q_6 - m_5 d_2 a_{c5} + m_6 d_2 a_{c6}) \cos(2\, q_1 + 2\, q_3 + q_4 + q_5)$$
$$+ (-2\, m_5 d_3 a_{c5} + 2\, m_6 d_3 a_{c6} - 2\, m_6 d_3 q_6) \cos(2\, q_1 + 2\, q_3 + 2\, q_4 + q_5)$$
$$+ (-m_6 d_2 d_3 - m_5 d_2 d_3 - m_4 d_2 a_{c4}) \sin q_4 + m_4 d_2 b_{c4} \cos q_4$$

$$c_{144} = c_{414} = (-2\, m_5 d_3 a_{c5} + 2\, m_6 d_3 a_{c6} - 2\, m_6 d_3 q_6) \cos(2\, q_1 + 2\, q_3 + 2\, q_4 + q_5)$$

$$c_{145} = c_{415} = (-m_6 d_3 q_6 + m_6 d_3 a_{c6} - m_5 d_3 a_{c5}) \cos(2\, q_1 + 2\, q_3 + 2\, q_4 + q_5)$$

$$c_{146} = c_{416} = -m_6 d_3 \sin(2\, q_1 + 2\, q_3 + 2\, q_4 + q_5) - m_6 q_6 + m_6 a_{c6}$$

$$c_{151} = c_{511} = (-m_6 d_3 q_6 + m_6 d_3 a_{c6} - m_5 d_3 a_{c5}) \cos(2\, q_1 + 2\, q_3 + 2\, q_4 + q_5)$$

$$+(-m_6d_2q_6 - m_5d_2a_{c5} + m_6d_2a_{c6})\cos(2q_1 + 2q_3 + q_4 + q_5)$$

$$+(m_6q_2q_6 + m_5q_2a_{c5} - m_6q_2a_{c6})\sin(2q_1 + q_3 + q_4 + q_5)$$

$$c_{152} = c_{512} = (-m_5a_{c5} + m_6a_{c6} - m_6q_6)\cos(2q_1 + q_3 + q_4 + q_5)$$

$$c_{153} = c_{513} = (-m_6d_3q_6 + m_6d_3a_{c6} - m_5d_3a_{c5})\cos(2q_1 + 2q_3 + 2q_4 + q_5)$$

$$+(-m_6d_2q_6 - m_5d_2a_{c5} + m_6d_2a_{c6})\cos(2q_1 + 2q_3 + q_4 + q_5)$$

$$c_{154} = c_{514} = (-m_6d_3q_6 + m_6d_3a_{c6} - m_5d_3a_{c5})\cos(2q_1 + 2q_3 + 2q_4 + q_5)$$

$$c_{156} = c_{516} = m_6a_{c6} - m_6q_6$$

$$c_{161} = c_{611} = -m_6q_2\cos(2q_1 + q_3 + q_4 + q_5) - m_6d_2\sin(2q_1 + 2q_3 + q_4 + q_5)$$

$$-m_6d_3\sin(2q_1 + 2q_3 + 2q_4 + q_5) - m_6a_{c6} + m_6q_6$$

$$c_{162} = c_{612} = -m_6\sin(2q_1 + q_3 + q_4 + q_5)$$

$$c_{163} = c_{613} = m_6q_6 - m_6d_2\sin(2q_1 + 2q_3 + q_4 + q_5) - m_6a_{c6}$$

$$-m_6d_3\sin(2q_1 + 2q_3 + 2q_4 + q_5)$$

$$c_{164} = c_{614} = m_6q_6 - m_6d_3\sin(2q_1 + 2q_3 + 2q_4 + q_5) - m_6a_{c6}$$

$$c_{165} = c_{615} = m_6q_6 - m_6a_{c6}$$

$$c_{331} = (m_5q_2d_2 + m_6q_2d_2 + m_3q_2a_{c3} + m_4q_2d_2)\cos q_3 - m_3q_2b_{c3}\sin q_3$$

$$+(m_4q_2a_{c4} + m_5q_2d_3 + m_6q_2d_3)\cos(q_3 + q_4) + m_4q_2b_{c4}\sin(q_3 + q_4)$$

$$+(-2m_5d_3a_{c5} + 2m_6d_3a_{c6} - 2m_6d_3q_6)\cos(2q_1 + 2q_3 + 2q_4 + q_5)$$

$$+(2m_6d_2a_{c6} - 2m_6d_2q_6 - 2m_5d_2a_{c5})\cos(2q_1 + 2q_3 + q_4 + q_5)$$

$$+(m_6q_2q_6 + m_5q_2a_{c5} - m_6q_2a_{c6})\sin(2q_1 + q_3 + q_4 + q_5)$$

$$c_{332} = q_4) + (-m_5a_{c5} + m_6a_{c6} - m_6q_6)\cos(2q_1 + q_3 + q_4 + q_5)$$

$$+(-m_6d_2 - m_3a_{c3} - m_4d_2 - m_5d_2)\sin q_3 + m_4b_{c4}\cos(q_3$$

$$+(-m_5d_3 - m_6d_3 - m_4a_{c4})\sin(q_3 + q_4) - m_3b_{c3}\cos q_3$$

$$c_{333} = (-2m_5d_3a_{c5} + 2m_6d_3a_{c6} - 2m_6d_3q_6)\cos(2q_1 + 2q_3 + 2q_4 + q_5)$$

$$+(2m_6d_2a_{c6} - 2m_6d_2q_6 - 2m_5d_2a_{c5})\cos(2q_1 + 2q_3 + q_4 + q_5)$$

$$
\begin{aligned}
c_{334} &= (-2\,m_5 d_3 a_{c5} + 2\,m_6 d_3 a_{c6} - 2\,m_6 d_3 q_6)\cos(2\,q_1 + 2\,q_3 + 2\,q_4 + q_5) \\
&\quad + (-m_6 d_2 q_6 - m_5 d_2 a_{c5} + m_6 d_2 a_{c6})\cos(2\,q_1 + 2\,q_3 + q_4 + q_5) \\
&\quad + (m_5 d_2 d_3 + m_6 d_2 d_3 + m_4 d_2 a_{c4})\sin q_4 - m_4 d_2 b_{c4}\cos q_4 \\
c_{335} &= (-m_6 d_3 q_6 + m_6 d_3 a_{c6} - m_5 d_3 a_{c5})\cos(2\,q_1 + 2\,q_3 + 2\,q_4 + q_5) \\
&\quad + (-m_6 d_2 q_6 - m_5 d_2 a_{c5} + m_6 d_2 a_{c6})\cos(2\,q_1 + 2\,q_3 + q_4 + q_5) \\
c_{336} &= -m_6 d_2 \sin(2\,q_1 + 2\,q_3 + q_4 + q_5) - m_6 d_3 \sin(2\,q_1 + 2\,q_3 + 2\,q_4 + q_5) \\
&\quad + m_6 a_{c6} - m_6 q_6 \\
c_{341} &= c_{431} = (m_4 q_2 a_{c4} + m_5 q_2 d_3 + m_6 q_2 d_3)\cos(q_3 + q_4) + m_4 d_2 b_{c4}\cos q_4 \\
&\quad + (-2\,m_5 d_3 a_{c5} + 2\,m_6 d_3 a_{c6} - 2\,m_6 d_3 q_6)\cos(2\,q_1 + 2\,q_3 + 2\,q_4 + q_5) \\
&\quad + (-m_6 d_2 q_6 - m_5 d_2 a_{c5} + m_6 d_2 a_{c6})\cos(2\,q_1 + 2\,q_3 + q_4 + q_5) \\
&\quad + (-m_6 d_2 d_3 - m_5 d_2 d_3 - m_4 d_2 a_{c4})\sin q_4 + m_4 q_2 b_{c4}\sin(q_3 + q_4) \\
&\quad + (m_6 q_2 q_6 + m_5 q_2 a_{c5} - m_6 q_2 a_{c6})\sin(2\,q_1 + q_3 + q_4 + q_5) \\
c_{342} &= c_{432} = (-m_5 a_{c5} + m_6 a_{c6} - m_6 q_6)\cos(2\,q_1 + q_3 + q_4 + q_5) \\
&\quad + (-m_5 d_3 - m_6 d_3 - m_4 a_{c4})\sin(q_3 + q_4) + m_4 b_{c4}\cos(q_3 + q_4) \\
c_{343} &= c_{433} = (-2\,m_5 d_3 a_{c5} + 2\,m_6 d_3 a_{c6} - 2\,m_6 d_3 q_6)\cos(2\,q_1 + 2\,q_3 + 2\,q_4 + q_5) \\
&\quad + (-m_6 d_2 q_6 - m_5 d_2 a_{c5} + m_6 d_2 a_{c6})\cos(2\,q_1 + 2\,q_3 + q_4 + q_5) \\
&\quad + (-m_6 d_2 d_3 - m_5 d_2 d_3 - m_4 d_2 a_{c4})\sin q_4 + m_4 d_2 b_{c4}\cos q_4 \\
c_{344} &= c_{434} = (-2\,m_5 d_3 a_{c5} + 2\,m_6 d_3 a_{c6} - 2\,m_6 d_3 q_6)\cos(2\,q_1 + 2\,q_3 + 2\,q_4 + q_5) \\
c_{345} &= c_{435} = (-m_6 d_3 q_6 + m_6 d_3 a_{c6} - m_5 d_3 a_{c5})\cos(2\,q_1 + 2\,q_3 + 2\,q_4 + q_5) \\
c_{346} &= c_{436} = -m_6 d_3 \sin(2\,q_1 + 2\,q_3 + 2\,q_4 + q_5) - m_6 q_6 + m_6 a_{c6} \\
c_{351} &= c_{531} = (-m_6 d_3 q_6 + m_6 d_3 a_{c6} - m_5 d_3 a_{c5})\cos(2\,q_1 + 2\,q_3 + 2\,q_4 + q_5) \\
&\quad + (-m_6 d_2 q_6 - m_5 d_2 a_{c5} + m_6 d_2 a_{c6})\cos(2\,q_1 + 2\,q_3 + q_4 + q_5) \\
&\quad + (m_6 q_2 q_6 + m_5 q_2 a_{c5} - m_6 q_2 a_{c6})\sin(2\,q_1 + q_3 + q_4 + q_5) \\
c_{352} &= c_{532} = (-m_5 a_{c5} + m_6 a_{c6} - m_6 q_6)\cos(2\,q_1 + q_3 + q_4 + q_5)
\end{aligned}
$$

$$
\begin{aligned}
c_{353} &= c_{533} = (-m_6 d_3 q_6 + m_6 d_3 a_{c6} - m_5 d_3 a_{c5}) \cos(2\,q_1 + 2\,q_3 + 2\,q_4 + q_5) \\
&\quad + (-m_6 d_2 q_6 - m_5 d_2 a_{c5} + m_6 d_2 a_{c6}) \cos(2\,q_1 + 2\,q_3 + q_4 + q_5) \\
c_{354} &= c_{534} = (-m_6 d_3 q_6 + m_6 d_3 a_{c6} - m_5 d_3 a_{c5}) \cos(2\,q_1 + 2\,q_3 + 2\,q_4 + q_5) \\
c_{356} &= c_{536} = m_6 a_{c6} - m_6 q_6 \\
c_{361} &= c_{631} = -m_6 q_2 \cos(2\,q_1 + q_3 + q_4 + q_5) - m_6 d_2 \sin(2\,q_1 + 2\,q_3 + q_4 + q_5) \\
&\quad - m_6 d_3 \sin(2\,q_1 + 2\,q_3 + 2\,q_4 + q_5) - m_6 a_{c6} + m_6 q_6 \\
c_{362} &= c_{632} = -m_6 \sin(2\,q_1 + q_3 + q_4 + q_5) \\
c_{363} &= c_{633} = m_6 q_6 - m_6 d_2 \sin(2\,q_1 + 2\,q_3 + q_4 + q_5) - m_6 a_{c6} \\
&\quad - m_6 d_3 \sin(2\,q_1 + 2\,q_3 + 2\,q_4 + q_5) \\
c_{364} &= c_{634} = m_6 q_6 - m_6 d_3 \sin(2\,q_1 + 2\,q_3 + 2\,q_4 + q_5) - m_6 a_{c6} \\
c_{365} &= c_{635} = m_6 q_6 - m_6 a_{c6} \\
c_{441} &= (m_4 q_2 a_{c4} + m_5 q_2 d_3 + m_6 q_2 d_3) \cos(q_3 + q_4) + m_4 d_2 b_{c4} \cos q_4 \\
&\quad + (-2\,m_5 d_3 a_{c5} + 2\,m_6 d_3 a_{c6} - 2\,m_6 d_3 q_6) \cos(2\,q_1 + 2\,q_3 + 2\,q_4 + q_5) \\
&\quad + (-m_6 d_2 q_6 - m_5 d_2 a_{c5} + m_6 d_2 a_{c6}) \cos(2\,q_1 + 2\,q_3 + q_4 + q_5) \\
&\quad + (-m_6 d_2 d_3 - m_5 d_2 d_3 - m_4 d_2 a_{c4}) \sin q_4 + m_4 q_2 b_{c4} \sin(q_3 + q_4) \\
&\quad + (m_6 q_2 q_6 + m_5 q_2 a_{c5} - m_6 q_2 a_{c6}) \sin(2\,q_1 + q_3 + q_4 + q_5) \\
c_{442} &= (-m_5 a_{c5} + m_6 a_{c6} - m_6 q_6) \cos(2\,q_1 + q_3 + q_4 + q_5) \\
&\quad + (-m_5 d_3 - m_6 d_3 - m_4 a_{c4}) \sin(q_3 + q_4) + m_4 b_{c4} \cos(q_3 + q_4) \\
c_{443} &= (-2\,m_5 d_3 a_{c5} + 2\,m_6 d_3 a_{c6} - 2\,m_6 d_3 q_6) \cos(2\,q_1 + 2\,q_3 + 2\,q_4 + q_5) \\
&\quad + (-m_6 d_2 q_6 - m_5 d_2 a_{c5} + m_6 d_2 a_{c6}) \cos(2\,q_1 + 2\,q_3 + q_4 + q_5) \\
&\quad + (-m_6 d_2 d_3 - m_5 d_2 d_3 - m_4 d_2 a_{c4}) \sin q_4 + m_4 d_2 b_{c4} \cos q_4 \\
c_{444} &= (-2\,m_5 d_3 a_{c5} + 2\,m_6 d_3 a_{c6} - 2\,m_6 d_3 q_6) \cos(2\,q_1 + 2\,q_3 + 2\,q_4 + q_5) \\
c_{445} &= (-m_6 d_3 q_6 + m_6 d_3 a_{c6} - m_5 d_3 a_{c5}) \cos(2\,q_1 + 2\,q_3 + 2\,q_4 + q_5) \\
c_{446} &= -m_6 d_3 \sin(2\,q_1 + 2\,q_3 + 2\,q_4 + q_5) - m_6 q_6 + m_6 a_{c6}
\end{aligned}
$$

$$
\begin{aligned}
c_{451} &= c_{541} = (-m_6 d_3 q_6 + m_6 d_3 a_{c6} - m_5 d_3 a_{c5}) \cos(2q_1 + 2q_3 + 2q_4 + q_5) \\
&\quad + (-m_6 d_2 q_6 - m_5 d_2 a_{c5} + m_6 d_2 a_{c6}) \cos(2q_1 + 2q_3 + q_4 + q_5) \\
&\quad + (m_6 q_2 q_6 + m_5 q_2 a_{c5} - m_6 q_2 a_{c6}) \sin(2q_1 + q_3 + q_4 + q_5) \\
c_{452} &= c_{542} = (-m_5 a_{c5} + m_6 a_{c6} - m_6 q_6) \cos(2q_1 + q_3 + q_4 + q_5) \\
c_{453} &= c_{543} = (-m_6 d_3 q_6 + m_6 d_3 a_{c6} - m_5 d_3 a_{c5}) \cos(2q_1 + 2q_3 + 2q_4 + q_5) \\
&\quad + (-m_6 d_2 q_6 - m_5 d_2 a_{c5} + m_6 d_2 a_{c6}) \cos(2q_1 + 2q_3 + q_4 + q_5) \\
c_{454} &= c_{544} = (-m_6 d_3 q_6 + m_6 d_3 a_{c6} - m_5 d_3 a_{c5}) \cos(2q_1 + 2q_3 + 2q_4 + q_5) \\
c_{456} &= c_{546} = m_6 a_{c6} - m_6 q_6 \\
c_{461} &= c_{641} = -m_6 q_2 \cos(2q_1 + q_3 + q_4 + q_5) - m_6 d_2 \sin(2q_1 + 2q_3 + q_4 + q_5) \\
&\quad - m_6 d_3 \sin(2q_1 + 2q_3 + 2q_4 + q_5) - m_6 a_{c6} + m_6 q_6 \\
c_{462} &= c_{642} = -m_6 \sin(2q_1 + q_3 + q_4 + q_5) \\
c_{463} &= c_{643} = m_6 q_6 - m_6 d_2 \sin(2q_1 + 2q_3 + q_4 + q_5) \\
&\quad - m_6 d_3 \sin(2q_1 + 2q_3 + 2q_4 + q_5) - m_6 a_{c6} \\
c_{464} &= c_{644} = m_6 q_6 - m_6 d_3 \sin(2q_1 + 2q_3 + 2q_4 + q_5) - m_6 a_{c6} \\
c_{465} &= c_{645} = m_6 q_6 - m_6 a_{c6} \\
c_{551} &= (-m_6 d_3 q_6 + m_6 d_3 a_{c6} - m_5 d_3 a_{c5}) \cos(2q_1 + 2q_3 + 2q_4 + q_5) \\
&\quad + (-m_6 d_2 q_6 - m_5 d_2 a_{c5} + m_6 d_2 a_{c6}) \cos(2q_1 + 2q_3 + q_4 + q_5) \\
&\quad + (m_6 q_2 q_6 + m_5 q_2 a_{c5} - m_6 q_2 a_{c6}) \sin(2q_1 + q_3 + q_4 + q_5) \\
c_{552} &= (-m_5 a_{c5} + m_6 a_{c6} - m_6 q_6) \cos(2q_1 + q_3 + q_4 + q_5) \\
c_{553} &= (-m_6 d_3 q_6 + m_6 d_3 a_{c6} - m_5 d_3 a_{c5}) \cos(2q_1 + 2q_3 + 2q_4 + q_5) \\
&\quad + (-m_6 d_2 q_6 - m_5 d_2 a_{c5} + m_6 d_2 a_{c6}) \cos(2q_1 + 2q_3 + q_4 + q_5) \\
c_{554} &= (-m_6 d_3 q_6 + m_6 d_3 a_{c6} - m_5 d_3 a_{c5}) \cos(2q_1 + 2q_3 + 2q_4 + q_5) \\
c_{556} &= m_6 a_{c6} - m_6 q_6 \\
c_{561} &= c_{651} = -m_6 q_2 \cos(2q_1 + q_3 + q_4 + q_5) - m_6 d_2 \sin(2q_1 + 2q_3 + q_4 + q_5)
\end{aligned}
$$

$$-m_6 d_3 \sin(2\,q_1 + 2\,q_3 + 2\,q_4 + q_5) - m_6 a_{c6} + m_6 q_6$$

$$c_{562} = c_{652} = -m_6 \sin(2\,q_1 + q_3 + q_4 + q_5)$$

$$c_{563} = c_{653} = m_6 q_6 - m_6 d_2 \sin(2\,q_1 + 2\,q_3 + q_4 + q_5)$$
$$-m_6 d_3 \sin(2\,q_1 + 2\,q_3 + 2\,q_4 + q_5) - m_6 a_{c6}$$

$$c_{564} = c_{654} = m_6 q_6 - m_6 d_3 \sin(2\,q_1 + 2\,q_3 + 2\,q_4 + q_5) - m_6 a_{c6}$$

$$c_{565} = c_{655} = m_6 q_6 - m_6 a_{c6}$$

B.3 Potential Functions

The potential functions ϕ_k below were not printed in section 5.1.1 on page 72.

$$\begin{aligned}
\phi_1 &= (-m_4 q_2 - m_2 q_2 - m_5 q_2 + m_2 a_{c2} - m_3 q_2 - m_1 a_{c1} - m_6 q_2)\, g \cos q_1 \\
&\quad -m_3 g b_{c3} \cos(q_1 + q_3) + m_4 g b_{c4} \cos(q_1 + q_3 + q_4) \\
&\quad + (-m_6 a_{c6} + m_5 a_{c5} + m_6 q_6)\, g \cos(q_1 + q_3 + q_4 + q_5) \\
&\quad + (-m_6 d_2 - m_3 a_{c3} - m_4 d_2 - m_5 d_2)\, g \sin(q_1 + q_3) \\
&\quad + (-m_5 d_3 - m_6 d_3 - m_4 a_{c4})\, g \sin(q_1 + q_3 + q_4) \\
\phi_2 &= (-m_2 - m_3 - m_4 - m_5 - m_6)\, g \sin q_1 \\
\phi_3 &= -m_3 g b_{c3} \cos(q_1 + q_3) + m_4 g b_{c4} \cos(q_1 + q_3 + q_4) \\
&\quad + (-m_6 a_{c6} + m_5 a_{c5} + m_6 q_6)\, g \cos(q_1 + q_3 + q_4 + q_5) \\
&\quad + (-m_6 d_2 - m_3 a_{c3} - m_4 d_2 - m_5 d_2)\, g \sin(q_1 + q_3) \\
&\quad + (-m_5 d_3 - m_6 d_3 - m_4 a_{c4})\, g \sin(q_1 + q_3 + q_4) \\
\phi_4 &= (-m_6 a_{c6} + m_5 a_{c5} + m_6 q_6)\, g \cos(q_1 + q_3 + q_4 + q_5) \\
&\quad + (-m_5 d_3 - m_6 d_3 - m_4 a_{c4})\, g \sin(q_1 + q_3 + q_4) \\
&\quad + m_4 g b_{c4} \cos(q_1 + q_3 + q_4) \\
\phi_5 &= (-m_6 a_{c6} + m_5 a_{c5} + m_6 q_6)\, g \cos(q_1 + q_3 + q_4 + q_5) \\
\phi_6 &= m_6 g \sin(q_1 + q_3 + q_4 + q_5)
\end{aligned}$$